EXAMINING THE TIME-DEPENDENT CHANGES IN THE BUBBLE STRUCTURE OF WHOLE EGG AND EGG WHITE FOAMS AND BATTERS USING SMALL STRAIN SHEAR OSCILLATORY RHEOLOGY, LARGE STRAIN SHEAR FLOW RHEOLOGY AND IMAGE ANALYSIS TECHNIQUES

by

Jeremy E. Spencer

A thesis submitted to the Faculty of Graduate Studies of

The University of Manitoba

In partial fulfillment of the requirements of the degree of

MASTER OF SCIENCE

Department of Food Science

University of Manitoba

Winnipeg, Manitoba

THE UNIVERSITY OF MANITOBA

FACULTY OF GRADUATE STUDIES

*****

COPYRIGHT PERMISSION

EXAMINING THE TIME-DEPENDENT CHANGES IN THE BUBBLE STRUCTURE OF WHOLE EGG AND EGG WHITE FOAMS AND BATTERS USING SMALL STRAIN SHEAR OSCILLATORY RHEOLOGY, LARGE STRAIN SHEAR FLOW RHEOLOGY AND IMAGE ANALYSIS TECHNIQUES

by

Jeremy E. Spencer

A Thesis/Practicum submitted to the Faculty of Graduate Studies of The University of Manitoba in partial fulfillment of the requirement of the degree of

Master of Science

I hereby declare that I am the sole author of this thesis.

I authorize the University of Manitoba to lend this thesis to other institutions or individuals for the purpose of scholarly research.

Jeremy E. Spencer

I further authorize the University of Manitoba to reproduce this thesis by photocopying or by other means, in total or in part, at the request of other institutions or individuals for the purpose of scholarly research.

Jeremy E. Spencer

Acknowledgements

I would like to thank Dr. Martin Scanlon for his guidance and patience over the past two years. I will forever be grateful of his support and teachings which have helped me develop scientifically, professionally and as a person. I have learned so much from you and could not have asked for a better advisor. I would like to extend a genuine thank you to Dr. Susan Arntfield who has provided me answers to numerous questions or pointed me in the right direction on just about anything I could throw at her. Thank you for having a genuine interest in all students and being my 'go to' person. I would also like to thank my other committee member Dr. John Page and all of the graduate students I have worked with in Food Science and Physics – I have learned so much from all of you. To all of the staff and professors in the Food Science Department, thank you for all of your support and teachings over the past six years. To Dr. Blank, thank you for allowing an unskilled microbiologist to TA your course and for always bringing your uplifting sense of humor to the department.

I am appreciative of all of the financial assistance I have received over the past two years from the Canadian Wheat Board, and through Dr. Scanlon's NSERC grant. Thank you to UMSU and UMGSA for providing travel grants, and to Innovatech Egg Products, and John Thoroski, for supplying eggs for the research.

Last but not least, I would like to thank all of my friends and family that have been there for me the past two years, especially to my parents who have provided me with so much love and support, without all of you I would have gone insane.

Abstract

Foam structure is responsible for texture and mouth-feel in a variety of foods. The stability of foams during processing greatly affects the appearance and the texture of the resulting product. Angel food and sponge cake textures are ultimately determined by the air bubbles entrained into the foam (batter) and their stability over time. Gravity-driven drainage and pressure-difference-driven diffusion of the gas alter the numbers and sizes of air bubbles in the foam and directly affect foam rheology. Whole egg and egg white foams (and their corresponding batters) were prepared according to typical sponge cake and angel food cake recipes, respectively. Eight mix times ranging from 0-1065 s were used to achieve a range in densities (1225 to 235 kg m^{-3}) within the four different systems. Ten consecutive frequency sweeps (0.1267 – 62.81 rad s^{-1}), at a controlled stress of 0.02 Pa (a stress within the linear viscoelastic regime of all systems), were performed to monitor changes in G' and G'' over time. Procedures described by Cohen-Addad *et al.* (1998) scaled rheological data successfully onto a single master curve. A plot of the rheological scaling factor versus time allowed characterization of the time-dependent evolution of the foam or batter. For short mix times (where foams and batters were dilute emulsions of bubbles) slopes of these plots approached +1, indicative of drainage dominating rheological changes. For long mix times a slope of -0.5 was approached, so that disproportionation was the dominant factor. Thirty consecutive shear rate ramps (1.452 – 145.2 s^{-1}) were used to monitor changes in yield stress and shear-thinning viscosity as a function of time. For whole egg foams, viscosity increased as more air was entrained with longer mix time. For egg white foams, viscosity also increased, but these foams began to exhibit a yield stress at a bubble fraction of ~0.65. Image analysis was used to monitor bubble size distribution

changes over the same time period to confirm mechanisms of foam evolution. Models previously employed on industrial foams and emulsions and similar soft glassy materials were adapted and applied to the foam and batter systems. Ultimately, using the three experimental procedures and the models designed for similar systems, the role of surface-active ingredients and bubble packing density can assist in understanding foam and batter deterioration so that cake appearance and texture can be optimized.

Table of Contents

List of Figures

List of Tables

Chapter 1: Introduction

The textural quality of foam cakes (angel food and sponge cake), is directly related to the air bubbles incorporated into the batter during the mixing stage (Pyler, 1988). Initially, mixing incorporates air into the eggs, but upon continued mixing the air cells become increasingly smaller and the foam or batter eventually reaches a maximum bubble volume fraction (Pyler, 1988). Factors affecting the amount of air entrained and the size distribution of the bubbles include mixing time and speed, type of mixing blade, egg temperature, and the surface tension and viscosity of the batter (Sahi & Alava, 2003). In turn, the volume fraction of bubbles and their sizes largely govern the rheological properties of the foam or batter (Weaire & Hutzler, 1999). However, because rheological properties are dynamically evolving in these wet foams (Cipelletti & Ramos, 2002; Gopal & Durian, 2003), the resulting quality of the sponge or angel food cake is sensitive to the time between mixing and the stabilization of foam structure that occurs during baking (Bennion & Bamford, 1973; Pyler, 1988).

At low mix times, the volume fraction of air bubbles entrained in the foam or batter is low, and, as is the case with dilute emulsions (Mason, 1999), the system essentially behaves as a viscous fluid. As the volume fraction of bubbles increases the emulsion-like material becomes a foam (Weaire & Hutzler, 1999), and behaves as a viscoelastic solid at low stresses and exhibits a yield stress (Cohen-Addad *et al.,* 1998; Lauridsen *et al.,* 2002). At high bubble concentrations and at stresses greater than the yield stress, foams flow as viscous fluids (Cohen-Addad & Höhler, 2001). The basis for resistance to flow at low stresses is that the bubbles become jammed rather than flowing around one another (Gopal & Durian, 2003). For food foams, the presence of polymeric surface-active compounds, such as proteins (Wilde, 2000), can complicate analyses of foam properties.

Assessments of how polymeric components affect the rheological properties of foams of a given volume fraction and bubble size distribution compared to surfactant stabilized foams is very much an area of active research (Murray & Ettelaie, 2004; Saint-Jalmes *et al.*, 2005).

Foams age, and there is a resulting change in their rheological properties (Weaire & Hutzler, 1999). The rate and extent of changes in foam rheology depend on mechanisms such as gravity driven drainage, pressure difference driven disproportionation between bubbles, and coalescence of the bubbles (Cohen-Addad *et al.*, 1998; Cox *et al.*, 2004; Hammershøj *et al.*, 1999; Herzhaft, 1999; Sahi & Alava, 2003; Weaire *et al.*, 1993). For synthetic foams (aerosol-generated shaving creams), an evolution of the shear moduli occurs over time (aging) according to a scaling law, whereby the frequency dependent complex shear moduli of foams of different ages scale with changes in the size of the bubbles and with changes in relaxation times of bubble motions (Cohen-Addad *et al.*, 1998).

In order to address the above outlined problems, integration of knowledge and experiments previously employed on emulsions and industrial foams needs to be applied to complex food foams. Although the macro-structure of food foams is the same as industrial foams, the multi-component nature of food foams leads to greater complexity and alters the mechanical response. By applying rheological analyses used on industrial foams the mechanical response of the complex food foams can be examined. Examining the differences in mechanical response of industrial foams and food foams may allow for the adaptation of existing theories and models on similar cellular materials to understand the mechanical behavior of food foams and lead to an overall better understanding of food structure stability. Ultimately, a better understanding of structural rearrangements in

foams would allow for the cake mixing and formulation processes to be optimized and ensure that desired bubble structure is maintained throughout the cake making process so as to attain good texture in the final product.

My research objectives are to use small strain rheological experiments, previously used on emulsions and industrial foams, to monitor the frequency dependence of both the elastic and viscous components of foams and batters of various bubble volume factions from two different egg systems. Similar to the small strain techniques, large strain rheological experiments previously used on emulsions and industrial foams will be employed to monitor the shear flow properties of the same foams and batters and common flow behavior models (Newtonian, Power-Law, Herschel-Buckley) will be used to characterize foams and batters of different bubble volume fractions. In both the small and large strain cases, the behavior of the foams and batters will be monitored over a one hour period to study the aging effects of the systems. An attempt to employ a scaling procedure previously used on industrial foams will be made in order to condense aging data from both the small strain and large strain rheological analyses onto a single master curve to allow for easier interpretation. From the single master curves, the objective is to characterize differences in aging mechanisms occurring in foams of different bubble volume fractions by analyzing both small strain and large strain rheological data and interpreting them in the light of existing foam literature. In order to account for differences in the rheological response with time due to changes in bubble sizes, image analysis techniques will be employed to monitor changes in bubble size and bubble size distribution of foams of various bubble volume fractions from both egg systems over a one hour period. Finally, in order to integrate all the experimental results and get an overall look at the foams' rheological response, small and large strain rheological results

will be analyzed with image analysis results utilizing theories and models that are applicable for foams/emulsion of similar nature.

Chapter 2: Review of Literature

2.1 Introduction

Predicting and understanding the mechanical response and underlying structural and dynamic properties of food foams allows for the optimization of many food production methods (Brooker, 1993; Thakur *et al*, 2003; Lau & Dickinson, 2004). Optimization of these methods leads to greater consistency and therefore quality, in the end texture of foods. Many foods, such as bread, cakes, chocolate, ice cream, and whipped dairy products, exhibit foam-like structures. Of particular interest are baked goods which exist as liquid foams and eventually become solid foams during baking.

Foams are a two phase system created by entraining air (the dispersed phase) into a continuous medium; in cake making this is usually done by means of mechanical mixing (Herzhaft, 1999; Weaire & Hutzler, 1999). All other things being equal, varying the mix time changes the amount of air incorporated into the continuous phase of the foam. Generally, in the cake making process a foam is created by mixing all the required ingredients, with the exception of flour, for a specified length of time. Once the desired amount of air has been entrained, the flour is gently folded into the foam to create the cake batter. Ingredients, as well as the inherent properties of the cake mix (viscosity and surface tension) determine the size and amount of bubbles that can be entrained for a given mix time. In turn, the size and amount of bubbles plays a large role in determining the mechanical response of the foam (Weaire & Hutzler, 1999).

Ingredients and mixing parameters play a role in defining the initial structure of the foam, but foams are dynamic and their structures are constantly evolving with time (Cipelletti & Ramos, 2002; Gopal & Durian, 2003). In many cases this evolution results in a loss of the desired foam structure. A significant number of researchers have explored

the mechanisms by which foam structures evolve with time, as well as potential means of controlling the foam structure decay (Weaire *et al*, 1993; Cohen-Addad *et al,* 1998; Hamershøj *et al*, 1999; Herzhaft, 1999; Sahi & Alava, 2003; Cox *et al*, 2004). Recently, theories and models which have been used to study industrial foams and emulsions (Princen & Kiss, 1986; Cohen-Addad, *et al*, 1998) have been applied to a food system (Pal, 2006). Further understanding of how these models can be adapted to fully characterize the complex nature of foods would allow for greater prediction, and thus optimization, of the end textural quality of food foams.

2.2 Cake Texture & Technology

Angel food cakes, made from egg whites, and sponge cakes, made from whole eggs, are both classified as foam type cakes. One of the major quality aspects of all cakes is texture. The textural quality of foam cakes is directly related to the air bubbles which are incorporated into the batter during the mixing stage (Carlin, 1944; Pyler, 1988). Initially, mixing incorporates air bubbles into the eggs, but upon continued mixing the bubbles become increasingly smaller and the foam or batter eventually reaches a maximum bubble volume fraction (Pyler, 1988; Jang *et al*, 2005). Factors affecting the amount of air entrained and the size distribution of the bubbles include mixing time and speed, type of mixing blade, egg temperature, and the surface tension and viscosity of the batter (Sahi & Alava, 2003; Jang *et al*, 2005).

Following mixing, the bubbles incorporated into the foam are not stable and undergo changes with time as discussed below (Sections 2.3.3.1, 2.3.3.2). As a result of these foam aging phenomena, the end quality of the angel food or sponge cake is sensitive to the time between mixing and the stabilization of the foam structure that occurs during baking (Bennion & Bamford, 1973; Pyler, 1988). Foam stabilization prior to the baking

stage is a result of the presence of an emulsifying agent, which in cake production, is either a lipid or a protein. In angel food cakes there are little or no lipids, hence the proteins act as the stabilizer forming strong viscoelastic films around the bubbles (Sahi & Alava, 2003). Sponge cakes, made from whole eggs, contain both the lipid fraction supplied by the yolk as well as the proteins in the egg. Sahi and Alava (2003) explain that the presence of two types of emulsifiers often has a detrimental effect on foam stability and formation due to competition between the two.

2.3 Foams

2.3.1 Foam Formation

Foams are a dispersion of two phases in which gas bubbles are entrapped or dispersed in a liquid or solid continuous phase (Murray & Ettelaie, 2004; Damodaran, 2005). Foams can exist in several different forms (liquid, solid, monodispersed, polydispersed, varying gas fractions) and, although their underlying structures may display similarities, different types of foams exhibit very different mechanical properties depending upon the nature of the foam (Weaire & Hutzler, 1999). The similarities in structure between solid and liquid foams is to be expected as many solid foams originate from liquid foams, as in the case of cakes in which the liquid foam batter is set during baking to create a solid foam. For the purpose of this research, only the science associated with liquid foams, in which the gas (air) is dispersed in a liquid continuous phase, was examined.

Aqueous foams are formed by entraining gas into the continuous phase. Generally this is done by one of two methods – agitation by mechanical mixing or aeration by dissolving the gas phase in the liquid phase. In aeration, the liquid and gas

phases are passed through a porous medium which entrains air bubbles into the continuous phase; by varying the flow rates of gas and continuous phase, bubble volume fraction can be varied (Herzhaft, 1999; Weaire & Hutzler, 1999). When using mechanical mixing to generate foams, considerations are the blade type on the mixer, the speed of mixer rotation, and of course the duration of mixing. For both angel food and sponge cakes, a wire whip at medium speed is recommended to generate the foam structure for a time predetermined to achieve desired bubble volume fraction (Pyler, 1988; Jang *et al*, 2005). In these types of cakes, flour is always gently folded in following foam formation with the emphasis on maintaining the created foam structure.

A major consideration in foam formation is how much air is entrained into the continuous phase; this is referred to in the literature as 'foam quality' (Herzhaft, 1999) or foam wetness (Weaire & Hutzler, 1999), where a dry foam would be a high quality foam containing very little liquid, and a wet foam would be of low quality. In cases where more liquid than bubbles exist, the substance is not considered a foam but is often referred to as a bubbly liquid. Throughout this thesis, foam quality is referred to as 'bubble volume fraction' represented by ϕ, where substances with a bubble volume fraction less than 0.50 ($\phi < 0.50$), would be considered bubbly liquids. Herzhaft (1999) claims that when using a mixer to entrain the air, foam quality or bubble volume fraction cannot be accurately controlled.

2.3.2 Foam Structure

Although the makeup of aqueous foams is generally the same, non-continuous bubbles dispersed through a continuous medium, disparities in the shapes of bubbles do

occur as the bubble volume fraction (ϕ) changes, which leads to variation in the foam structure.

In low bubble volume fraction systems, such as the aforementioned bubbly liquids ($\phi < 0.50$), bubbles are spaced well apart from each other and are spherical in shape (Weaire & Fortes, 1994; Mason, 1999; Butt *et al*, 2006); this shape attempts to minimize the bubble surface area and thus the free energy of the system (Damodaran, 2005). As more air is entrained into the system, bubble spacing begins to become limited. Eventually, the bubbles become compressed and deform from their initial spherical state to polyhedral shapes (Figure 1) (Mason, 1999). The compressed bubbles consist of two main parts – a face (or faces) known as the lamella and liquid-filled Plateau borders at their edges or intersections, as seen in Figure 2 (Weaire & Fortes, 1994).

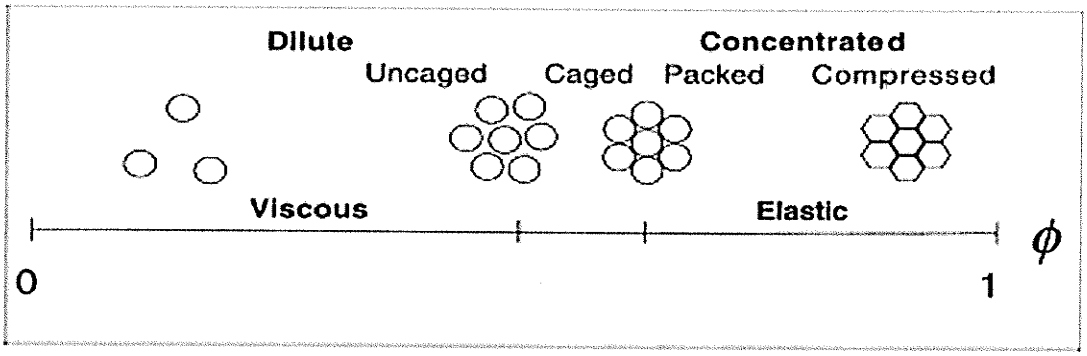

Figure 1: Schematic of changes in bubble structure of a monodispersed foam with changes in bubble volume fraction (ϕ) (Reprinted from Current Opinions in Colloid and Interface Science, v.4, TG Mason, New Fundamental Concepts in Emulsion Rheology, p. 232, Copyright (1999), with permission from Elsevier).

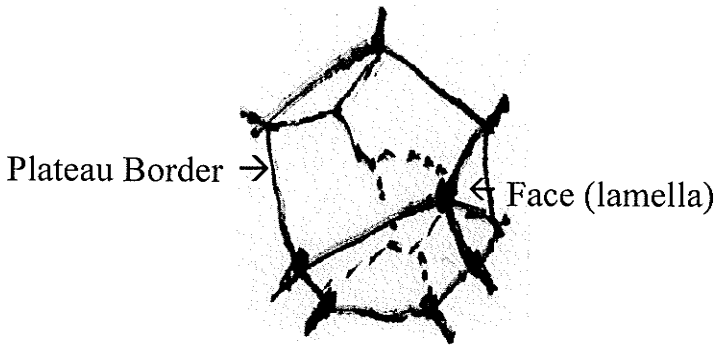

Figure 2: Schematic of a typical bubble in a compressed foam with multiple faces (lamellae) and Plateau borders at the intersections of the lamella (Adapted from Weaire & Fortes, 1994).

The bubble volume fraction at which this packing begins to occur is dependent upon whether the bubbles in the foam are monodispersed or polydispersed. Assuming that bubbles in foams behave similarly to the dispersed liquids in emulsions (liquids dispersed in liquids), monodispersed bubbles become packed at a bubble volume fraction of 0.64 (Mason, 1999). Polydispersed bubbles allow for more air to be entrained before exhibiting packing, a bubble volume fraction of approximately 0.74 is required before packing and sphere deformation begins (Princen & Kiss, 1986). Figure 3 (A) shows a foam at a bubble volume fraction below the compressed packing fraction, while Figure 3 (B) shows a different foam that has exceeded the bubble volume fraction necessary for compression of the bubbles to occur and thus the bubble shapes have deformed from their initial spherical shape.

The compression of the bubbles together as bubble volume fraction increases, results in a resistance to flow of the foam at low applied stresses. This resistance is due to the bubbles jamming together and not being able to effortlessly pass by each other (Gopal & Durian, 2003). As applied stress is increased, and the bubbles are forced to pass by one another, the foams begin to flow as viscous liquids. The stress at which the

foam changes from a non- flowing elastic material to a flowing viscous material is known as the yield stress (Princen & Kiss, 1986; Cohen-Addad *et al*, 1998; Weaire & Hutzler, 1999).

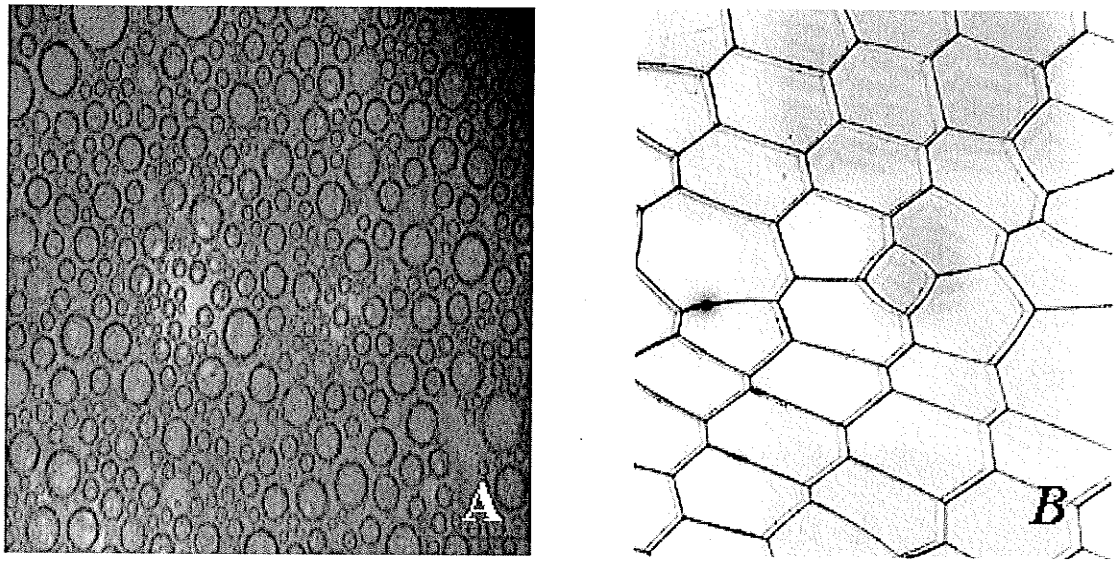

Figure 3: Two different foams: at a bubble volume fraction below the compressed packing fraction (A) (*obtained from experimental work*) *and beyond the bubble volume fraction at which packing occurs* (B) (*Public domain photo*).

Foams, like emulsions and colloids (solids dispersed in liquids), present interesting challenges when it comes to studying their mechanical behavior. Two major problems arise. First, foams consist of two different phases and the mechanical response of the complex foam differs from each of the individual component responses (Weaire *et al*, 1993; Durian, 1995; Weaire & Hutzler, 1999). Second, foams are dynamic and constantly evolving, and this presents the challenge of time dependency on their mechanical response (Cohen-Addad *et al*, 1998; Weaire & Hutzler, 1999; Marze *et al*, 2005). Mechanisms associated with evolution of properties with time are discussed in detail in sections 2.3.3.1 & 2.3.3.2.

2.3.2.1 Air/Water Interfaces & Surface Tension

When foams are created by entraining the gas into the liquid, an interface or surface is created (Butt *et al*, 2006). At this interface a tensile force exists, similar to that of a balloon, which maintains the bubble shape (Butt *et al*, 2006). Energy input is required to change the form or shape of the interface. The work input per unit surface area required to change the shape of the interface is called the surface tension (Butt *et al*, 2006) and is usually given units of J m^{-2} or N m^{-1} .

Likewise with other dispersions, foams are thermodynamically unstable and the dispersed gas and continuous liquid phase strive to separate into individual components (see section 2.3.3). Foams and emulsions are only completely stable (in equilibrium) when the gas and liquid phase are completely separated, thus minimizing the free energy (Damodaran, 2005; Butt *et al*, 2006). In lower bubble volume fraction foams, bubble shapes are spherical, a shape that minimizes surface area and thus free energy. As bubble volume fraction increases (~>0.74 for polydispersed foams), crowding occurs, causing bubbles to deform in shape to a polyhedron and form multiple lamellae with increased surface area (Princen & Kiss, 1986; Mason, 1999).

Numerous methods exist to measure the surface tension of liquids. One of the more widely used methods is the Wilhelmy Plate method (Figure 4). The Wilhelmy Plate method uses a flat plate (usually made of platinum) which is lifted out of the liquid in question. The maximum force is registered when contact between the surface of the liquid and the plate occurs. The platinum plate is roughened such that the angle of contact between the liquid and the plate is virtually 0°. The surface tension (γ) can then be calculated using Equation 1.

$$\gamma = \frac{F}{L \times \cos\theta} \qquad [1]$$

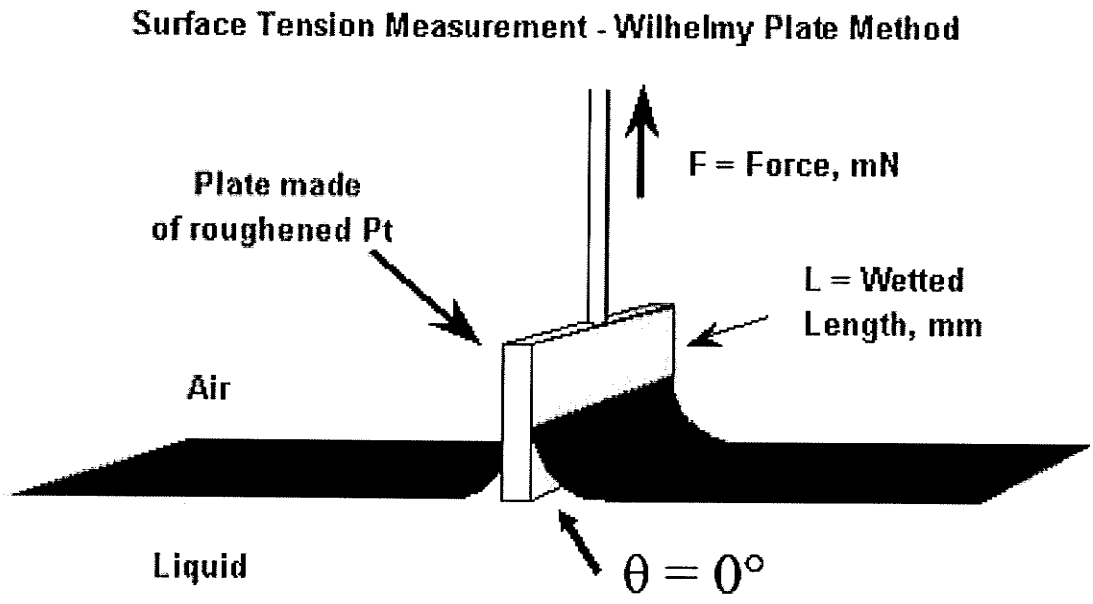

Figure 4: Diagram of the Wilhelmy Plate method for determining surface tension of a liquid (Kruss, Germany – www.kruss.info).

In order to counteract the drive to decrease surface free energy, surface active molecules (emulsifiers) are added as ingredients that will adsorb at the gas liquid interface. In foods these emulsifiers are generally surfactants such as lipids or polymers such as proteins (Wilde, 2000; Sahi & Alava, 2003; Butt *et al*, 2006). Surfactants help lower the surface tension at the gas liquid interface as well as create a repulsive force between adjacent interfaces (Butt *et al*, 2006). Decreased surface tension stabilizes the interface from rupturing, while the repulsive forces keep the bubbles separate, both of which slow the rate of separation of the gas from the liquid phase and thus increase foam stability (Murray & Ettelaie, 2004; Damodaran, 2005; Butt *et al*, 2006).

For each type of surface active molecule the mechanism differs, but the role of each is to stabilize the foam. However, when both surfactants and proteins exist in the same system, a synergistic effect is not always seen. Often a decrease in foam stability

occurs due to competition for adsorption of the surfactants and proteins at the interface (Wilde, 2000; Murray & Ettelaie, 2004).

Polymer type surface active agents such as proteins form viscoelastic films around bubbles by cross-linking with other neighboring protein molecules (Murray & Ettelaie, 2004). Due to the fact that proteins have polar and non-polar regions, when they are adsorbed at the air-water interface of the bubble, the protein unfolds in order to minimize free energy (Phillips, 1981; Damodaran, 2005). That is, the hydrophobic portions of the proteins will reside within the bubble while the hydrophilic regions reside in the continuous phase.

Surfactant type surface active molecules stabilize foams and emulsions by forming a fluid adsorbed layer, rather than a viscoelastic film as is the case for proteins (Wilde, 2000). This fluidity allows the surfactant to migrate to regions of the foam where surfactant levels are less concentrated and therefore where more stabilization is needed. This ability to migrate is known as the Marangoni effect (Wilde, 2000; Damodaran, 2005).

2.3.3 Foam Stability

Aqueous foams by nature are unstable (Wilde, 2000; Murray & Ettelaie, 2004; Damodaran, 2005). In order to decrease total surface free energy, foams are driven to separate into their component parts – liquid and gas (Heller & Kuntamukkula, 1987; Murray & Ettelaie, 2004; Damodaran, 2005). When gas is entrained into the liquid medium during foam formation a gas liquid interface is created which in turn increases the overall free energy of the system. The stability of foams largely depends upon the properties of the interface (specifically surface tension) which separates the bubbles and the liquid continuous phase (Wilde, 2000; Murray & Ettelaie, 2004; Damodaran, 2005).

In order to slow the decay of foams, surfactants are used to minimize the surface tension (Meinders & van Vliet, 2004; Damodaran, 2005). As previously mentioned these emulsifiers are usually of protein or lipid nature in foods (Sahi & Alava, 2003).

Two prominent macroscopic mechanisms of foam decay exist – drainage and disproportionation (Weaire & Hutzler, 1999), each of which is discussed in detail in the following sections (2.3.3.1 & 2.3.3.2) as well as how the changes in the foam make up affect the rates of each of these decay processes.

2.3.3.1 Drainage

Since the continuous phase of aqueous foam is liquid, it is able to flow. The force of gravity causes flow of the liquid continuous phase out of the foam structure resulting in separation of the dispersed gas phase and the continuous liquid phase. Drainage has therefore become one of the well known and researched mechanisms of foam decay (Weaire & Hutzler, 1999; Saint-Jalmes & Langevin, 2002; Murray & Ettelaie, 2004; Damodaran, 2005). It is worthy to note that in more rigid-like foams (solid foams) drainage is not likely to exist or it exists at a significantly lower rate, as in cakes and breads that have been set by baking (Murray & Ettalaie, 2004). Drainage of the liquid continuous phase across the bubble lamella film can lead to film thinning and as a result may cause bubbles coming into contact with each other to coalesce (Damodaran, 2005), thus altering the desired bubble structure and, as a result, the rheological properties (see Sction 2.5). The rate of drainage can be significantly decreased by altering the physical properties of the foam. Increasing the viscosity of the medium or varying the surfactant can both play a role in slowing the rate of drainage (Heller & Kuntamukkula, 1987; Saint-Jalmes & Langevin, 2002; Murray & Ettalaie, 2004; Damodaran, 2005).

Two main experiments have been used to attempt to quantify rates and extents of drainage in foam systems – the forced drainage experiment and the free drainage experiment (Weaire & Hutzler, 1999; Saint-Jalmes & Langevin, 2002). In forced drainage experiments, surfactant solutions are continuously poured from the top of the foam and the passage of liquid through the foam monitored. In free drainage experiments, no additional liquid is added, only the liquid present in the foam is allowed to drain and consequently settle to the bottom of the foam. Regardless of the method used to quantify drainage, the route the liquid travels remains the same. Liquid drains from the bubble lamella to the Plateau borders and eventually, by force of gravity, through the network of Plateau borders to the bottom of the system (Maurdev *et al*, 2006). Plateau borders vary in size depending upon the bubble volume fraction; as bubble volume fraction increases, Plateau borders become increasingly smaller. Therefore, the rate of drainage varies tremendously from system to system depending upon the bubble volume fraction (Weaire & Hutzler, 1999).

Viscosity of the medium can alter the rate of liquid drainage. An increase in viscosity slows the rate of liquid drainage out of the lamella and through the Plateau borders (Heller & Kuntamukkula, 1987; Saint-Jalmes & Langevin, 2002; Murray & Ettelaie, 2004; Damodaran, 2005). The use of surface active agents to decrease surface tension can also have the effect of slowing the rate of drainage. As the surfactants form layers at the gas liquid interface, they decrease the lamella thickness, which in turn slows the rate of drainage through the lamella (Damodaran, 2005). This is especially the case when proteins are used as the surfactant; the proteins unfold and their hydrophilic portions protrude into the Plateau borders thus increasing the resistance to liquid flow within the Plateau boarders (Maurdev *et al*, 2006).

Recent experiments have looked at the use of electrical conductivity to study the rate and extent of drainage (Pugh, 2005). Electrical conductivity through foam is a function of the liquid fraction in the foam; as liquid content is increased, conductivity is increased (Weaire & Hutzler, 1999). Therefore, one would expect the conductivity to increase near the bottom of a draining foam as a function of the rate of drainage. Weaire and Hutzler (1999) provide mathematical expressions relating the conductivity of foam to liquid contents and conclude that the bubble size has little effect on conductivity.

2.3.3.2 Disproportionation

Disproportionation, also known as Ostwald ripening, is the process of gas diffusion from smaller bubbles to larger bubbles (Cohen-Addad *et al*, 1998; Weaire & Hutzler, 1999; Meinders & van Vliet, 2004; Murray & Ettelaie, 2004). Disproportionation results in a coarsening of the foam due to shrinkage of the smaller bubbles and an increase in the larger bubble sizes. As a result, the mean bubble size increases and bubble size distributions become broadened and the mean is shifted towards a larger value. Weaire and Hutzler (1999) showed that the coarsening of bubble sizes due to disproportionation follows Equation 2:

$$R \propto t^{1/2} \qquad [2]$$

where R = bubble radius and t = time.

The driving force behind gas diffusion is the difference in Laplace pressures (ΔP) between small and large bubbles which is calculated by the Laplace equation (Equation 3) (Cohen-Addad et al, 1998; Damodaran, 2005).

$$\Delta P = \frac{2\gamma}{R} \qquad [3]$$

where γ = surface tension and R = bubble radius.

The rate and extent of gas diffusion is correlated with the surfactant that is absorbed at the gas liquid interface which increases the elasticity at the interface. In order to completely prevent gas diffusion, bubbles have to be contained within a completely impervious elastic continuous phase, as is the case in solid foams (Murray & Ettelaie, 2004). However, gas diffusion can be slowed in aqueous foams by increasing the viscosity of the medium and by using surfactants which increase the elasticity at the interface.

As disproportionation occurs, smaller bubbles shrink and their gas diffuses to larger bubbles. In order for these bubbles to shrink, work must be done against both the interfacial elasticity and the viscosity of the continuous medium (Murray & Ettelaie, 2004). In foams, a viscous component exists, associated with their viscoelastic character. The viscous component will continue to allow some shrinkage of the smaller bubbles and thus gas diffusion to the larger bubbles, regardless of the surfactant used (Murray & Ettelaie, 2004). Murray and Ettelaie (2004) explain that even the most well packed monolayer of low molecular weight surfactants allows gas to diffuse due to the dynamic nature of the packing in which fluctuations occur. Larger surfactants, such as proteins, are no better at completely eliminating gas diffusion since they form three dimensional structures with many paths throughout allowing the gas molecules to pass through (Murray & Ettelaie, 2004).

When proteins are used as the surfactant a second mechanism affects the rate of disproportionation along with the increase in interfacial elasticity. When the bubbles shrink and eventually disappear, the proteins at the gas liquid interface are forced into the continuous phase. The rate at which the protein desorbs from the interface and dissolves

into the continuous phase affects the rate at which the bubble can shrink – for most proteins this desorption and dissolving is slow (Damodaran, 2005).

The bubble volume fraction of a foam also plays a role in determining the rate and extent of disproportionation (Weaire & Hutzler, 1999). An increase in bubble volume fraction increases the contact between bubbles (Figure 2) which, in turn, increases the film area (consequently Plateau border areas are decreased), resulting in a faster gas volume transfer according to Fick's Law (Equation 4) (Weaire & Hutzler, 1999).

$$\text{Volume rate of gas transfer} = \kappa \times \text{film area} \times \text{pressure difference} \quad [4]$$

where κ = permeability constant for the diffusing gas ($m^2\ s\ kg^{-1}$).

Although they are two distinct mechanisms of foam aging, drainage and disproportionation are interrelated. If an increase in bubble volume fraction decreases the Plateau border area one would expect that the rate and extent of drainage would decrease since the Plateau borders are the paths by which liquid drains through the foam (Weaire & Hutzler, 1999; Saint-Jalmes & Langevin, 2002). Alternatively, as drainage occurs, a thinning of the films between bubbles occurs due to the liquid passing by and as a result, permeability of the gas is increased and disproportionation is enhanced (Weaire & Hutzler, 1999). Therefore in low bubble volume fraction foams, Plateau borders are larger implying that drainage would initially be dominant. In foams approaching a dry limit ($\phi \rightarrow 1$), Plateau borders are small, limiting the drainage paths. In these high bubble volume fraction foams, film areas are large which results in an increase in the volume of gas transfer according to Fick's law (Equation 4). Therefore, in high bubble volume fraction systems, disproportionation is the dominant aging mechanism (Weaire & Hutzler, 1999).

2.4 Image Analysis for Characterization of Foam Structure

2.4.1 2D Analysis

Imaging of foam systems presents challenges due to the three dimensional nature of the bubble structure. In transmission, foams cannot be easily imaged due to the fact that bubble sizes are often much smaller than the sample thickness causing overlapping effects in the images (Gonatas *et al*, 1995; Sahi & Alava, 2003). As in many other areas of foam research, a two dimensional approach is generally taken to analyze foam images and thus calculate a bubble size distribution. The general approach to creating a two dimensional image is to sandwich the foam sample between two microscope slides (Weaire & Hutzler, 1999; Sahi & Alava, 2003; Jang *et al*, 2005). Depending upon the spacer thickness used between the slides a single layer of bubbles could potentially be captured in order to eliminate bubble overlap when imaging. In polydispersed systems there is often a compromise between deforming the large bubbles by having too small a gap between the slides, and having some of the smaller bubbles overlap. In polydispersed foam cases, Sahi and Alava (2003) explain that the smaller bubbles which were not constrained by the gap thickness were still prone to overlapping; therefore some error may occur due to the inability to identify and measure these bubbles. Regardless of the gap used, both Sahi and Alava (2003) and Jang *et al* (2005) used image analysis software to measure areas of the bubbles, and then calculate an equivalent circle diameter; that is, the bubbles were assumed to be circular. These diameters were used to then calculate a sphere volume which estimates the volume of the three dimensional bubbles in the foam. Sahi and Alava (2003) imposed a correcting factor on the circle diameters which were greater than the gap width of their two microscope plates to account for any flattening of the bubble that had occurred. Weaire & Hutzler (1999)

confirm that this method of imaging foams is an ideal way to quantify the effects of disproportionation over time, by taking a series of time-delayed photographs and monitoring the changes in bubble size with time.

2.4.2 3D Analysis

Only recently have experiments looked at imaging foam samples three dimensionally. Indirect methods such as multiple light scattering techniques based on diffusion of light have been used to predict mean bubble sizes and changes with time (Cipelletti & Ramos, 2002; Mayer *et al*, 2004). However, as Gonatas *et al* (1995) point out, these techniques rely on a model and do not provide a direct picture of the three dimensional foam structure. Weaire and Hutzler (1999) also agree that although light scattering techniques have become useful in past years to study foams, often a high degree of interpretation and statistical analysis is necessary.

More direct methods for three dimensional imaging have been used recently. Magnetic resonance imaging (MRI), has been introduced by Gonatas *et al* (1995) to probe the interior of foams, although not without complications and limitations. Since MRI is only sensitive to the liquid portion of foams, foams of high bubble volume fraction are often difficult to analyze using this method. Furthermore, the resolution of medical MRI machines is often not high enough to accurately display very small bubble sizes (Gonatas *et al*, 1995).

Optical tomography is a three dimensional imaging method that uses a series of two dimensional photos to reconstruct a three dimensional image. The two dimensional photos are obtained by transmitting and scattering a light source through cross sections of the object. Thomas *et al* (1998) successfully used optical tomography to obtain two dimensional slices of a foam structure and then used computer generation to reconstruct a

three dimensional image. Likewise with MRI, difficulties and limitations can arise dependent upon the liquid content of the foam which may affect the ability of the light source to transmit through the foam without refracting (Thomas *et al*, 1998).

2.4.3 Surface-Volume Mean Radius – R32

When dealing with polydispersed foams, as is the case in many food systems, the average radius (R_{av}) is not an accurate representation of the overall bubble sizes in the system. For this reason, Princen and Kiss (1986) introduced a parameter, the surface-volume mean radius, R_{32}, (sometimes referred to as the Sauter mean radius (Marze *et al*, 2005), which, when characterizing the size distribution, takes into account the polydispersity exhibited by many foam and emulsion systems.

For low bubble volume fraction bubbly liquid systems calculation of R_{32} is rather straightforward due to the lack of bubble compression and therefore all bubbles retain spherical shapes. Princen and Kiss (1986) used a Coulter counter to obtain a size distribution histogram of their foams. From this distribution the average volume and surface area of the bubbles can be calculated as follows:

$$V = \frac{4}{3}\pi \frac{\sum_i n_i R_i^3}{\sum_i n_i} \qquad [5]$$

$$S = 4\pi \frac{\sum_i n_i R_i^2}{\sum_i n_i} \qquad [6]$$

where V = average volume, S = average surface area, R_i = is the mean radius in distribution bin i, n_i= is the number of bubbles in distribution bin i. By taking the ratio of the average volume to the surface area the following equation is obtained:

$$\frac{V}{S} = \frac{\frac{4}{3}\pi \frac{\sum_i n_i R_i^3}{\sum_i n_i}}{4\pi \frac{\sum_i n_i R_i^2}{\sum_i n_i}} = \frac{\sum_i n_i R_i^3}{3\sum_i n_i R_i^2} \qquad [7]$$

R_{32} is then the characteristic dimension defining the size distribution of bubbles:

$$R_{32} = \frac{\sum_i n_i R_i^3}{\sum_i n_i R_i^2} = \frac{3V}{S} \qquad [8]$$

In foams, the calculation of R_{32} is not as straightforward due to the fact that the compression of the bubbles at $\phi > 0.74$ (for polydispersed foams) leads to bubbles being polyhedra rather than spheres (Mason, 1999). The change in shape of the bubble is accompanied by an increase in the surface area even though the volume remains the same. Since Equation 8 assumes the bubbles are spherical, a correction factor needs to be applied in order for the measure of bubble size to be valid for these high bubble volume fraction foams. Princen and Kiss (1986) explain that in these compressed systems, a variety of polyhedral shapes exist with the average number of lamella per bubble being somewhere between 12 and 14. Taking into account the variation in polyhedral shapes Princen and Kiss (1986) suggested that the ratio of surface areas approximated to:

$$S_{poly} / S_{sphere} \sim 1.10$$

where S_{poly} is the surface area of the polyhedral bubbles and S_{sphere} is the surface area of a sphere of equivalent volume. By incorporating this correction factor for surface area, we can alter the Princen and Kiss equation to account for compression of the bubbles in high bubble volume fraction foams (Equation 9):

$$R_{32} = \frac{\sum_i n_i R_i^3}{1.10 \sum_i n_i R_i^2} \qquad [9]$$

Similar to previous experimental studies (McGinnis & Little, 2002; Bordel *et al*, 2006) our experimental work used image analysis rather than a Coulter counter to obtain the size histogram of the bubble distributions. However, instead of measuring volumes, our two-dimensional imaging technique measures the perimeter of each bubble and then assumes the bubbles to be circular in order to calculate a radius. Using this radius and the geometric equations of a sphere the surface area and volume of the bubble can be determined and R_{32} can be calculated from the measured perimeters.

2.5 Rheology

The bulk rheological properties of foams are largely dependent upon the inherent bubble structures of the foam. Changes in bubble volume fraction, bubble size distributions, and surfactants used to stabilize the bubbles greatly affect the resulting mechanical response of the bulk material (Mason, 1999). Furthermore, foams are dynamic; therefore the structure changes with time and so do the mechanical properties (Cohen-Addad *et al*, 1998; Weaire & Hutzler, 1999; Marze *et al*, 2005).

2.5.1 Static Shear Modulus

The static shear modulus (G_0) of a foam is a value which represents the elastic stored energy of a material in its free standing or static state; that is no stress applied to it. Since methods of determining the shear modulus require applying a mechanical force, as in a stress, and measuring the responding strain, the static elastic modulus value is often a predicted value rather than an experimentally determined value. The static value has

been estimated in two ways. Strain ramp (or stress ramp) plots for G' show a plateau range (or stress/strain independent G' values) at low strain or stress amplitudes. This plateau value for G' has been used as the static shear modulus G_0 (Marze *et al*, 2005). Frequency sweeps show a similar plateau (or frequency independent regime) at low frequencies; Mason *et al* (1997) use this plateau as the value for the static shear modulus G_0. It is important to note that in both of the aforementioned cases, bubble volume fractions (or dispersed phase fractions in the case of emulsions) were very high; that is the experimental foam was approaching its dry limit.

Regardless of the method used to predict or calculate a static shear modulus, it is well agreed that the magnitude of the static shear modulus of foams is a function of the overpressure of the trapped gas (Princen & Kiss, 1986; Coughlin *et al*, 1996; Mason *et al*, 1997; Weaire & Hutzler, 2003; Marze *et al*, 2005). Overpressure is calculated from the surface tension of the continuous liquid phase, divided by the total interfacial area and volume of the dispersed gas (Princen & Kiss, 1986; Coughlin *et al*, 1996). Marze *et al* (2005) simply state this as surface tension divided by average bubble radius. However, more precisely, the equation should take into account the mean surface-volume radius, R_{32}. Adapting from these factors, Coughlin *et al* (1996) present an equation to estimate the overpressure (Equation 10):

$$\Delta P = \frac{2\gamma}{R_{32}}\left(\frac{0.00283}{1-0.9639\phi}+0.989\right) \qquad [10]$$

where γ is the surface tension of the continuous liquid phase, R_{32} is is the surface-volume mean radius of the dispersed phase (as discussed in Section 2.4.3) and ϕ is the bubble volume fraction. Using the calculated ΔP and static modulus values determined by a novel punch indentation technique, Coughlin *et al* (1996) found the ratio of the static

modulus to the overpressure to be around 0.18. Again as in most experiments on foams, these tests were done on foams of very high bubble volume fractions.

Using surface tension, bubble volume fraction, $R_{32,}$ and experimental trials, Princen and Kiss (1986) developed an equation to predict the static modulus of foams of high bubble volume fraction (ϕ >0.74). Equation 11 shows that the only variables that affect the static shear modulus, and thus the elastic response, of a foam are the surface tension of the continuous phase and the size and volume fraction of the dispersed phase.

$$G_0 = 1.769\frac{\gamma}{R_{32}}\phi^{1/3}(\phi - 0.712) \qquad [11]$$

2.5.2 Small Strain Rheology

Foams are viscoelastic materials, that is, they contain both a viscous component which allows them to flow, and an elastic component which resists flow and stores elastic energy. In small strain oscillatory shear rheology, the viscous and elastic components are represented by the loss modulus (G'') and storage modulus (G') respectively. These moduli are obtained by shearing the sample at different frequencies at a controlled stress or strain and measuring the response of the sample as the oscillation changes directions.

When examining the frequency dependence of any viscoelastic system, it is first necessary to ensure that oscillatory tests are carried out at a stress or strain within the linear viscoelastic regime of that particular system. Outside this range, damage may be caused to the structure of the foam which will result in moduli values that are not indicative of the response of the undamaged bubble structure (Marze *et al*, 2005).

Many researchers have looked at the shear storage modulus (G') and loss moduli (G'') for freshly formed foams of high bubble volume fractions (Princen & Kiss, 1986; Cohen-Addad *et al*, 1998; Gopal & Durian, 2003). Previous experimental works have

shown that for these un-aged high bubble volume fraction (ϕ = 0.93) foams, G' is greater than G'' at all frequencies examined, with G' ranging between 400-450 Pa and G'' being more than an order of magnitude less - around 40 Pa at a frequency of 1 Hz (Khan *et al*, 1988; Cohen-Addad *et al*, 1998). As these high bubble volume fraction foams age, both G' and G'' decrease, with G' decreasing to around 300 Pa after a one hour period and G'' decreasing to around 30 Pa (Cohen-Addad *et al*, 1998). Although the viscoelastic frequency response of lower bubble volume fraction foams and bubbly liquids is not widely reported in the literature, it is assumed that these bubbly liquid systems follow similar trends to those observed in dilute emulsions and colloids as the bubble volume fraction is varied. Mason and Weitz (1995) show that in colloidal suspensions at low volume fraction of the dispersed phase (ϕ = 0.50), G'' is greater than G', and the suspension exhibits primarily a viscous response. As the volume fraction of the dispersed phase increases (ϕ > 0.56), G' becomes greater than G'' and the suspension is predominantly elastic (Mason & Weitz, 1995), a result which is confirmed by Cohen-Addad *et al*'s (1998) high bubble volume fraction foams.

The moduli response of foams is also dependent upon the frequency at which the shearing takes place. Cohen-Addad *et al* (1998) showed that commercial shaving foams exhibited a slight increase in G' as a function of frequency; a result which has also been shown in colloidal suspensions (Mason & Weitz, 1995). The frequency dependence of the imaginary part of the shear modulus G'' has been shown to be more complicated. At low frequencies, G' has remained somewhat constant, but as frequency is increased, a sharp increase in G'' is apparent (Cohen-Addad *et al*, 1998). The point at which this sharp increase occurs suggests that there is a time-dependent transition from more resistant to less resistant behavior; this transition is known as a relaxation of the material.

The time at which relaxation occurs varies depending on the material and in certain cases may be much greater than the experimental timescale (e.g., relaxation in concrete) (Reiner, 1964). In Cohen-Addad's (1998) high bubble volume fraction foams the frequency at which this sharp increase occurred varied depending upon foam age. Frequencies are inversely related to the time of testing and thus a distribution of relaxation times, dependent upon foam age (Cohen-Addad *et al*, 1998), is apparent at constant bubble volume fractions.

2.5.3 Large Strain Rheology

Bubble volume fraction plays a key role in the mechanical response of foams. As is the case with dilute emulsions, bubbly liquids with low bubble volume fraction essentially behave as viscous fluids (Mason, 1999). As the bubble volume fraction increases the liquid-like material becomes a foam (Weaire & Hutzler, 1999), and begins to behave as a viscoelastic solid at low stresses (Sollich *et al*, 1997; Cohen-Addad *et al*, 1998; Mason, 1999; Weaire & Hutzler, 1999). The key point is that the resistance to flow happens at low stresses; beyond a certain stress, known as the yield stress, the foam will begin to flow as a viscous liquid. The nature of the elastic response, or resistance to flow, is that, at high bubble volume fractions, the bubbles become jammed at low stresses rather then being easily able to flow around one another (Gopal & Durian, 2003). Beyond the yield stress the bubbles can deform and flow around each other resulting in the viscous flow of the foam (Weaire & Hutzler, 1999; Gopal & Durian, 2003). The viscosity of the system beyond the yield stress is shear rate dependent (Princen & Kiss, 1986). A mathematical model for the prediction of the yield stress of foams was proposed in a classic foam rheology paper by Princen and Kiss (1986). The model takes into account three main properties of foams that dictate the majority of their mechanical

response: surface tension, bubble volume fraction, and R_{32}, parameters that have all been discussed throughout this literature review. Princen and Kiss (1986) show that for high bubble volume fraction systems ($\phi > 0.74$) the yield stress (σ_0) can be determined by Equation 12:

$$\sigma_y = 1.28\frac{\gamma}{R_{32}}\phi^{1/3}F_{\max}(\phi) \qquad [12]$$

where σ_y = yield stress, γ = surface tension, R_{32} = surface-volume mean radius, ϕ = bubble volume fraction and $F_{max}(\phi)$ = the dimensionless mean contribution of a single bubble to the yield stress. F_{max} (ϕ) is greatly affected by ϕ and was determined experimentally by Princen (1985).

As a result of this model and other experimental studies, yield stress has been found to increase with bubble volume fraction assuming R_{32} and surface tension remain constant (Rouyer *et al*, 2005). This is an expected result when considering Mason's (1999) work on monodispersed systems in which droplets in emulsions or bubbles in foams begin to become jammed at a bubble volume fraction of 0.64 and increasingly more jamming occurs as bubble volume fraction increases. Princen and Kiss (1986) expanded on this to show that polydispersed systems begin to exhibit this behavior at bubble volume fractions beyond 0.74. Below these critical bubble volume fractions (0.64 and 0.74 for monodispersed and polydispersed foams, respectively) bubble jamming is not seen and thus no yield stress is exhibited.

Although bubble volume fraction plays a large role, bubble size also affects the yield stress of foams. The Princen and Kiss model incorporates the measure of bubble size (R_{32}) used for polydispersed foams. As the R_{32} increases, the average bubble size

increases and the yield stress decreases as bubbles are now able to pass by each other more readily (Gardiner *et al*, 1998; Rouyer *et al*, 2005).

2.5.4 Time Dependence

The study of freshly formed foams is simple compared to the difficult task of studying foams over time due to the dynamic nature of the foam. Foams age, and there is a resulting change in their rheological properties (Cohen-Addad *et al*, 1998; Weaire & Hutzler, 1999). The rate and extent of changes in foam rheology depend on mechanisms such as gravity-driven drainage (Section 2.3.3.1) and pressure-difference-driven disproportionation (Section 2.3.3.2) (Weaire *et al*, 1993; Cohen-Addad *et al*, 1998; Hammershøj *et al*, 1999; Herzhaft, 1999; Sahi & Alava, 2003; Cox *et al*, 2004).

In foams where disproportionation is dominant, an observed increase in the mean bubble size takes place; thus a decrease in the specific surface arises and as a result a decrease in the elastic response and G' occurs (Cohen-Addad *et al*, 1998). In other words, foams which coarsen via disproportionation with time exhibit a softening effect with time. When examining aging data of the large strain response of foams, a decrease in yield stress and in apparent viscosity can be seen with time (Coughlin *et al*, 1996); an expected result when considering the Princen and Kiss (1986) equation for predicting yield stress (Equation 12). The equation suggests that as disproportionation occurs, R_{32} increases and as a result yield stress is lowered.

The aging effects on G'' are similar to those of G' in that an overall decrease occurs with age. However, as Cohen-Addad *et al* (1998) point out, the frequency at which the sharp increase in G'' (as discussed in Section 2.5.2) occurs is shifted towards lower frequencies with aging time.

Elaborating on work done by Princen and Kiss (1986), Cohen-Addad et al (1998) found that the complex shear modulus, G^*, follows a scaling law in regards to aging time, whereby all G^* curves can be superimposed onto a reference curve at an arbitrarily chosen reference time, by dividing the moduli by a given parameter, $b(t,t_0)$, and multiplying the frequencies by another parameter, $a(t,t_0)$, such that:

$$G^*(\omega, t) = b(t,t_0)G^*(\omega a(t,t_0),t_0) \qquad [13]$$

The viscoelastic scaling factor, $b(t,t_0)$, was derived from considerations of how the static elastic modulus of a foam of a constant volume fraction of bubbles (Princen & Kiss, 1986) would evolve due to changes in mean gas cell size arising from disproportionation. In this way, the complex shear modulus as a function of frequency at any given time of aging, $G^*(\omega, t)$, is related to its counterpart at an arbitrarily chosen aging time of t_0, $G^*(\omega, t_o)$ by:

$$G^*(\omega, t) = b(t,t_o)\ G^*\ (\omega, t_o) \qquad [14]$$

Cohen-Addad *et al* (1998) also point out that the scaling of data solely by one parameter, $b(t,t_o)$, as suggested by the Princen and Kiss model (1986) did not lead to a master curve for their data. The point at which the plot of G'' versus frequency emerges from a plateau region to a positive slope is shifted towards a lower frequency. This distribution in rheological relaxation times requires a second scaling factor, $a(t,t_0)$ in order to fit rheological data to a master curve. In this case frequencies are multiplied by the $a(t,t_0)$ scaling factor. The mathematical expression for scaling using both the $b(t,t_o)$ and $a(t,t_0)$ scaling factors is shown in Equation 13.

In the case of Cohen-Addad's foam, (a foam which approaches the dry limit; that is bubble fractions >90%), logarithmic plots of the scaling factor $b(t,t_o)$ versus aging time produce a continuous line with a slope of approximately −0.5. Recall from Equation 2

that the bubble radius changes due to disproportionation and is proportional to $t^{0.5}$. Princen and Kiss (1986) showed that the evolution of the shear modulus is inversely proportional to the bubble radius (Equation 11).

$$G \propto R^{-1} \qquad [15]$$

Associating Equation 2 and Equation 15 leads to Equation 16

$$G \propto t^{-1/2} \qquad [16]$$

This states that the modulus is inversely proportional to the square root of time. According to the slopes of the scaling factor graphs, Cohen and Addad's (1998) high bubble volume fraction foams show good agreement with a theoretical prediction that the static modulus, G_0, (see section 2.5.1) at a given time evolves by a square root dependence in relation to the static modulus at the arbitrarily chosen time (Princen & Kiss, 1986; Cohen-Addad *et al*, 1998; Weaire & Hutzler, 1999).

Chapter 3: Materials & Methods

3.1 Recipes

Recipes for two different egg system cakes, angel food with egg whites (Table 1) and sponge cake with whole eggs (Table 2) were selected based on simplicity and minimum ingredients in order to limit variables in the experiments. The ingredients were

Table 1: Typical Angel Food Cake Recipe adapted from Pyler (1988).

Ingredient	Composition
Flour	30 g
Sugar	83 g
Egg White	83 g
Salt	1.15 g
Cream of tartar	1.25 g

Table 2: Typical Sponge Cake Recipe adapted from Bennion & Bamford (1973).

Ingredient	Composition
Eggs (Whole)	150 g
Sugar	120 g
Flour	120 g

proportionally scaled up from the original recipes to meet the volume needs of the experiments (i.e., enough sample for the analyses of density and rheological properties). Two foam systems were produced for each egg system (Table 1 and 2). In the first system of each, referred to as our foam, the flour was omitted from each recipe; in the second, the full recipe was used in making foams to which flour was systematically added, referred to as batters (see Section 3.3). The distinction between the systems with and without flour (batters and foams respectively) allowed for analysis of the developed bubble structure itself in the foams, and analysis of how the addition of flour affected the structure.

3.2 Foam & Batter Materials

3.2.1 Eggs

A series of preliminary tests were conducted to determine the best of three various egg products (shelled, liquid or powdered) in producing consistent foams and batters as well as ease of preparation. As a result, liquid whole egg and liquid egg albumen (Innovatech, Winnipeg, MB) were chosen for the sponge cake and angel food cake recipes, respectively. Liquid egg products were frozen in portioned containers and kept frozen until required. Products were thawed overnight at refrigeration (4°C) temperatures the day before an experiment. Thawed eggs were kept refrigerated until just prior to weighing out in a beaker.

3.2.2 Dry Ingredients

An all purpose flour with as few additives as possible (Sunspun, Toronto, ON) was selected for this study. A finely powdered icing sugar (Rogers Sugar Ltd., Vancouver, B.C.) was used as suggested by Pyler (1988) to promote more consistent mixing. Only the angel food recipe called for the use of salt, which was a standard table salt (Sifto Canada, Inc., Mississauga, ON). The angel food recipe also called for the use of a small amount of cream of tartar (Nabisco, Etobicoke, ON).

3.3 Mixing Procedures

Foam and batter preparation followed a standard mixing procedure as outlined below. The liquid egg (white or whole depending on the experiment) was added to the mixing bowl followed by all the dry ingredients with the exception of the flour. Mixing took place on a variable speed kitchen food mixer (KitchenAid, St. Joseph, MI). Mixing started out on speed *one* for 15 seconds followed immediately by a 15 second scrape

down period using a plastic spatula to ensure all the dry ingredients were mixed in with the egg and were not sticking to the sides of the bowl. After the scrape down, the mixer was turned on for an additional 15 seconds at speed *one,* followed immediately by running the mixer at speed *six* for the remainder of the mixing time, as required by the particular experiment (Table 3). Total mixing times were selected based on preliminary experiments in order to cover a wide range of densities in the foams and batters.

Table 3: High speed and total mix times for mix levels 1 – 8.

Mix Level	Time at Speed Six (*s*)	Total Mixing Time (*s*)
1	0	45
2	30	75
3	60	105
4	120	165
5	180	225
6	345	390
7	705	750
8	1065	1110

For those experiments where flour was added (i.e., the creation of a batter not a foam), the following procedure was used. Following the creation of the egg foam at a given mixing time, the mixer was stopped and then the flour was added in promptly and carefully to the middle of the mixing bowl. The mixer was then turned on to speed *one* for 15 seconds followed by a 15 second scrape down period using a plastic spatula. The batter was then mixed for an additional 30 seconds at speed *one*. No high speed mixing was performed following flour addition, on the grounds that flour should be folded in so as not to disrupt the structure already developed in the foam (Pyler, 1988). Mix times at low speed for the flour addition were based on preliminary trials in which the flour was visually assessed for homogeneous distribution within the foam.

Immediately following mixing, a portion of the foam or batter was carefully poured (or scooped, depending on foam or batter consistency) into a beaker designated

for density measurements (Section 3.4). Secondly, a portion (25-30 mL) was carefully poured (or scooped) into the rheometer sample cup for either small or large strain rheometric analysis (Sections 3.5.3 or 3.5.4).

3.4 Density Measurements

Following mixing, the foam/batter was poured into one of three pre-calibrated spout-less 200 mL beakers whose exact volume (0.195% error) had been predetermined. Excess foam/batter was then skimmed off using a glass stirring rod such that the foam or batter's top surface was even with the top of the beaker. The filled beaker was then set aside until the rheometric experiments had been started. We are able to do this because the weight of the foam/batter in the beaker does not change over time although its volume might. Once the rheometer was started the beaker was cleaned off and weighed (2 decimal places i.e. to 10 mg accuracy) in order to determine the density of the foam or batter.

3.5 Rheological Analyses

Both small and large strain experiments were conducted on an AR 2000 (TA Instruments, New Castle, DE) controlled stress rheometer at a controlled temperature of 25°C ± 0.2°C. Both large and small strain tests were conducted using a 14.0 mm concentric cylinder configuration with a 15.0 mm sample cup, thus creating a 1.0 mm annulus (TA Instruments, New Castle, DE).

3.5.1 Sample Loading

Due to differences in the consistencies of the foams and batters, it was necessary to use different methods to fill the sample cup of the rheometer. In all cases the sample cup

was removed from the rheometer for ease of filling. For higher density, more fluid foams and batters, a glass funnel was used to pour approximately 25 mL of the sample into the sample cup. Lower density foams and batters were less likely to flow into the sample cup, and so it was necessary to scoop portions of the sample and place it at the bottom of the sample cup using a plastic spatula. In these cases a secondary spatula was used to scrape the foam/batter off the primary spatula into the bottom of the sample cup being careful not to create large air voids within the sample cup. Once the sample was in the sample cup, the sample cup was placed back in the rheometer, the head of the rheometer (with the concentric cylinder geometry attached) was lowered into the sample and the experiment was started.

3.5.2 Preliminary Experiments

To ensure that we were working within the linear viscoelastic regime of the materials a series of preliminary stress sweeps were conducted at three different frequencies (0.6284, 6.284 and 62.84 rad s^{-1}) (Figures 8-10, Section 4.2). The samples were chosen to cover a wide range of densities and to cover all of the systems (i.e., angel food foam and batter, and sponge foam and its batter). The results for all were then overlaid onto one graph and the linear viscoelastic region was selected. As a result, a controlled stress of 0.02 Pa was used for all small strain experiments.

3.5.3 Small Strain Rheology

Small strain rheological tests were conducted on the AR 2000 rheometer using an oscillatory frequency sweep over a frequency range of 0.1267 rad s^{-1} to 62.83 rad s^{-1} at a controlled stress of 0.02 Pa. Each frequency sweep took approximately 372 s. The aging

characteristics of the foams and batters were determined from performing ten consecutive identical frequency sweeps on the same sample for a total aging time of 3720 s.

3.5.4 Large Strain Rheology

Large strain rheological tests were conducted using a continuous ramp procedure consisting of 30 consecutive shear rate ramps on the same sample with a one minute rest period between each. Shear rates were ramped from 1.452 s^{-1} to 145.2 s^{-1} in each step. The consecutive steps were again performed to determine the effects of aging on the large strain rheological properties. In contrast to the small strain measurements, disruption of the foam or batter structure during measurement is expected. Therefore, the one minute rest period was chosen to allow the foam/batter to equilibrate between consecutive shearing steps.

3.6 Image Analysis

In order to further investigate aging mechanisms in the foams, image analysis was used to monitor changes in bubble size distributions with aging time. Using a Nikon Coolpix 4500 digital camera (camera settings outlined in Table 4) and a Zeiss Universal Research microscope, 22 images were taken on selected foam systems over a one hour period.

Table 4: Nikon Coolpix 4500 camera options for image analysis of foam samples.

Nikon Coolpix 4500 Option	Selected Setting
Resolution	1600 × 1200 pix.
Aperture	Fixed F4.5
Shutter Speed	Variable (1/8 – 1/125 s)
White Balance	Cloudy
Focus	Continuous

A stage graticule was used to focus and zoom in the camera prior to the start of each experimental run and sample loading, such that the field of view was 0.7 mm x 0.52 mm, and as a result, 2300 pixels were equal to 1 mm.

Foam samples were mixed following the standard mixing procedure as outlined in Section 3.3. A few drops of the sample were then transferred using a plastic spatula onto a microscope slide. Two 1 mm spacers made from microscope slide cover slips were placed on each side of the sample and another microscope slide was placed on top creating a 1 mm sample thickness which mimics the annulus used in the rheometric analyses. The sample was then carefully loaded onto the microscope stage ensuring that the two microscope slides holding the sample did not move and create any shearing effects.

Camera shutter speed was set to variable and automatically adjusted by the camera (1/8 – 1/125 s) to allow for different amounts of light depending upon the system and the bubble size; this was necessary to obtain clear pictures. Intervals of approximately three minutes were used in order to capture the bubble systems at times approximately equal to, and at the half way point of each aging time associated with the small strain rheological analysis, i.e., since each frequency sweep took approximately six minutes, pictures were taken every three minutes. Camera focus was set to continuous to minimize the time before each picture was taken, so the actual shot took place as close to the set interval as possible.

Using the pixel to millimeter calibration, Image J (v. 1.35q), shareware imaging analysis software program was used to adjust the image and automatically measure bubble size in an unbiased manner. The following processes were used to obtain bubble sizes. The background (the smooth continuous portion of the image that is not an object

of interest in the image) was subtracted using Image J's automated subtract background command. Secondly, the color images were converted to 8-bit grey-scale images, and then the built-in enhanced contrast option (saturated pixels set to 0.5%) was applied. Image J's adjust image threshold option was used to convert to a binary image, the image threshold automatically determined by the software; the default values for thresholding as selected by Image J for each individual picture were applied. The images were then inverted such that the interiors of the bubbles were filled. The analyze particle option allowed for automated measurement of the perimeter of the highlighted particles. In order to eliminate measurement of any noise particles only those bubbles which had perimeters greater than 0.01 mm and whose circularity values were greater than 0.15 were measured. Perimeter values were then converted to radius values based on the assumption that the particles were spherical in shape.

In order to confirm the validity of the image analysis technique used, radius values (from a whole foam at a mix time of 345 s) for images with no aging time (lots of small bubbles) and images at one hour aging time (fewer larger bubbles), as calculated by Image J and as measured manually were compared (Figure 5). Figure 5 shows good agreement between the two methods, supporting the accuracy of the automated analysis procedures. Error bars on Figure 5 represent 3 replicates of pictures taken on different samples of the whole egg foam at the same mix time.

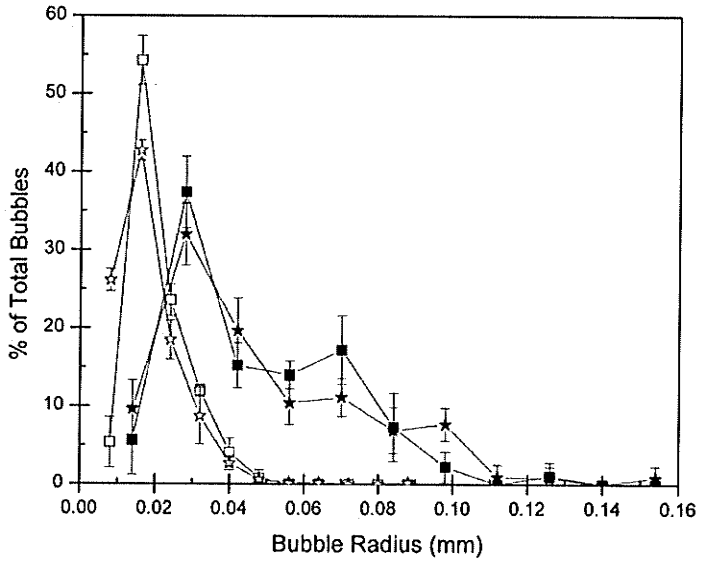

Figure 5: Comparison of bubble radius size distributions from a whole egg foam mixed for 345 s as obtained automatically by Image J software (□,■)*, and by manual measurement using callipers* (☆,★) *at aging times of less than one minute* (open symbols) *and one hour* (closed symbols). *Error bars represent one standard deviation from the mean achieved from three replicates.*

3.7 Experimental Design

A total 192 rheological experiments were conducted, encompassing the two cake recipes (angel food or sponge), whether or not flour was added (foam or batter), eight mix times, two rheological analyses (small and large strain), and triplicates of each experiment. In order to completely randomize the experiments, each experiment was assigned a number (1-192), and a random number list for these 192 numbers was generated to determine the order in which the experiments were conducted. Both small and large strain experiments were randomized together.

Systems for image analysis were chosen on the basis of the small strain scaling factor plots (Figures 25 & 26, Section 4.5), in order to cover a range in bubble evolution behavior. Only foams (whole egg and egg white) were analyzed due to the opacity of the

batters and the difficulty in obtaining clear bubble images. All chosen foam systems were analyzed in duplicate with experimental order randomized by assigning a number and generating a random number table.

Chapter 4: Small Strain Rheology Results & Discussion

4.1 Density & Bubble Volume Fraction

Mechanical mixing of egg systems leads to the incorporation of air bubbles into the system resulting in a foam being created with a lower density than the initial ingredients. Air is first incorporated into the eggs but upon longer mixing the air bubbles are subdivided and become increasingly smaller until a maximum bubble volume fraction (lowest density) is achieved (Pyler, 1988). The eight different mix times produced foams and batters with a density range of 1225 to 235 kg m^{-3} (Figure 6).

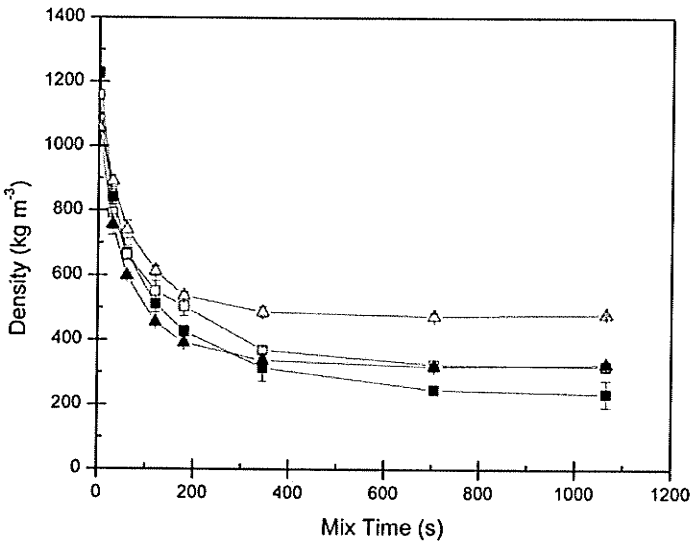

Figure 6: Changes in foam/batter density as a function of mix time for whole egg foams (▲), whole egg batters (△), egg white foams (■), and egg white batters (□).

In most cases error bars resulting from six replicates on Figure 6 are concealed by the data points. In all four systems a plateau was reached as mix time approached the maximum value (1065 s), indicating that the lowest density possible had been achieved at this mix time. Egg white foams reached the lowest density of all four systems (235 kg

m^{-3}), while the whole egg batter had the highest density (480 kg m^{-3}) at the maximum mix time. Variation in the densities at a given mixing time between the egg white and whole egg systems arises from two things. First, there is the effect of lipids, which are present in the whole egg systems. Lipids can have a detrimental effect on foam stability and formation by competing with the egg white proteins for adsorption at the air-water interface, thus resulting in less air being entrained in the whole egg systems (Sahi & Alava, 2003). Secondly, there is the effect of the recipe differences between the two cake systems, as outlined in Section 3.1, sponge cake recipes call for more sugar than the angel food recipes, thus increasing the overall density of the system at the initial mix time (0 s).

Within the whole egg and egg white systems there was a distinct upward shift in the density following flour addition at a given mix time (i.e., from foams to batters). However in the whole egg systems the shift was approximately two times the shift seen in the egg white systems. This difference is assumed to be due to the recipe differences between the sponge cake and angel food cake systems, in which the sponge cake calls for more flour to be added (Section 3.1).

Assuming that there is little or no air entrained into the systems at the initial mix time (0 s at high speed), that is, the materials are merely blended together, we can calculate the volume fraction of bubbles at different mix times for each system (Figure 7) by using Equation 17. The same trends in volume fraction occur as in density (Figure 6); however, the bubble fraction becomes one of the main characteristics of foams needed for applying many of the models developed for industrial foams - hence the conversion from density.

$$\phi = 1 - \frac{\rho(t)}{\rho_0} \qquad [17]$$

where: ϕ = bubble fraction, $\rho(t)$ = density at mix time t, ρ_0 = density at mix time 0.

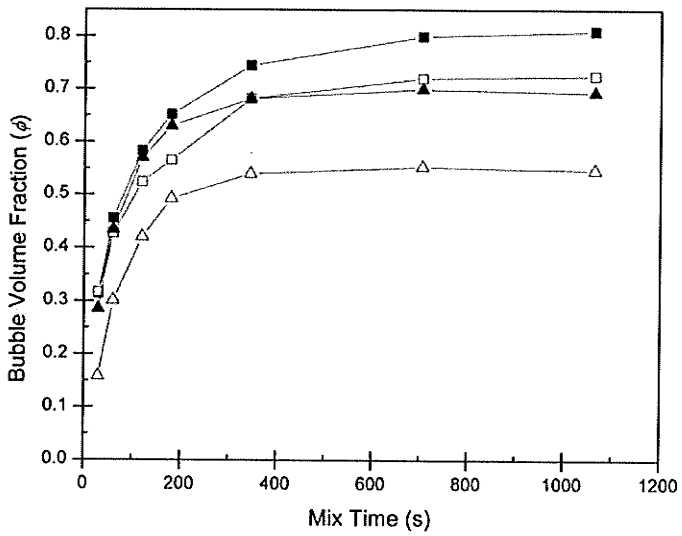

Figure 7: Changes in bubble volume fraction (ϕ) as a function of mix time for whole egg foams (▲), whole egg batters (△), egg white foams (■), and egg white batters (□).

4.2 Linear Viscoelastic Regions

In order to ensure stresses applied to the four different systems did not destroy the structure developed during mixing, it was important to make certain that the applied stress is within the linear viscoelastic region for each system. This is the region in which the shear moduli are independent of the applied stress. At greater stresses we see a breakdown in structure and thus a decrease in G'. Three selected trials were strategically chosen to cover both the range in densities and the varying systems that were used in the overall experiment. These foams and batters were subjected to stress sweeps (0.002 – 5 Pa) at three different frequencies (0.6284 rad s^{-1}, 6.284 rad s^{-1}, 62.84 rad s^{-1}) which

covered the range of frequencies used during small strain analyses. Figures 8, 9 & 10 show the chosen controlled stress (0.02 Pa) for subsequent frequency sweeps to be well within the linear viscoelastic region of all systems. In certain cases, at low frequencies, a linear region was not clearly evident (Figure 9); in those cases it was ensured that the chosen stress of 0.02 Pa was sufficiently small that the structure had not broken down. For Figure 9, structure changes at the slow rate of testing are likely responsible for the rise in G' with increasing stress.

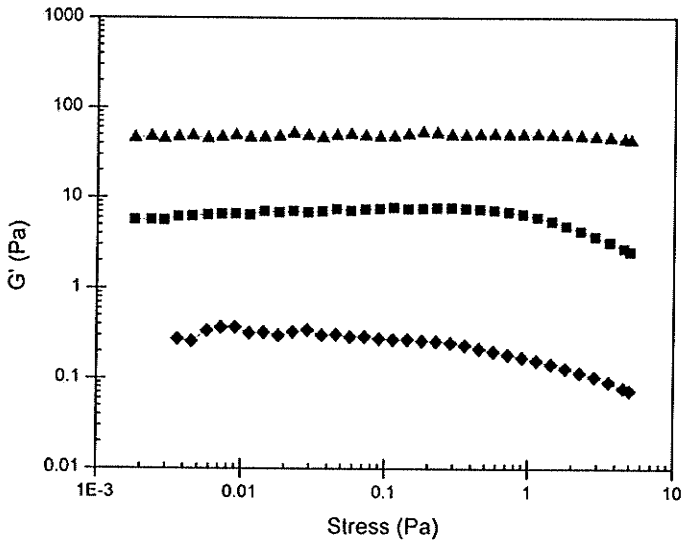

Figure 8: Changes in the shear modulus (G') as a function of increasing stress on a whole egg foam that had been mixed for 30 s at three different frequencies, 0.6284 rad s^{-1} (◆), 6.284 rad s^{-1} (■), and 62.84 rad s^{-1} (▲).

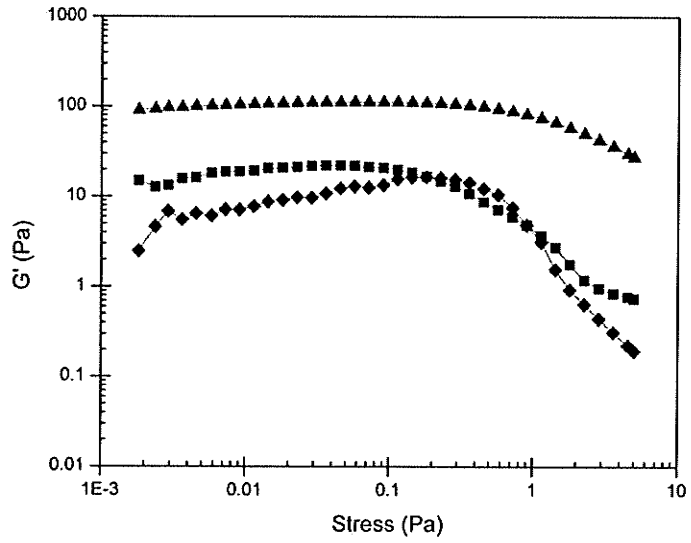

Figure 9: Changes in the shear modulus (G') as a function of increasing stress on an egg white foam that had been mixed for 30 s at three different frequencies, 0.6284 rad s^{-1} (◆), 6.284 rad s^{-1} (■), and 62.84 rad s^{-1} (▲).

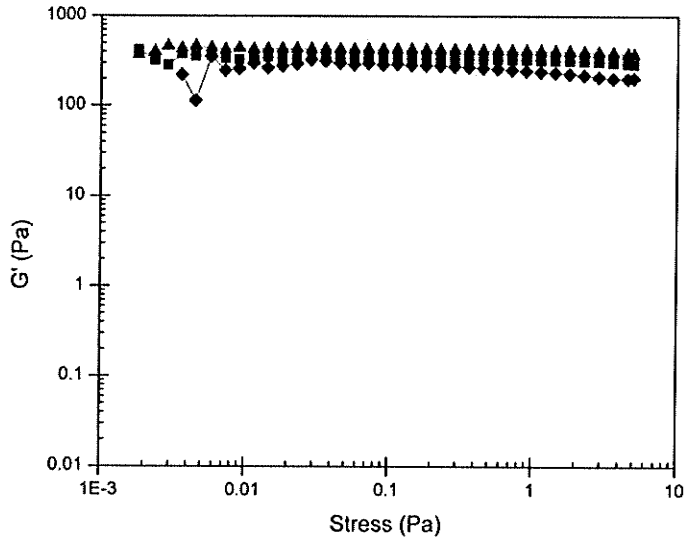

Figure 10: Changes in the shear modulus (G') as a function of increasing stress on an egg white batter that had been mixed for 1065 s at three different frequencies, 0.6284 rad s^{-1} (◆), 6.284 rad s^{-1} (■), and 62.84 rad s^{-1} (▲).

4.3 Frequency Sweeps

In order to look at the changes in G' and G'' with mix time and aging time, selected plots of the frequency sweeps which cover all four systems and also cover a range in densities are shown in Figures 11 through 19. In each case aging times of 675 s, 1788 s, and 3643 s were selected to cover the approximately one hour period in which the foam/batter was allowed to evolve. In cases where G' and G'' were fairly close, separate plots of each modulus were used in order to limit congestion on the graphs. Conversely, in cases where there was a significant separation of G' and G'' one plot was used to show the difference. Error bars resulting from the average of the three replicates are shown on every third data point for a given aging time, again to limit congestion on the plots. When looking at the comparison of egg whites and whole eggs, there is a large difference in the shear moduli between the two systems, whether foams are being looked at (Figures 15 & 17) or batters (Figures 18 & 19). In all cases the storage and loss moduli of the egg white systems were greater than those of the whole egg systems for a given mix time. This difference in the moduli between systems is amplified as more air is entrained into the systems, indicating that the egg whites are capable of producing much stiffer foams, an expected result when considering the fact that egg white systems are able to entrain significantly more air ($\phi = 0.81$ at 1065 s mix time) as compared to the whole egg systems ($\phi = 0.69$ at 1065 s mix time). For both whole egg and egg white systems, G' and G'' show an increase as a function of frequency at a given aging time. However the trends in G'' with time at the high bubble volume fraction egg white foams (Figure 17) are different than those of the whole egg systems. Based on visual assessment, it seems that as a certain bubble volume fraction ($\phi > \sim 0.60$) is reached, G'' shows a plateau at

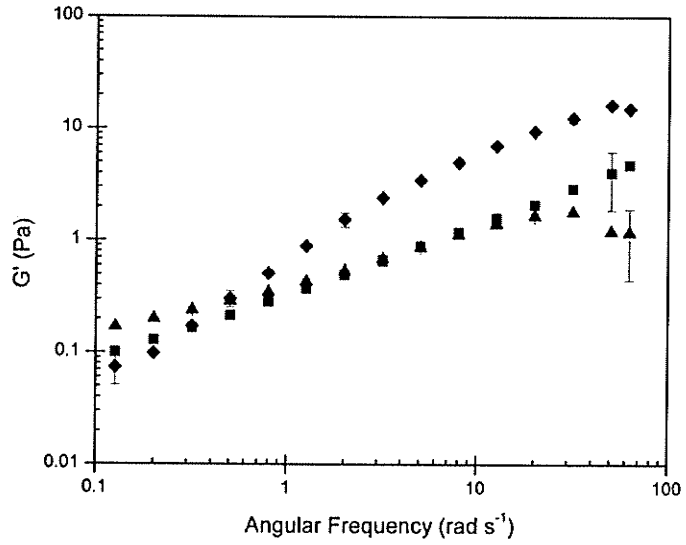

Figure 11: Frequency response of the shear storage modulus (G′) of a whole egg foam that had been mixed for 30 s ($\phi = 0.29$) at three different aging times, 675 s (◆), 1788 s (■), and 3643 s (▲).

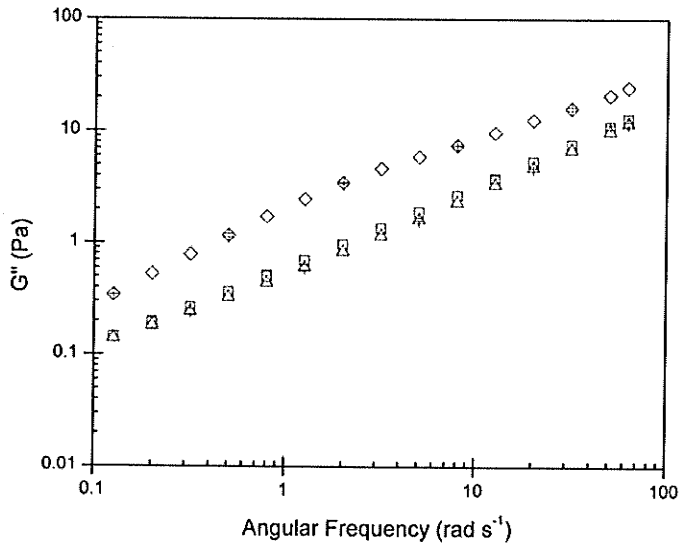

Figure 12: Frequency response of the shear loss modulus (G′′) of a whole egg foam that had been mixed for 30 s ($\phi = 0.29$) at three different aging times, 675 s (◇), 1788 s (□), and 3643 s (△).

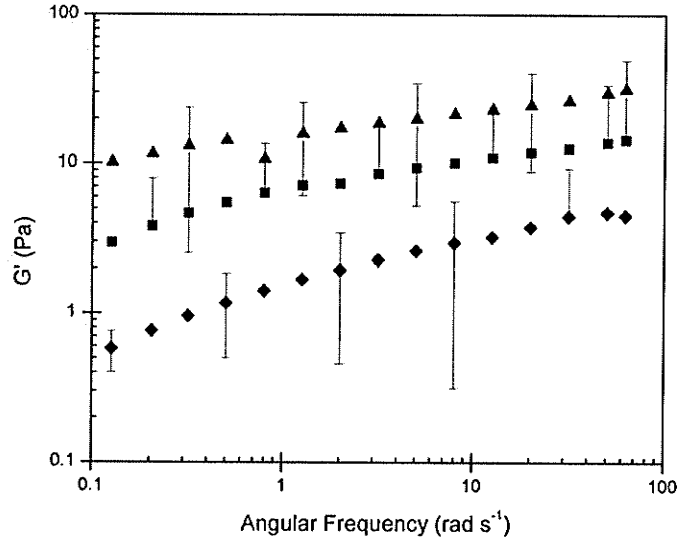

Figure 13: Frequency response of the shear storage modulus (G') of an egg white foam that had been mixed for 30 s ($\phi = 0.31$) at three different aging times, 675 s (◆), 1788 s (■), and 3643 s (▲).

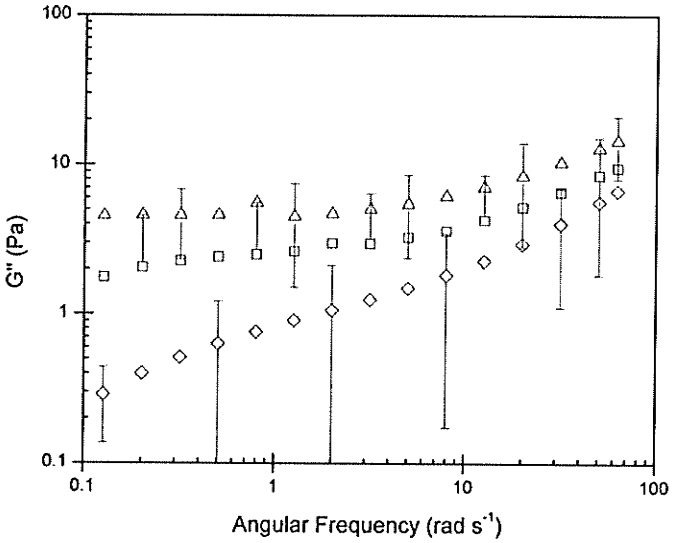

Figure 14: Frequency response of the shear loss modulus (G'') of an egg white foam that had been mixed for 30 s ($\phi = 0.31$) at three different aging times, 675 s (◇), 1788 s (□), and 3643 s (△).

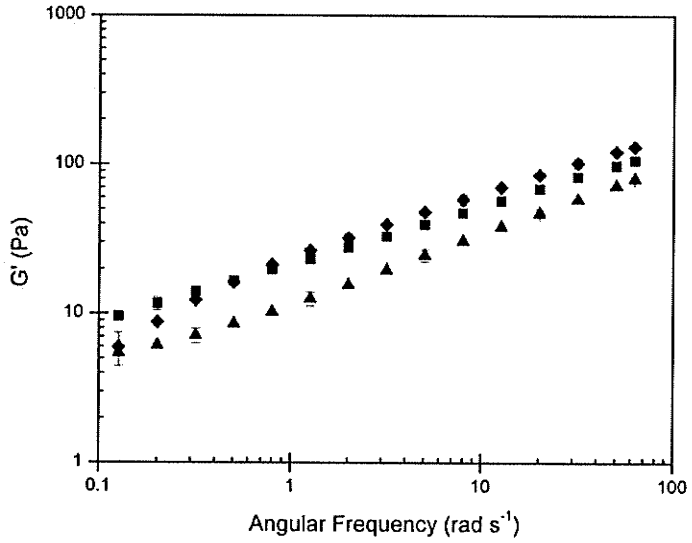

Figure 15: Frequency response of the shear storage modulus (G') of a whole egg foam that had been mixed for 1065 s ($\phi = 0.69$) at three different aging times, 675 s (◆), 1788 s (■), and 3643 s (▲).

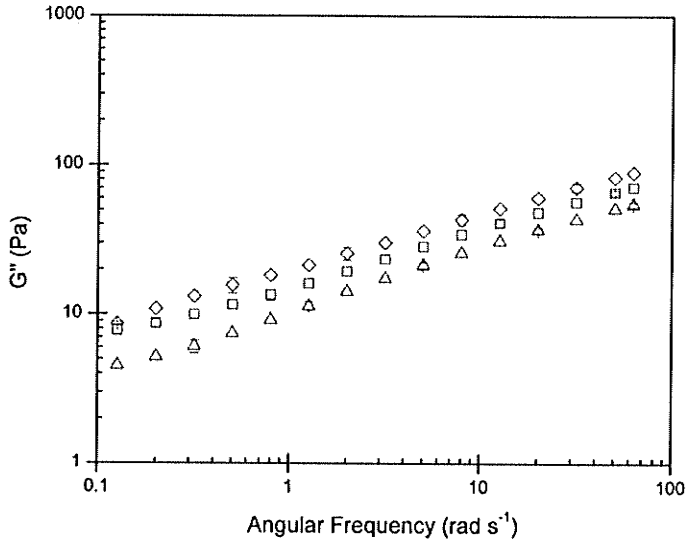

Figure 16: Frequency response of the shear loss modulus (G'') of a whole egg foam that had been mixed for 1065 s ($\phi = 0.69$) at three different aging times, 675 s (◇), 1788 s (□), and 3643 s (△).

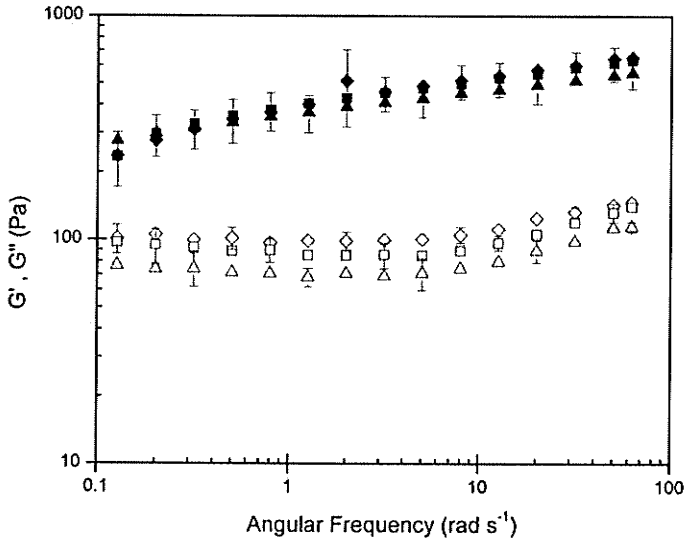

Figure 17: Frequency response of the shear storage modulus (solid symbols) (*G'*) *and shear loss modulus* (open symbols) (*G''*) *of an egg white foam that had been mixed for 180 s* ($\phi = 0.65$) *at three different aging times, 675 s* (◆,◇), *1788 s* (■,□), *and 3643 s* (▲,△).

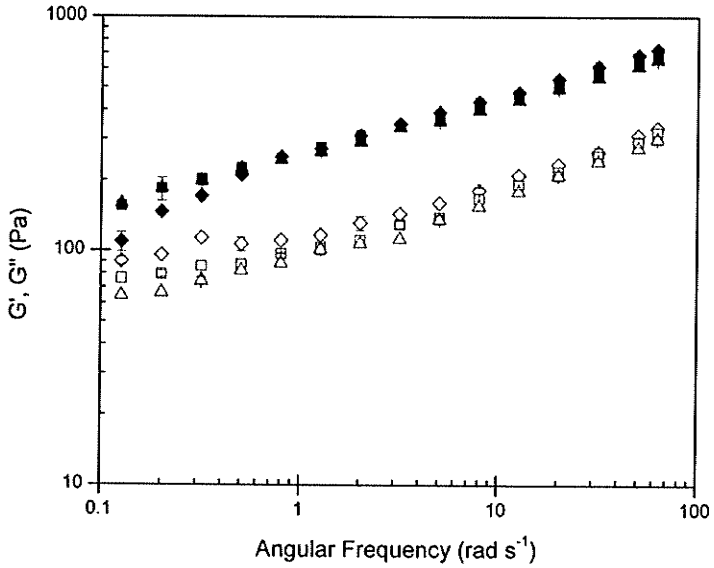

Figure 18: Frequency response of the shear storage modulus (solid symbols) (*G'*) *and shear loss modulus* (open symbols) (*G''*) *of a whole egg batter that had been mixed for 180 s* ($\phi = 0.49$) *at three different aging times, 675 s* (◆,◇), *1788 s* (■,□), *and 3643 s* (▲,△).

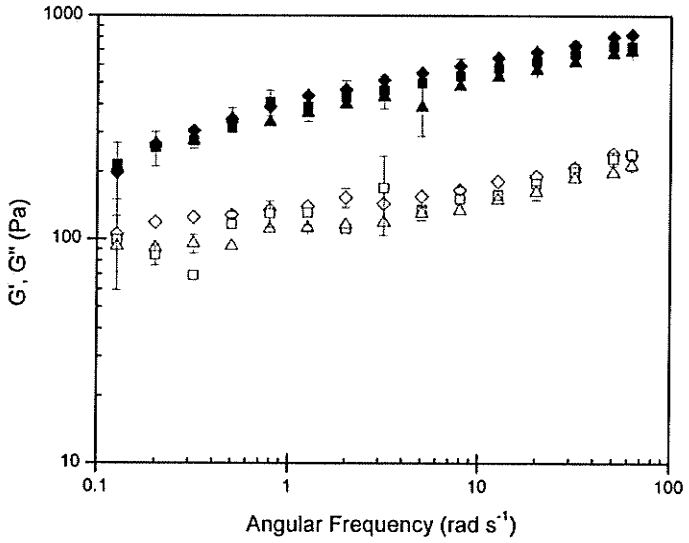

Figure 19: Frequency response of the shear storage modulus (solid symbols) (*G′*) *and shear loss modulus* (open symbols) (*G′′*) *of an egg white batter that had been mixed for 180 s* ($\phi = 0.56$) *at three different aging times, 675 s* (◆,◇), *1788 s* (■,□), *and 3643 s* (▲,△).

low frequencies; as frequency is increased a shallow minimum appears followed by a strong increase with further increase in frequency (Figure 17). This result is in contrast to a linear increase that is shown in all of the whole egg foam systems (Figures 12 & 16). Cohen-Addad *et al* (1998) show similar trends for both *G′* and *G′′* for high bubble volume fraction ($\phi > 0.90$) aerosol-generated shaving foams. Their results show a linear increase with frequency for *G′* and the low frequency plateau for *G′′* followed by the shallow minimum and then linear increase.

4.4 Scaling of Small Strain Rheological Data

In order to characterize the evolution of the foams and batters with aging time, the average moduli data (from three replicates) from eight consecutive frequency sweeps (aging times 1046 s- 3643 s) were scaled to the frequency sweep curve at a reference

aging time (t_0) of 675 s using procedures described by Cohen-Addad *et al* (1998) to produce a master curve of all aging time data. The aging time of 675 s was selected as the point of normalization since the data were perceived to be more consistent than the first aging time of 304 s. Note that aging times are taken as the median time of each frequency sweep. Scaling of the moduli to a single master curve involves shifting aged moduli data (either up or down depending upon how they evolve) to the curve at the reference time. Scaling factors ($b(t,t_0)$) are calculated as the average (frequency independent) ratio of the loss modulus G'' at a given aging time to the loss modulus at the reference aging time (675 s) as is shown in Equation 18.

$$b(t,t_0) = \frac{G''(\omega,t)}{G''(\omega,t_0)} \qquad [18]$$

The scaling factor was calculated using the G'' data, and then the same scaling factor was used to scale the G' data, i.e., the scaling of G' and G'' was not independent. Thus, we see a tighter fit to the master curve for G'' in all cases. Nevertheless, for most systems, the G'' scaling factor does well in reducing G' data onto a common curve. Selected scaled plots are shown in Figures 20-24, again, covering all four systems and varying bubble volume fractions (mix times). The quality of the scaling of the data depends on mix time: at higher mix times (Figures 22-24) the fit is superior to that at low mix times (Figures 20 & 21) for a given system. Similarly, the data seems to tighten at higher frequencies as opposed to the low frequency ends, especially at low mix times (Figures 20 & 21).

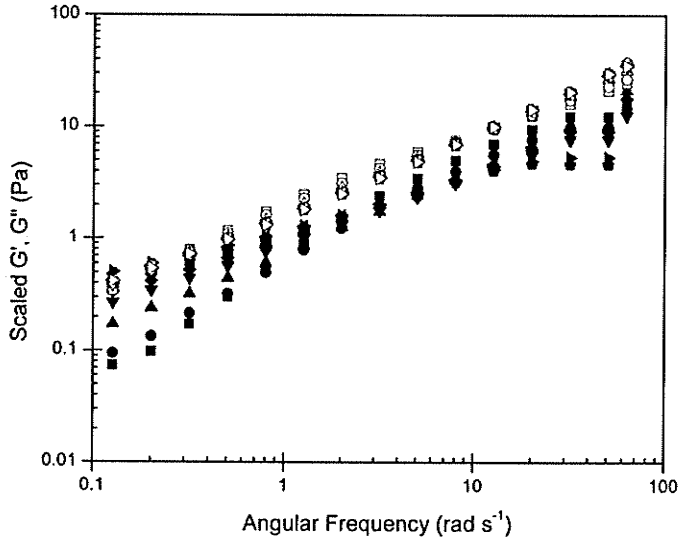

Figure 20: Shear storage modulus (solid symbols) (*G'*) *and loss modulus* (open symbols) (*G''*) *of a whole egg foam mixed for 30 s* ($\phi = 0.29$) *at various aging times (1046 s* (●,○)*, 1417 s* (▲,△)*, 1788 s* (▼,▽)*, 2159 s* (◆,◇)*, 2530 s* (★,☆)*, 2901 s* (⬟,⬠)*, 3272 s* (◀,◁)*, 3643 s* (▶,▷)*) scaled to an aging time of 675 s* (■,□).

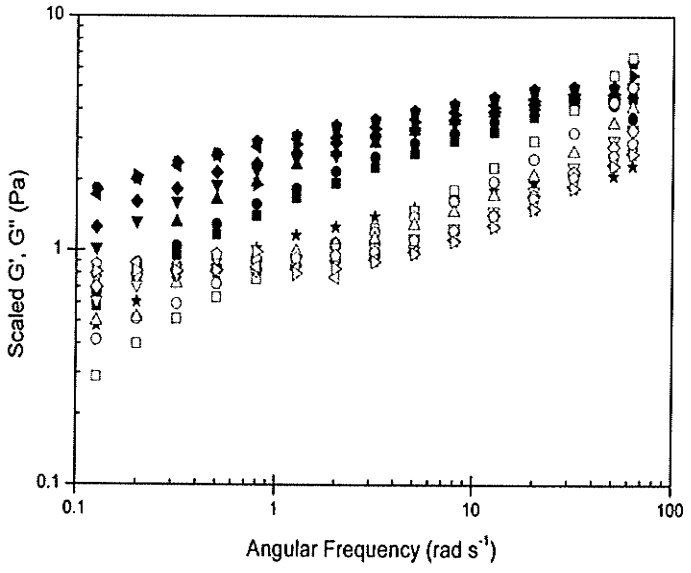

Figure 21: Shear storage modulus (solid symbols) (*G'*) *and loss modulus* (open symbols) (*G''*) *of an egg white foam mixed for 30 s* ($\phi = 0.31$) *at various aging times (1046 s* (●,○)*, 1417 s* (▲,△)*, 1788 s* (▼,▽)*, 2159 s* (◆,◇)*, 2530 s* (★,☆)*, 2901 s* (⬟,⬠)*, 3272 s* (◀,◁)*, 3643 s* (▶,▷)*) scaled to an aging time of 675 s* (■,□).

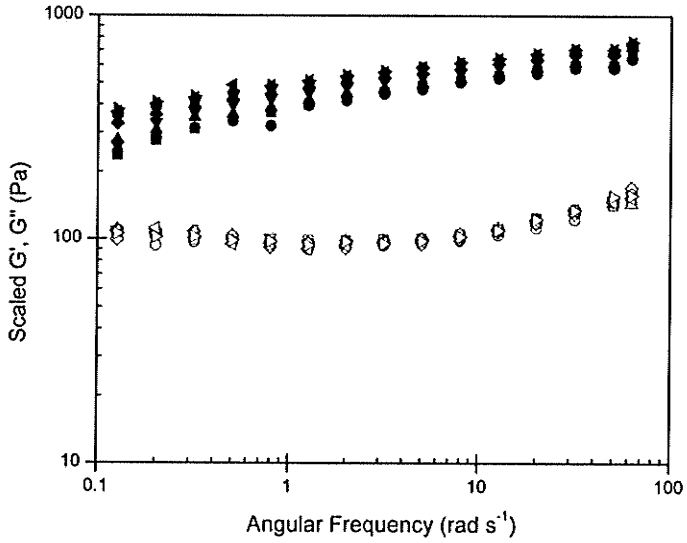

Figure 22: Shear storage modulus (solid symbols) (*G'*) *and loss modulus* (open symbols) (*G''*) *of an egg white foam mixed for 180 s* ($\phi = 0.65$) *at various aging times* (*1046 s* (●,○), *1417 s* (▲,△), *1788 s* (▼,▽), *2159 s* (◆,◇), *2530 s* (★,☆), *2901 s* (⬟,⬠), *3272 s* (◀,◁), *3643 s* (▶,▷)) *scaled to an aging time of 675 s* (■,□).

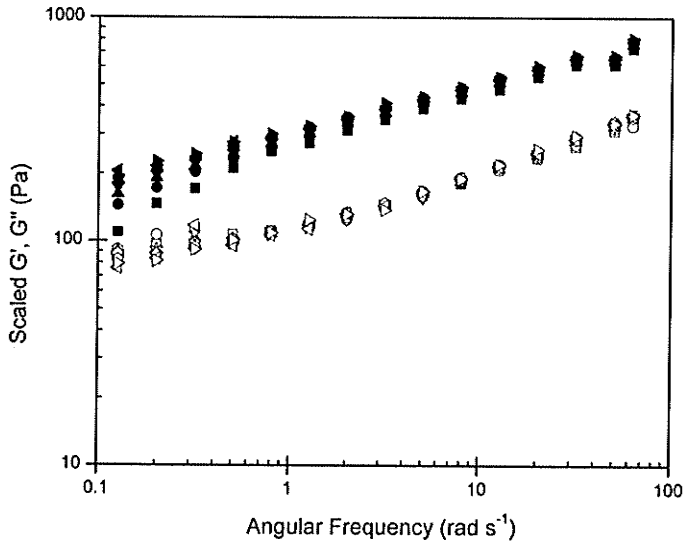

Figure 23: Shear storage modulus (solid symbols) (*G'*) *and loss modulus* (open symbols) (*G''*) *of a whole egg batter mixed for 180 s* ($\phi = 0.49$) *at various aging times* (*1046 s* (●,○), *1417 s* (▲,△), *1788 s* (▼,▽), *2159 s* (◆,◇), *2530 s* (★,☆), *2901 s* (⬟,⬠), *3272 s* (◀,◁), *3643 s* (▶,▷)) *scaled to an aging time of 675 s* (■,□).

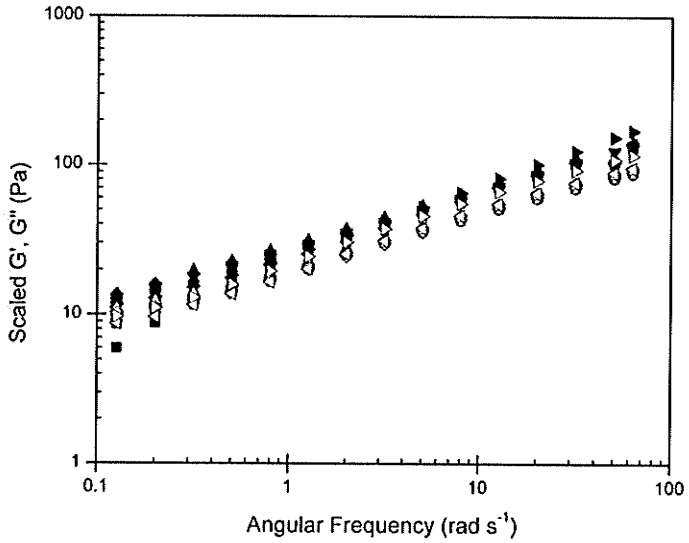

Figure 24: Shear storage modulus (solid symbols) (*G′*) *and loss modulus* (open symbols) (*G′′*) *of a whole egg foam mixed for 1065 s* ($\phi = 0.69$) *at various aging times* (*1046 s* (●,○), *1417 s* (▲,△), *1788 s* (▼,▽), *2159 s* (◆,◇), *2530 s* (★,☆), *2901 s* (⬟,⬠), *3272 s* (◀,◁), *3643 s* (▶,▷)) *scaled to an aging time of 675 s* (■,□).

4.5 Changes in Small Strain Rheology with Aging Time

The scaling of the *G′* and *G′′* data produces a scaling factor ($b(t,t_0)$) for a given aging time within a specific mix time (i.e., 9 data points per mix time, with aging time 675 having a scaling factor of 1). These factors are averaged over the entire frequency range, which allows us to eliminate one variable from the plot (frequency). Plots of the scaling factor versus aging time allow us to see the evolution of the rheology of the foams and batters directly. Furthermore, by plotting the different mix times on a single plot (Figures 25-28), we can see how foam or batter rheology evolve with aging time as more air is entrained into the system. In all cases, the initial point is (675 s, 1) since 675 s was the selected aging time chosen for this normalization procedure. For the two foam systems (Figures 25 & 26), there is a noticeable change in the slope of the scaling factor at a mix

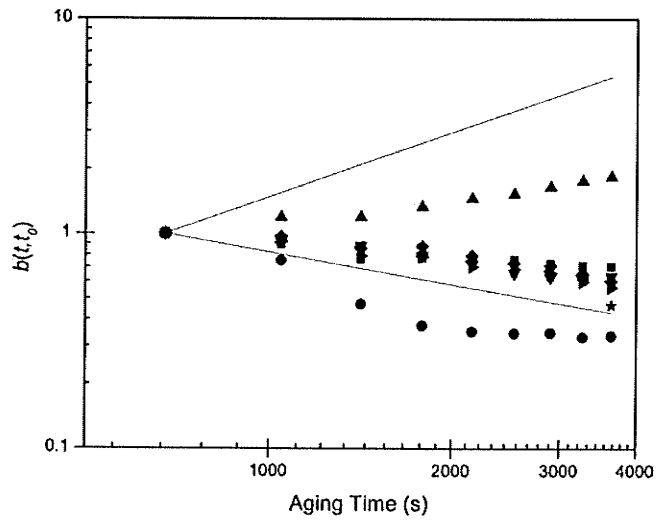

Figure 25: Change in modulus scaling factor $b(t,t_0)$, as a function of aging time for whole egg foams created by mixing for 0 s (■), 30 s (●), 60 s (▲), 120 s (▼), 180 s (◆), 345 s (◀), 705 s (▶), 1065 s (★). Solid lines represent slopes of +1 and −0.5.

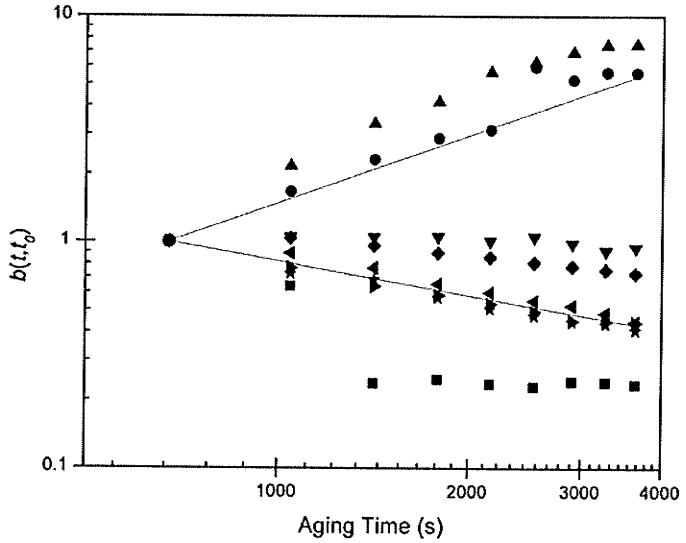

Figure 26: Change in modulus scaling factor $b(t,t_0)$, as a function of aging time for egg white foams created by mixing for 0 s (■), 30 s (●), 60 s (▲), 120 s (▼), 180 s (◆), 345 s (◀), 705 s (▶), 1065 s (★). Solid lines represent slopes of +1 and −0.5.

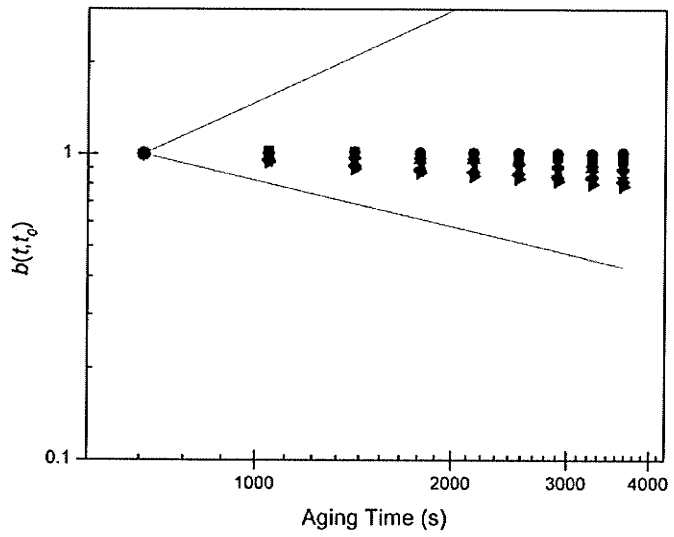

Figure 27: Change in modulus scaling factor $b(t,t_0)$, as a function of aging time for whole egg batters created by mixing for 0 s (■), 30 s (●), 60 s (▲), 120 s (▼), 180 s (◆), 345 s (◀), 705 s (▶), 1065 s (★). Solid lines represent slopes of +1 and −0.5.

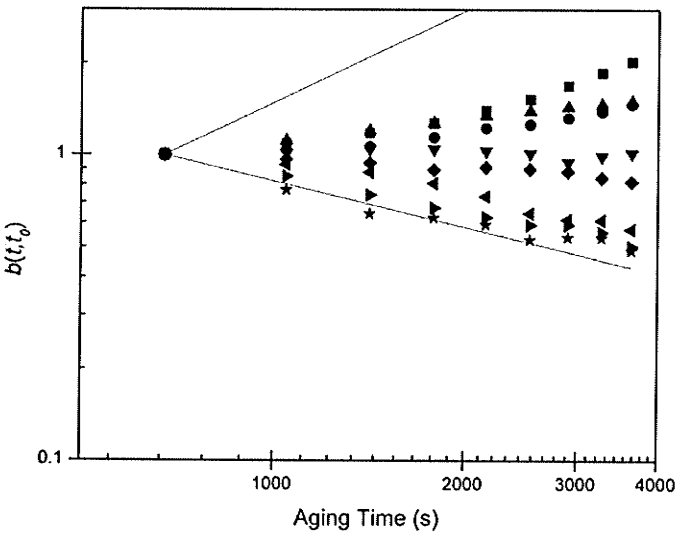

Figure 28: Change in modulus scaling factor $b(t,t_0)$, as a function of aging time for egg white batters created by mixing for 0 s (■), 30 s (●), 60 s (▲), 120 s (▼), 180 s (◆), 345 s (◀), 705 s (▶), 1065 s (★). Solid lines represent slopes of +1 and −0.5.

time of approximately 120 s. The slope changes from a positive slope at 60 s, which approaches +1, to a negative slope at 120 s which then begins approaches −0.5 as mix time is further increased. The goodness of fit indicates (with some exceptions) that the fits to the data are strong (Table 5).

Positive slopes indicate that a downward shift in the aged moduli data must occur in order to fit the reference curve, i.e., a stiffening occurs with aging time. This occurs in systems which have low bubble volume fractions ($\phi < \sim 0.45$) and can be explained by two things. First, since bubble volume fraction is low, the average thickness of the liquid films separating bubble is large, so that resistance to transfer of gas between bubbles is large; disproportionation effects are severely limited (Marze *et al*, 2005). Secondly, if disproportionation is limited, it is assumed that changes in the rheological response are caused by aging via liquid drainage. Drainage can lead to the formation of a dry foam skeleton as the liquid leaves the bubble network, thus causing an increase in the elastic response. This drained foam shows a demonstrated stiffening effect with aging time (Weaire & Hutzler, 1999). Hence we can say that as the slopes of the scaling factor versus aging time plots approach +1 drainage effects are the dominant aging mechanisms for that particular foam.

Negative slopes indicate that aged moduli data require an upward shift to fit the reference curve i.e., a decrease in the shear moduli occurs with aging time. As bubble volume fraction is increased the foams from both systems tend to approach a slope of −0.5; in fact, the high bubble volume fraction ($\phi > \sim 0.74$) egg white foams not only approach but reach this slope (Table 5). Weaire and Hutzler (1999) show that the coarsening (due to disproportionation) of high bubble volume fraction foams scales

Table 5: Slope and R^2 values for plots of scaling factor ($b(t,t_0)$) versus aging time.

	Whole Foam (Figure 25)			**White Foam (Figure 26)**			**Whole Batter (Figure 27)**			**White Batter (Figure 28)**		
Mix (s)	Slope (s^{-1})	ϕ	R^2	Slope (s^{-1})	ϕ	R^2	Slope (s^{-1})	ϕ	R^2	Slope (s^{-1})	ϕ	R^2
30	-0.682	0.29	0.887	1.09	0.31	0.954	0.002	0.16	0.064	0.234	0.32	0.928
60	0.358	0.43	0.969	1.19	0.46	0.965	-0.063	0.30	0.872	0.244	0.43	0.998
120	-0.325	0.57	0.95	-0.049	0.58	0.283	-0.078	0.42	0.938	-0.013	0.52	0.055
180	-0.295	0.63	0.909	-0.216	0.65	0.905	-0.117	0.49	0.988	-0.107	0.56	0.901
345	-0.29	0.68	0.969	-0.492	0.74	0.986	-0.118	0.54	0.993	-0.355	0.68	0.947
705	-0.331	0.70	0.971	-0.496	0.80	0.986	-0.14	0.55	0.999	-0.387	0.72	0.987
1065	-0.385	0.69	0.881	-0.524	0.81	0.986	-0.113	0.55	0.984	-0.391	0.73	0.951

according to a square root dependence on time (Equation 19), where R = bubble radius, t = time.

$$R \propto t^{1/2} \qquad [19]$$

Furthermore, Princen and Kiss (1986) showed that the static shear modulus of foams is inversely proportional to a measure of bubble size known as R_{32}, (Equation 20),

$$G = C\frac{\gamma}{R_{32}}\phi^{1/3} \Rightarrow G \propto R^{-1} \qquad [20]$$

where G = static shear modulus, C = constant, ϕ = bubble volume fraction, γ = surface tension, R_{32} = surface-volume mean radius, R = bubble radius. Combining Equations 19 and 20 leads to Equation 21 which shows that for high bubble volume fraction foams ($\phi > \sim 0.74$) the static shear modulus evolves inversely proportionally to a square root dependence on time.

$$G \propto t^{-1/2} \qquad [21]$$

This relationship is confirmed in our high bubble volume fraction ($\phi > \sim 0.74$) egg white foams as the evolution of their shear modulus with aging time approaches or reaches a −0.5 slope. Hence we can say that as the slopes of the scaling factor versus aging time plot approach −0.5 disproportionation is the dominant aging mechanism.

The addition of flour to the systems proves to have a stabilization effect, as the slope values are much closer to zero, regardless of whether they are positive (drainage dominating) or negative (disproportionation dominating). The reduction in drainage effects can be attributed to an increase in bulk viscosity caused by the addition of flour which slows the rate of drainage (Saint-Jalmes & Langevin, 2002). Reduced rates of disproportionation are likely due to adsorption of the flour particles at the bubble

interface. This reduces the difference in chemical potential for gas molecules inside and outside the bubbles which is the driving force for diffusion (Murray & Ettelaie, 2004). A summary of all slopes is given in Table 5.

Chapter 5: Large Strain Rheology Results & Discussion

5.1 Shear Rate Ramps

Similar to the small strain rheological results, representative graphs of the large strain rheological tests (shear rate ramps) were selected covering the complete range of densities and all four systems (Figures 29-34). In each case, aging times of 270 s, 1350 s, 2430 s and 3510 s are shown on the graphs to cover the approximately one hour period in which the foam/batter was allowed to age. Error bars resulting from the three replicates are shown on every fourth data point for a given aging time to limit congestion on the plot. At low mix times, where little bubble structure has developed there is significantly more error than at higher mix times; this larger error is presumed to arise from one of two things; sensitivity of the bubble network to the imposed shear stresses which result in collapse or rearrangement of the bubble network (Heller & Kuntamukkula, 1987), or rapid drainage leading to the collecting of liquid at the bottom of the rheometer resulting in variability of the torque measurements by the rheometer (Heller & Kuntamukkula, 1987). In Figure 34, showing the whole egg batter at a mix time of 180 s, the data at the aging time of 270 s (square symbols) did not follow the trends seen at other mix times. Beyond this aging time point there is very little change in the large strain response for the remainder of the one hour aging period. This unusual result is presumed to be due to the difficulty in loading the thick and sticky batters into the rheometer cup without creating voids; in some cases this was unavoidable and thus we see a settling period in the initial aging times for many of the batter systems.

Flow characteristics of all systems were looked at on the basis of two parameters: time independent behavior of the foams as a function of shear rate (Section 5.1.1) and time dependent changes in viscosity on the basis of foam aging (Section 5.3), the latter

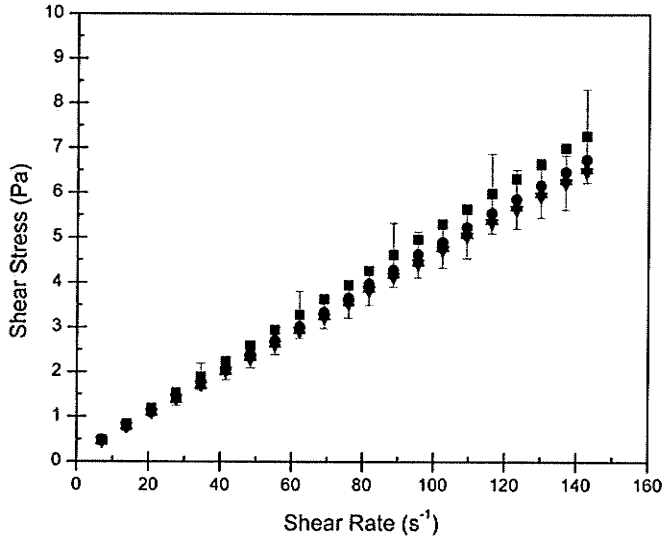

Figure 29: Shear stress response of egg white foams at a mixing time of 0 s (ϕ = ~0) subjected to shear rate ramps at four different aging times; 270 s (■), 1350 s (●), 2430 s (▲), 3510 s (▼).

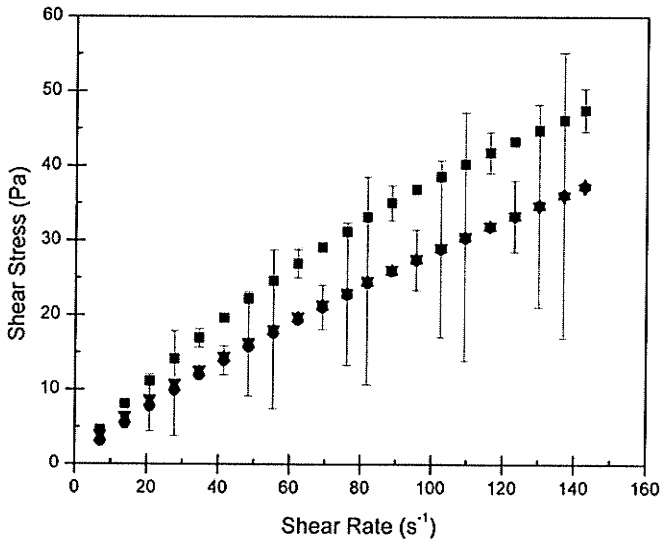

Figure 30: Shear stress response of whole egg foams at a mixing time of 30 s (ϕ = 0.29) subjected to shear rate ramps at four different aging times; 270 s (■), 1350 s (●), 2430 s (▲), 3510 s (▼).

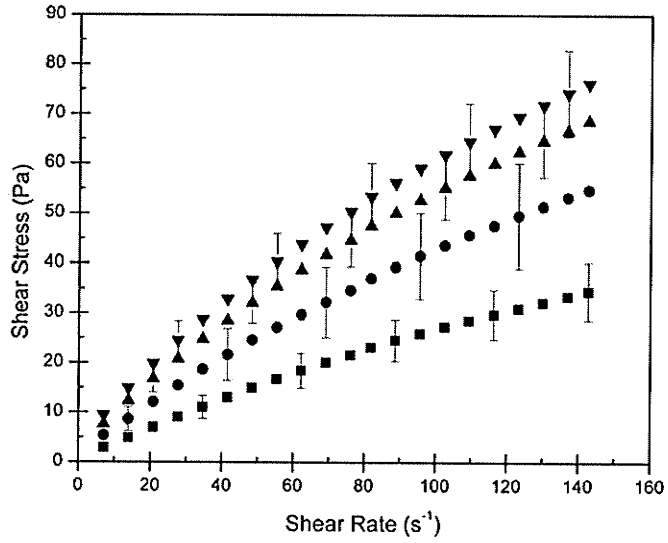

Figure 31: Shear stress response of egg white foams at a mixing time of 60 s (ϕ = 0.46) subjected to shear rate ramps at four different aging times; 270 s (■), 1350 s (●), 2430 s (▲), 3510 s (▼).

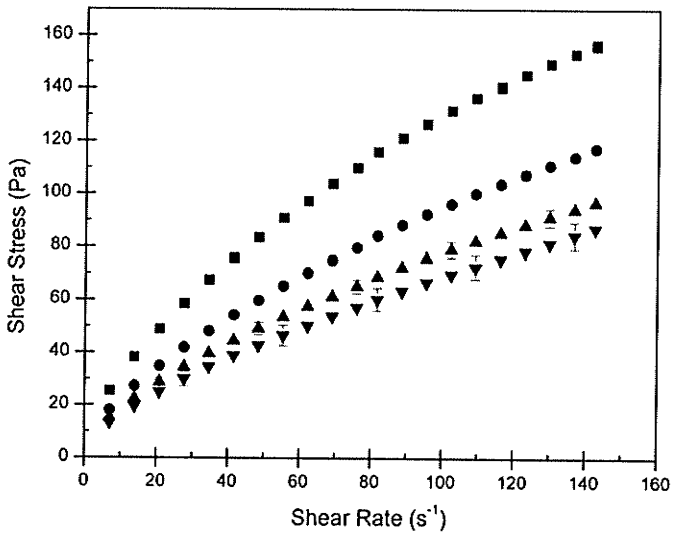

Figure 32: Shear stress response of whole egg foams at a mixing time of 1065 s (ϕ = 0.69) subjected to shear rate ramps at four different aging times; 270 s (■), 1350 s (●), 2430 s (▲), 3510 s (▼).

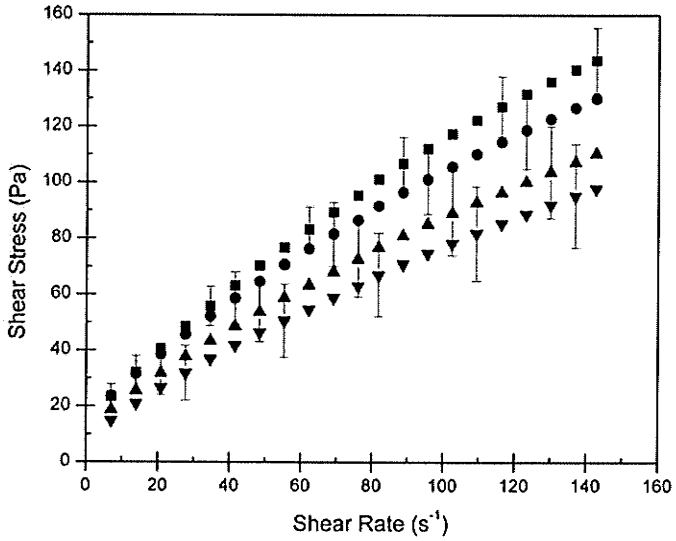

Figure 33 Shear stress response of egg white foams at a mixing time of 180 s (ϕ = 0.65) subjected to shear rate ramps at four different aging times; 270 s (■), 1350 s (●), 2430 s (▲), 3510 s (▼).

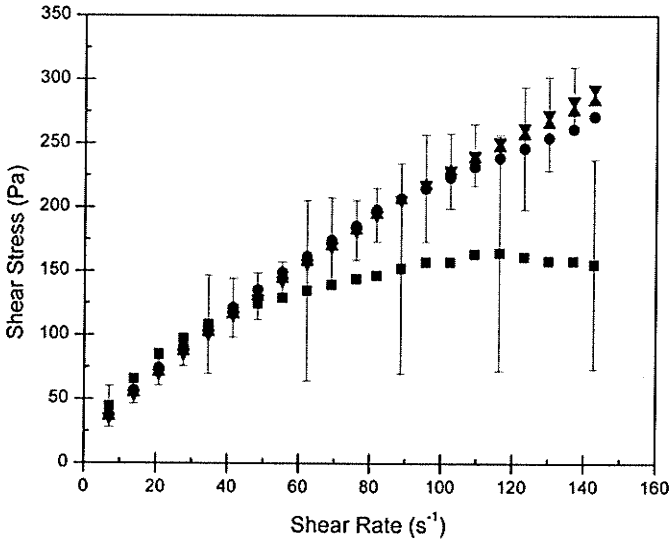

Figure 34: Shear stress response of whole egg batters at a mixing time of 180 s (ϕ = 0.49) subjected to shear rate ramps at four different aging times; 270 s (■), 1350 s (●), 2430 s (▲), 3510 s (▼).

being left until later in the discussion for purposes of introducing scaling techniques which were necessary to characterize time dependent effects. Finally, these parameters are then compared amongst each other on the basis of mix time (bubble volume fraction), and how the incorporation of flour to the foam (to create a batter) affects the flow properties.

5.1.1 Shear Rate Dependence

In the egg white foam systems Newtonian behavior is seen at the lowest mix time, 0 sec (Figure 29), a system which is essentially blended egg white and sugar. Beyond this mix time all the egg white systems (foams and batters) exhibit shear thinning behavior (Figures 31, 33). Similarly, all whole egg systems, foams and batters at all mix times, exhibit shear thinning behavior (Figures 30, 32, & 34). The shear thinning result is consistent with previously reported large strain shear flow behavior of foams (Yuan & Edwards, 1995; Sakiyan et al, 2004).

5.2 Scaling of Large Strain Rheological Data

The Cox-Merz rule states that the viscosity versus shear rate curve should be identical to the complex dynamic viscosity versus frequency curve when compared at similar rates of testing (Yu & Gunasekaran, 2001). Cox-Merz plots for the systems of section 5.1 are shown in Figures 35-39. As can be seen, the apparent viscosity values (open symbols) at a given age time do not fall directly on the same curve as the complex dynamic viscosity values (solid symbols). A shift downwards is apparent in all cases for large strain testing except for the whole foam at a mix time of 30 s. This shift downwards in apparent viscosity from the small strain calculated complex viscosity can once again be attributed to the sensitivity of the bubble network to the imposed shear

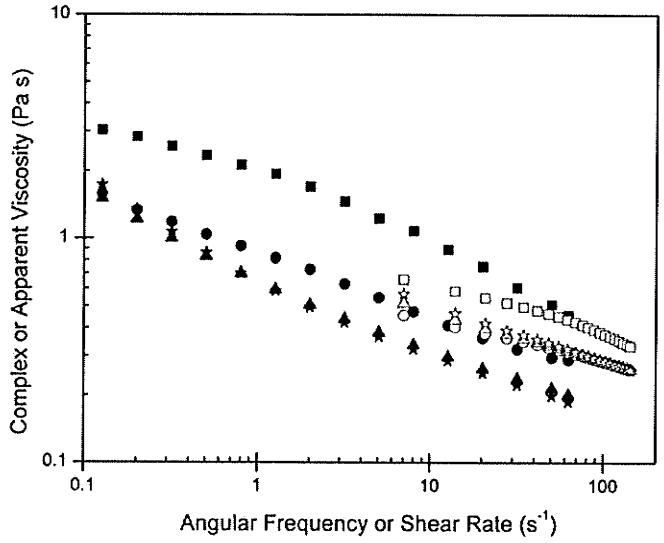

Figure 35: Cox-Merz plots for Whole Egg Foams at a mixing time of 30 s (ϕ = 0.29). Complex dynamic viscosity (closed symbols) *and apparent viscosity* (open symbols) *and shown for four different aging times; 270 s* (■,□), *1350 s* (●,○), *2430 s* (▲,△), *3510 s* (★,☆).

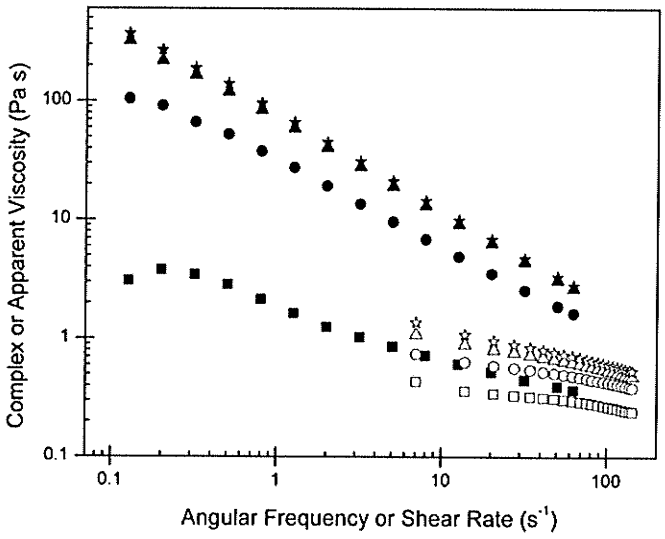

Figure 36: Cox-Merz plot for Egg White Foams at a mixing time of 60 s (ϕ = 0.46). Complex dynamic viscosity (closed symbols) *and apparent viscosity* (open symbols) *and shown for four different aging times; 270 s* (■,□), *1350 s* (●,○), *2430 s* (▲,△), *3510 s* (★,☆).

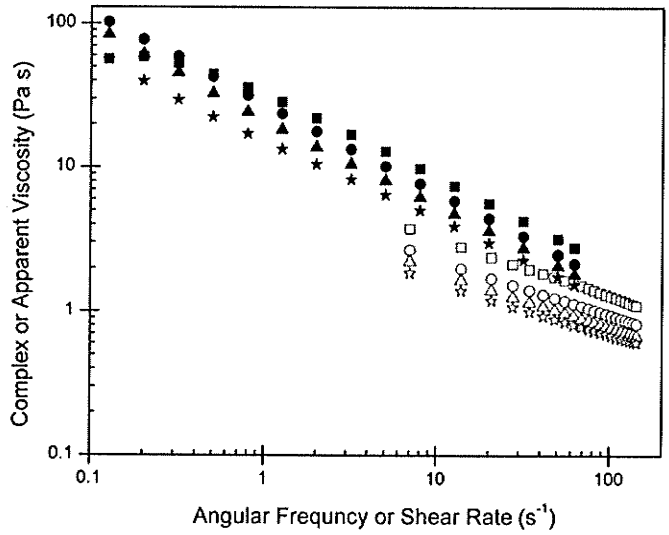

Figure 37: Cox-Merz plot for Whole Egg Foams at a mixing time of 1065 s (ϕ = 0.69). Complex dynamic viscosity (closed symbols) *and apparent viscosity* (open symbols) *and shown for four different aging times; 270 s* (■,□), *1350 s* (●,○), *2430 s* (▲,△), *3510 s* (★,☆).

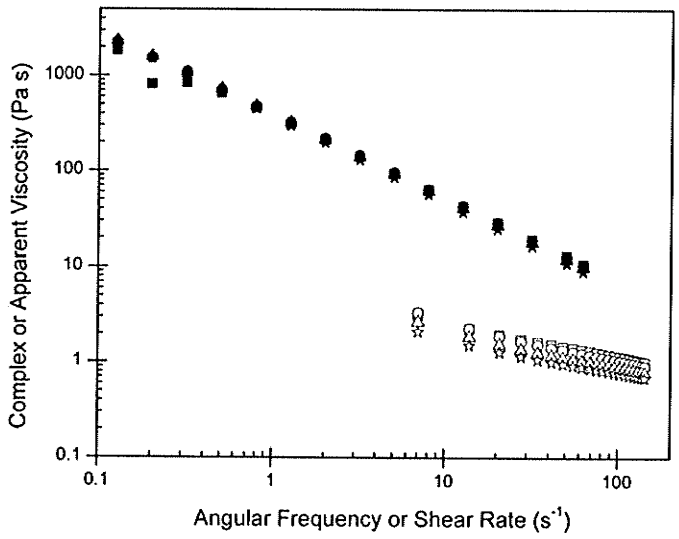

Figure 38: Cox-Merz plot for Whole Egg Foams at a mixing time of 180 s (ϕ = 0.65). Complex dynamic viscosity (closed symbols) *and apparent viscosity* (open symbols) *and shown for four different aging times; 270 s* (■,□), *1350 s* (●,○), *2430 s* (▲,△), *3510 s* (★,☆).

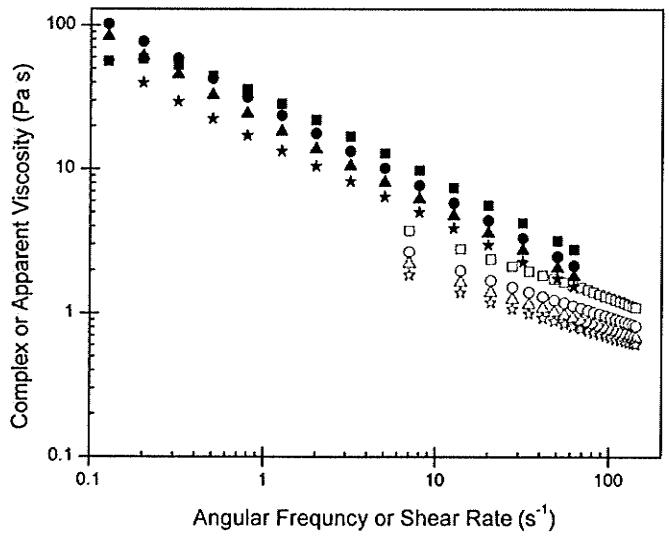

Figure 39: Cox-Merz plot for Whole Egg Batters at a mixing time of 180 s (ϕ = 0.49). Complex dynamic viscosity (closed symbols) *and apparent viscosity* (open symbols) *and shown for four different aging times; 270 s* (■,□), *1350 s* (●,○), *2430 s* (▲,△), *3510 s* (★,☆).

stresses which damage the internal bubble network (Heller & Kuntamukkula, 1987).

Making use of the Cox-Merz rule and analogous procedures to the small strain scaling (Section 4.4) large strain data was scaled to a single master curve in order to characterize the evolution of the foam/batter with aging time. The same procedures as described by Cohen-Addad *et al.* (1998) were used with the obvious exception that the scaling factor is now calculated as the ratio of stresses (σ) at a given aging time to a reference aging time (270 s) averaged over all shear rates ($\dot{\gamma}$) (Equation 22) as opposed to a ratio of moduli averaged over frequency as used in the small strain scaling. Shear stress data at each aging time are then divided by the appropriate scaling factor to shift the curve onto the reference curve. In these plots the data from 28 consecutive shear rate ramps were scaled to fit to an aging time of 270 s (Figures 40-44).

$$b^*(t,t_0) = \frac{\sigma(\dot{\gamma},t)}{\sigma(\dot{\gamma},t_0)} \qquad [22]$$

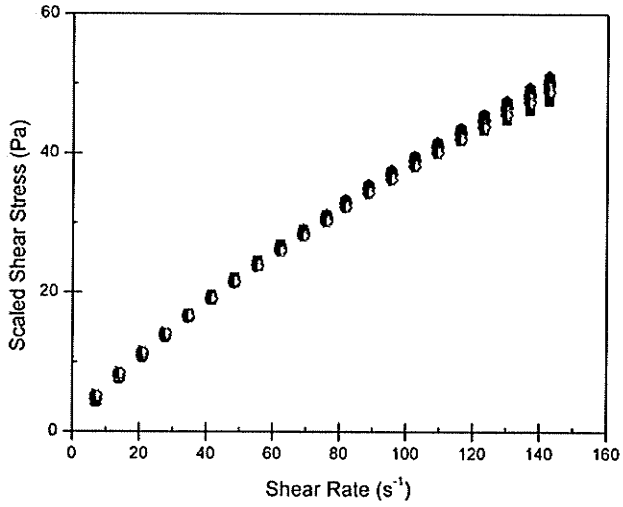

Figure 40: Scaled shear stress response of whole egg foams at a mixing time of 30 s (ϕ = 0.29) subjected to shear rate ramps. All aging times, 390 s (●), 510 s (▲), 630 s (▼), 750 s (◀), 870 (▶), 990 (◆), 1110 s (⬢), 1230 s (★), 1350 s (⬟), 1470 s (◕), 1590 s (▣), 1710 s (◓), 1830 s (◬), 1950 s (▽), 2070 s (◁), 2190 s (▷), 2310 s (◈), 2430 s (◒), 2550 s (☆), 2670 s (⬘), 2790 s (✳), 2910 s (◧), 3030 s (◐), 3150 s (◭), 3270 s (▼), 3390 s (◀), 3510 s (▶) were scaled to a reference aging time of 270 s (■).

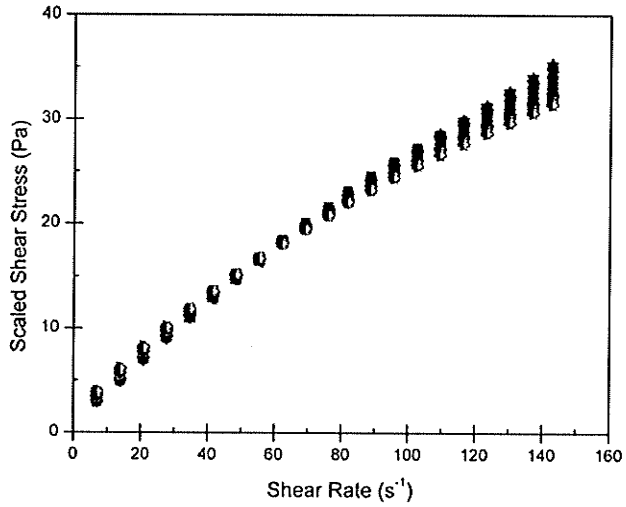

Figure 41: Scaled shear stress response of egg white foams at a mixing time of 60 s (ϕ = 0.46) subjected to shear rate ramps. All aging times, 390 s (●), 510 s (▲), 630 s (▼), 750 s (◀), 870 (▶), 990 (◆), 1110 s (⬢), 1230 s (★), 1350 s (⬟), 1470 s (◕), 1590 s (▣), 1710 s (◓), 1830 s (◬), 1950 s (▽), 2070 s (◁), 2190 s (▷), 2310 s (◈), 2430 s (◒), 2550 s (☆), 2670 s (⬘), 2790 s (✳), 2910 s (◧), 3030 s (◐), 3150 s (◭), 3270 s (▼), 3390 s (◀), 3510 s (▶) were scaled to a reference aging time of 270 s (■).

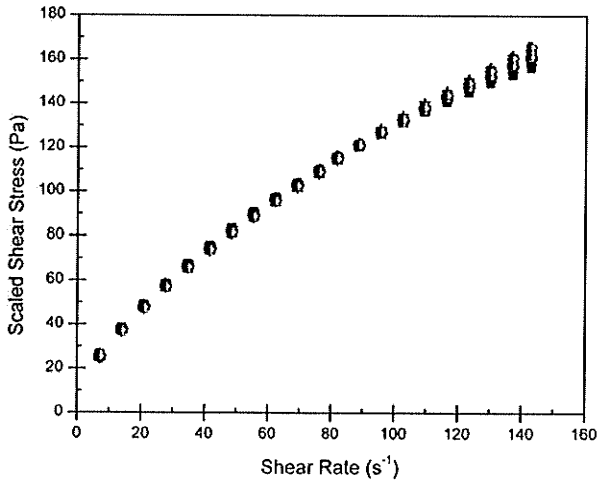

Figure 42 Scaled shear stress response of whole egg foams at a mixing time of 1065 s (ϕ = 0.69) subjected to shear rate ramps. All aging times, 390 s (●), 510 s (▲), 630 s (▼), 750 s (◀), 870 (▶), 990 (◆), 1110 s (⬢), 1230 s (★), 1350 s (⬟), 1470 s (◕), 1590 s (▬), 1710 s (◓), 1830 s (◬), 1950 s (▽), 2070 s (◁), 2190 s (▷), 2310 s (◈), 2430 s (◓), 2550 s (☆), 2670 s (⬟), 2790 s (✳), 2910 s (◧), 3030 s (◐), 3150 s (◭), 3270 s (▼), 3390 s (◀), 3510 s (▶) were scaled to a reference aging time of 270 s (■).

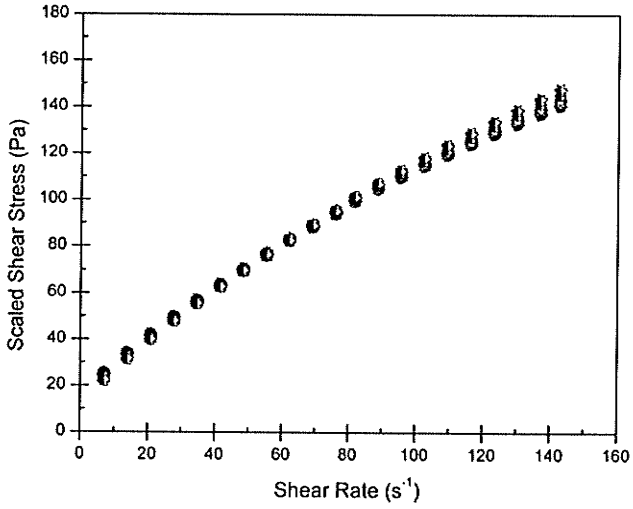

Figure 43: Scaled shear stress response of egg white foams at a mixing time of 180 s (ϕ = 0.65) subjected to shear rate ramps. All aging times, 390 s (●), 510 s (▲), 630 s (▼), 750 s (◀), 870 (▶), 990 (◆), 1110 s (⬢), 1230 s (★), 1350 s (⬟), 1470 s (◕), 1590 s (▬), 1710 s (◓), 1830 s (◬), 1950 s (▽), 2070 s (◁), 2190 s (▷), 2310 s (◈), 2430 s (◓), 2550 s (☆), 2670 s (⬟), 2790 s (✳), 2910 s (◧), 3030 s (◐), 3150 s (◭), 3270 s (▼), 3390 s (◀), 3510 s (▶) were scaled to a reference aging time of 270 s (■).

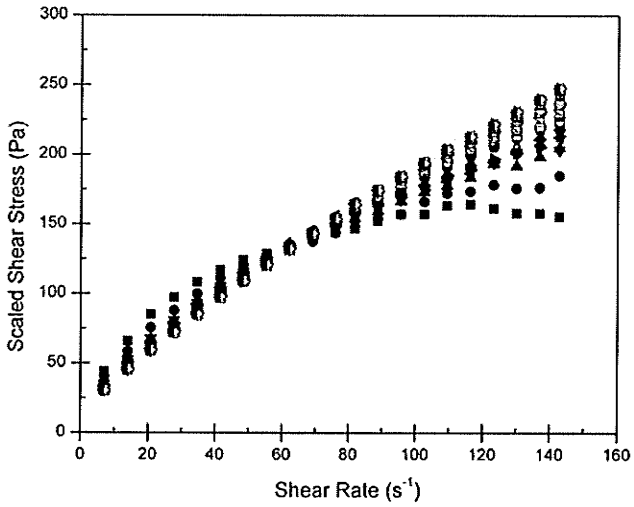

Figure 44: Scaled shear stress response of whole egg batters at a mixing time of 180 s (ϕ = 0.49) subjected to shear rate ramps. All aging times, 390 s (●), 510 s (▲), 630 s (▼), 750 s (◀), 870 (▶), 990 (◆), 1110 s (⬢), 1230 s (★), 1350 s (⬟), 1470 s (●), 1590 s (■), 1710 s (⬭), 1830 s (▲), 1950 s (▽), 2070 s (◁), 2190 s (▷), 2310 s (◈), 2430 s (⬭), 2550 s (☆), 2670 s (⬟), 2790 s (✳), 2910 s (◧), 3030 s (◐), 3150 s (◭), 3270 s (▼), 3390 s (◀), 3510 s (▶) were scaled to a reference aging time of 270 s (■).

The third shear rate ramp was selected as the point of normalization, and the initial two shear rate ramps were omitted from the scaling, as the data was seen to be more consistent from the point of 270 s on. The better consistency for the 270 s data, compared to that of earlier aging times, is likely due to a settling effect upon loading the sample into the rheometer cup. Especially with batter systems or high bubble volume fraction foam systems, the stiff nature of the sample made it difficult to fill the cup without creating sample discontinuities. These sample discontinuities presumably settled out with aging time and as a result of shearing. In most cases the large strain data scales exceptionally well to the reference aging time. There is a slight spread in the scaled data at the high shear rate end for low mix times of both the whole egg and egg white foams (Figures 40 & 41), but these systems still appear to scale onto a single master curve. This

spread disappears as mix time is increased in all foam cases, and the data fall seamlessly onto a single line (Figures 42 & 43). Figure 44, showing the whole egg batter at a mix time of 180 s does not scale as nicely as the foam systems due to the irregularity arising from the data at the reference aging time (270 s) as discussed in Section 5.1.

5.3 Comparison of Large Strain Rheological Data

Two separate plots showing selected mix times and the corresponding bubble volume fractions for whole egg and egg white foams (Figure 45 & 46) allows for an appreciation of how structure changes alter the rheological properties with increased mix time for these scaled data plots. Figure 45 shows values for shear stresses up to 60 Pa allowing visualization of the progression from a Newtonian fluid (in the case of the egg white at a mix time of 0 s) to power law fluids as bubble volume fraction is increased. Figure 46 expands the shear stress range to display the development of an obvious yield stress in the egg white foams with increased mix time. Initially, where $\phi = 0$, and at low bubble volume fractions ($\phi \leq 0.50$) whole egg foams are more viscous than egg white foams. This is presumably due to the presence of lipids which increase the bulk viscosity of the whole egg systems (Vadehra & Nath, 1973). Interestingly, at a mix time of 180 s both foam systems have almost an identical shear rate response and very similar bubble volume fractions (ϕ = 0.65 for egg whites and $\phi = 0.63$ for whole eggs), suggesting that the role of bubble volume fraction now plays a larger role than the bulk viscosity of the materials in determining the shear rate response. Beyond the mix time of 180 s the whole egg foams show very little further change in the large strain response and eventually reach a maximum bubble volume fraction of 0.70. Egg white foams, on the other hand, continue to become more viscous and allow far more air to be entrained, reaching a maximum bubble volume fraction of 0.81. This difference is due to the strong surface

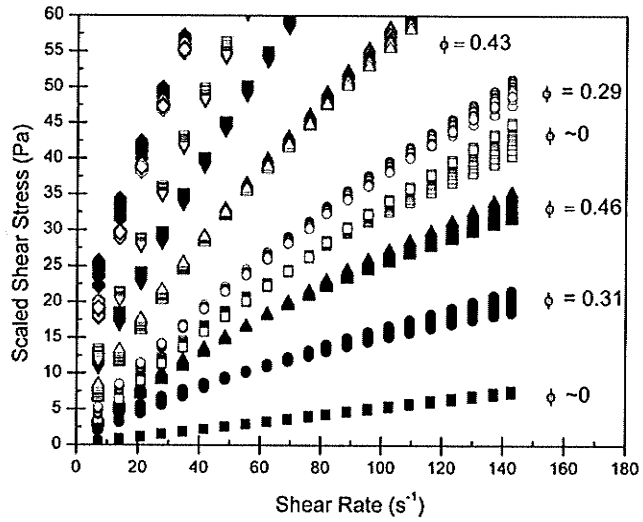

Figure 45: Change in large strain properties (independent of aging effects) for whole egg foams (open symbols) *and egg white foams* (closed symbols) *created from different mixing times 0 s,* (■,□), *30 s* (●,○), *60 s* (▲,△), *120 s* (▼,▽), *180 s* (◆,◇), *with corresponding bubble volume fractions, showing shear stresses up to 60 Pa to highlight evolution with mixing time at low stresses.*

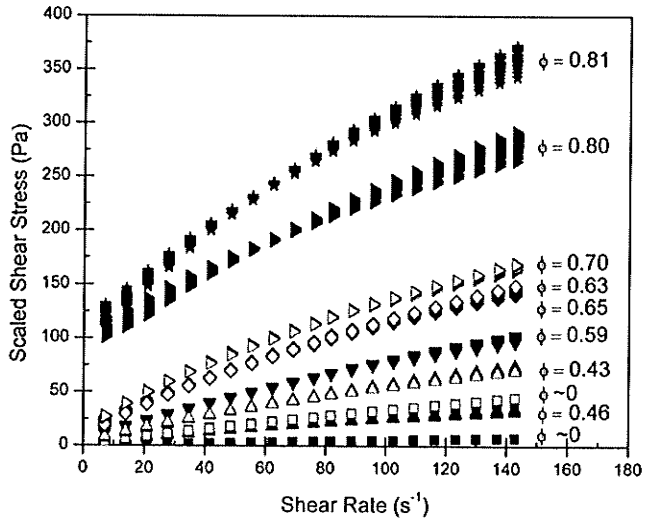

Figure 46: Change in large strain properties (independent of aging effects) for selected whole egg foams (open symbols) *and egg white foams* (closed symbols) *created from different mixing times 0 s,* (■,□), *60 s* (▲,△), *120 s* (▼), *180 s* (◆,◇), *705 s* (▶,▷), *1065 s* (★), *with corresponding bubble volume fractions* (ϕ) *displayed. The complete range of shear stresses is shown to highlight the development of a yield stress in high bubble volume fraction egg white foams.*

active properties of the egg white proteins (Phillips, 1981). Although the same proteins exist in the whole egg systems, lipids compete with the proteins for adsorption at the air-water interface, limiting the unfolding of the proteins at the interface and as a result limiting the protein-protein interactions that stabilize foam structure (Damodaran, 2005). Also, beyond the mix time of 180 s a distinct yield stress can be seen beginning to develop in the egg white foams; this is an expected result considering that at bubble volume fractions above ~0.65 the dispersed phase has been shown to become packed and thus gives an elastic response at low stresses (Mason, 1999). The yield stress has been shown to arise from jamming of the bubbles which occurs in high bubble volume fraction systems at low stresses (Gopal & Durian, 2003). Beyond the yield stress the bubbles can deform and flow around each other resulting in the viscous flow of the foam as shear rate is increased (Weaire & Hutzler, 1999; Gopal & Durian, 2003). Below bubble volume fractions of ~0.64 the foam-like systems are still considered as disordered emulsions and should behave as viscous fluids (Mason, 1999), a result that is confirmed by the Newtonian and power law systems in Figures 45 and 46. Power law and Herschel-Buckley fits from scaled large strain rheological data for whole egg foams (Table 6), egg white foams (Table 7), whole egg batters (Table 8), and egg white batters (Table 9) are provided.

Table 6: Power law and Herschel-Buckley fits for whole egg foams.

Whole Egg Foams							
Mix Time (s)	Power Law			Herschel-Buckley			
	k	n	r^2	Yield Stress	k	n	r^2
0	0.723	0.830	0.9992	0.000	0.723	0.830	0.9992
30	1.005	0.789	0.9990	0.423	0.837	0.835	0.9972
60	1.698	0.758	0.9980	1.340	1.231	0.834	0.9932
120	2.840	0.762	0.9992	1.861	2.150	0.828	0.9978
180	4.809	0.692	0.9995	3.837	3.390	0.768	0.9992
345	7.011	0.631	0.9996	5.267	4.886	0.706	0.9994
705	7.593	0.625	0.9995	5.759	5.248	0.702	0.9994
1065	7.349	0.623	0.9994	6.635	4.643	0.721	0.9992

Table 7: Power law and Herschel-Buckley fits for egg white foams.

Egg White Foams							
Mix Time (s)	Power Law			Herschel-Buckley			
	k	n	r^2	Yield Stress	k	n	r^2
0	0.076	0.914	0.9983	0.122	0.055	0.978	0.9985
30	0.670	0.680	0.9916	1.059	0.329	0.635	0.9655
60	0.755	0.766	0.9961	1.007	0.416	0.910	0.9856
120	2.566	0.740	0.9972	4.715	1.166	0.913	0.9946
180	6.602	0.616	0.9951	12.222	2.424	0.816	0.9951
345	33.282	0.458	0.9881	56.497	8.193	0.719	0.9903
705	44.929	0.360	0.9594	96.722	0.979	1.133	0.9423
1065	46.752	0.405	0.9777	94.738	3.734	0.904	0.9732

Table 8: Power law and Herschel-Buckley fits for whole egg batters.

Whole Egg Batters							
Mix Time (s)	Power Law			Herschel-Buckley			
	k	n	r^2	Yield Stress	k	n	r^2
0	23.648	0.736	0.9978	37.508	13.692	0.844	0.9996
30	24.098	0.703	0.9972	37.299	12.157	0.850	0.9943
60	17.814	0.695	0.9945	27.058	8.423	0.862	0.9836
120	15.319	0.674	0.9900	21.906	6.892	0.857	0.9621
180	8.539	0.664	0.9857	10.299	4.213	0.829	0.9433
345	7.396	0.633	0.9796	5.995	4.363	0.757	0.9316
705	8.229	0.651	0.9828	7.754	4.487	0.796	0.9408
1065	6.026	0.640	0.9737	4.551	3.541	0.771	0.9133

Table 9: Power law and Herschel-Buckley fits for egg white batters.

Egg White Batters							
Mix Time (s)	Power Law			Herschel-Buckley			
	k	n	r^2	Yield Stress	k	n	r^2
0	0.608	0.893	0.9969	0.132	0.459	0.981	0.9990
30	3.738	0.710	0.9988	2.999	2.351	0.826	0.9985
60	6.282	0.655	0.9993	7.136	3.368	0.797	0.9991
120	7.814	0.634	0.9986	9.019	4.135	0.773	0.9980
180	8.732	0.628	0.9979	10.028	4.691	0.760	0.9966
345	6.859	0.617	0.9925	6.215	4.067	0.729	0.9797
705	3.859	0.638	0.9921	3.210	2.407	0.742	0.9760
1065	3.007	0.643	0.9951	3.252	1.751	0.755	0.9886

5.4 Changes in Large Strain Rheology with Aging Time

The scaling of the shear stress data to a reference aging time produced a different scaling factor for each given aging time, with the reference curve having a scaling factor of one and, thus, remaining where it is. At all other aging times a scaling factor not equal to one is required to shift the data curves onto the reference curve. Plots of the scaling factors (Figures 47-50) versus aging time for all four systems allow us not only to

characterize the evolution in large strain rheological properties with aging time but also to observe how this evolution in foam rheology with aging time is affected by changes in mixing time for a given system (whites or whole eggs, foams or batters).

Slopes on the scaling factor graphs (Figures 47-50) are predominantly negative which indicates the thixotropic nature of the majority of the systems; that is, a reduction in apparent viscosity with aging time is observed. Although a rest period is imposed between each consecutive shear rate ramp, the reduction in viscosity may be enhanced due to continued shearing of the sample. Constant shearing at high rates may damage the bubble network, which may not be able to fully recover in the rest period, and as a result reduce the large strain response of the sample (Heller & Kuntamukkula, 1987).

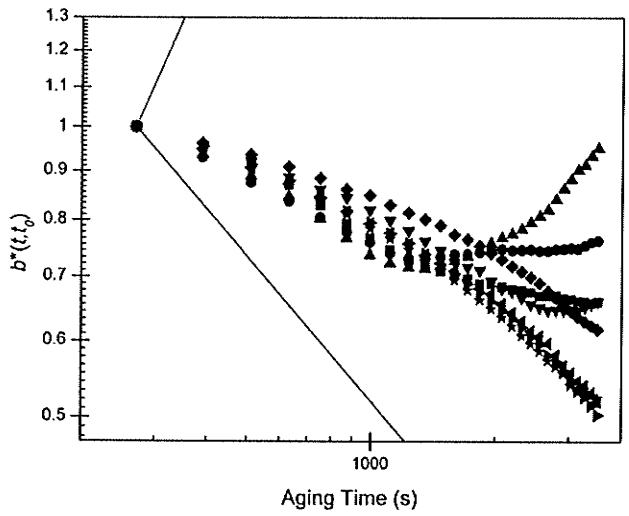

Figure 47 Change in shear stress scaling factor $b^*(t,t_0)$, as a function of aging time for whole egg foams created by mixing for 0 s (■), 30 s (●), 60 s (▲), 120 s (▼), 180 s (◆), 345 s (◀), 705 s (▶), 1065 s (★). Solid lines represent slopes of +1 and −0.5.

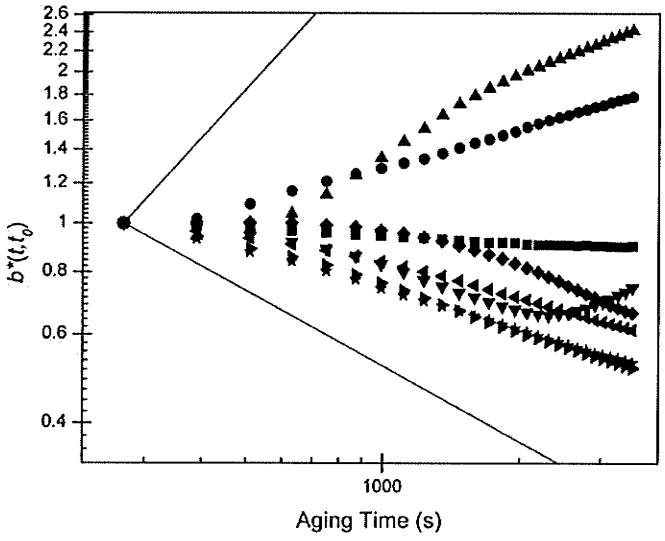

Figure 48 Change in shear stress scaling factor $b^*(t,t_0)$, as a function of aging time for egg white foams created by mixing for 0 s (■), 30 s (●), 60 s (▲), 120 s (▼), 180 s (◆), 345 s (◀), 705 s (▶), 1065 s (★). Solid lines represent slopes of +1 and −0.5.

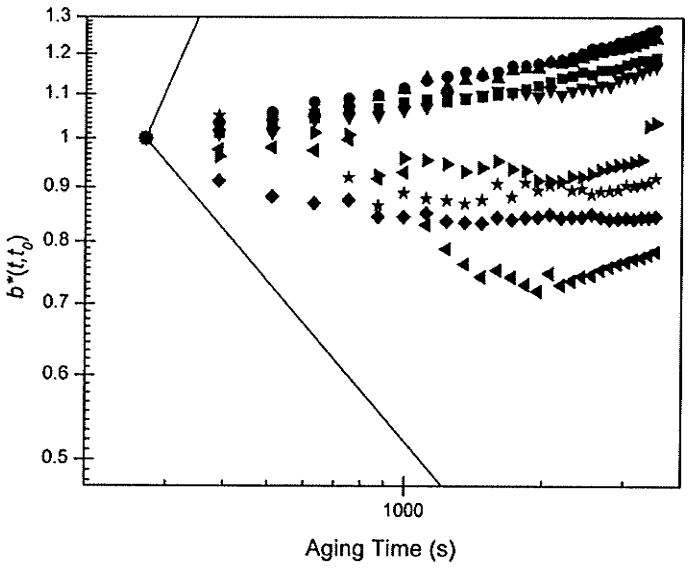

Figure 49 Change in shear stress scaling factor $b^*(t,t_0)$, as a function of aging time for whole egg batters created by mixing for 0 s (■), 30 s (●), 60 s (▲), 120 s (▼), 180 s (◆), 345 s (◀), 705 s (▶), 1065 s (★). Solid lines represent slopes of +1 and −0.5.

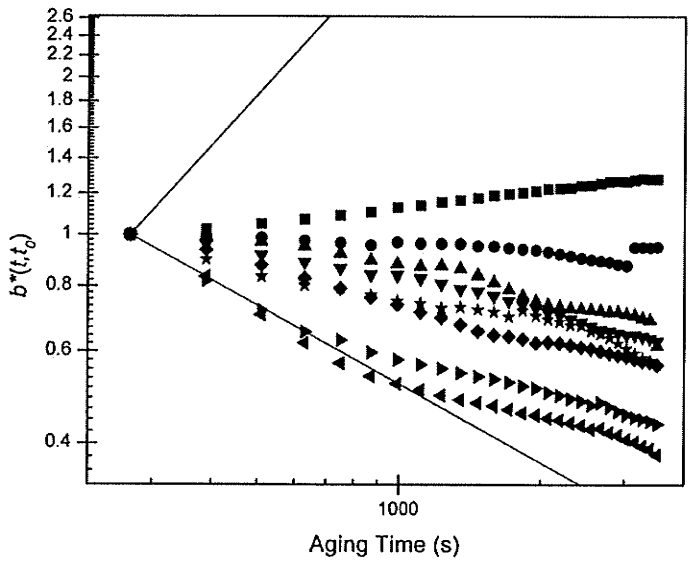

Figure 50 Change in shear stress scaling factor $b^*(t,t_0)$, as a function of aging time for egg white batters created by mixing for 0 s (■), 30 s (●), 60 s (▲), 120 s (▼), 180 s (◆), 345 s (◀), 705 s (▶), 1065 s (★). Solid lines represent slopes of +1 and −0.5.

The egg white foams at mix times of 30 s and 60 s display a positive slope in the scaling factors with aging time. Positive slopes on the scaling factor graphs indicate that a rheopectic behavior is observed; that is, an increase in apparent viscosity with aging time. This is not to be confused with shear thickening or dilatant materials which show an increase in apparent viscosity with increased shear rate. This is somewhat an expected result when considering the small strain scaling factor graphs (Figures 25-28, Section 4.5); in both the small and large strain scaling the same egg systems display positive slopes on both of the scaling factor graphs. At these bubble volume fractions, the "foam" behaves more like a disordered emulsion with the rate of gas diffusion between bubbles severely curtailed, and so drainage is the predominant aging mechanism (Marze et al., 2005). The drainage leads to the development of a dry foam skeleton, which imposes

rigidity in the sample (Weaire & Hutzler, 1999), thus increasing the shear rate response of the sample with aging time.

In certain cases, particularly in the whole egg foam systems (Figure 47), the slope of the scaling factor is negative up to a certain aging time and then becomes positive beyond this aging time. These systems are all in a range where both drainage and disproportionation aging effects are taking place (slopes between -0.5 and +1). This result would lead us to believe that initially, disproportionation effects are dominant, resulting in an increased average bubble size, and thus a decrease in viscosity (Weaire & Hutzler, 1999). As aging continues drainage effects become dominant, leading to the development of a dry foam skeleton, and thus an increase in viscosity (Weaire & Hutzler, 1999). The shift in dominant aging mechanism is supported by the fact that disproportionation can enhance drainage by increasing the Plateau border sizes, which are the paths for drainage (Weaire & Hutzler, 1999; Wang & Narsimhan, 2006).

The solid lines on Figures 47-50 represent slopes of +1 and -0.5 as in the small strain scaling factor graphs (Figures 25-28, Section 4.5). However, in the large strain case, the slopes of the scaling factor plots do not approach the +1 slope as they do in the small strain data. Slopes of +1 are indicative of drainage effects dominating the aging of the foam, and are seen in lower bubble volume fraction systems where disproportionation is limited due to lack of bubbles (Damodaran, 2005; Cohen-Addad et al, 1998). In addition, the slopes do not come as close to the -0.5 slope as the small strain aging data did. Slopes of -0.5 are indicative of disproportionation effects dominating; Weaire and Hutzler (1999) show that high bubble volume fraction foams scale according to a square root dependence on aging time. High bubble volume fraction egg white foams and batters (Figures 48 & 50 respectively) certainly approach this -0.5 slope but never fully

reach it as they do in their small strain counterparts (Figures 26 & 28, Section 4.5). Consequently, the effects of aging in the large strain response, whether by drainage or disproportionation, are not as pronounced as they are in the small strain results. This is likely due to the disturbance of the bubble structure caused by the large strain resulting in collapsing or rearranging of the bubble network that is in contact with the rotating surface (Heller & Kuntamukkula, 1987), as previously discussed.

Regardless of whether drainage or disproportionation effects dominate the evolution in structure; the rate of changes in the large strain response of batters is much less than that is seen for the foam systems. As is the case with the small strain response (Section 4.5), the reduction in drainage effects can be attributed to an increase in bulk viscosity caused by the addition of flour which slows the rate of drainage (Saint-Jalmes & Langevin, 2002). Reduced rates of disproportionation are likely due to adsorption of the flour particles at the bubble interface; this reduces the difference in chemical potential for gas molecules inside and outside the bubbles which is the driving force for diffusion (Murray & Ettelaie, 2004).

Chapter 6: Image Analysis

6.1 Image Acquisition

Six different foam systems were selected for image analysis based upon the small strain scaling factor graph slopes (Section 4.5). For both whole egg and egg whites, systems were selected which came closest to the +1 slope, 0 slope, and −0.5 slope, representing systems which exhibit a range between the two dominating aging mechanisms. Images were taken approximately every three minutes for one hour to represent the foam aging times used in the small strain rheological analysis as well as the midpoint of each of these aging times. Duplicate analyses of each selected system were carried out. Batter systems were not analyzed due to the opacity of the systems, and thus an inability to transmit light though the samples at the selected 1 mm thickness.

Figures 51 and 52 show egg white systems which exhibit a +1.19 slope and a −0.524 slope representing systems which display drainage-dominates aging effects and disproportionation-dominated aging effects respectively. Similarly, Figures 53 and 54 show whole egg systems which exhibit slopes of +0.358 and −0.385. It is visually apparent in Figures 51 and 53 (systems which approach a +1 slope) that there is very little change in the mean bubble size over the one hour period. However, as is seen in the small strain scaling factor graphs (Section 4.5 Figure 25 & Figure 26 for whole egg and egg white, respectively) there is significant change in the rheological response over this same time period. For systems which approach a +1 slope on the small strain scaling factor graphs, a stiffening effect is seen, that is, G' increases with aging time. This change in the rheology over the one hour period cannot be attributed to changes in bubble size or bubble volume as they both remain relatively constant over the one hour period (Figures 51 & 53).

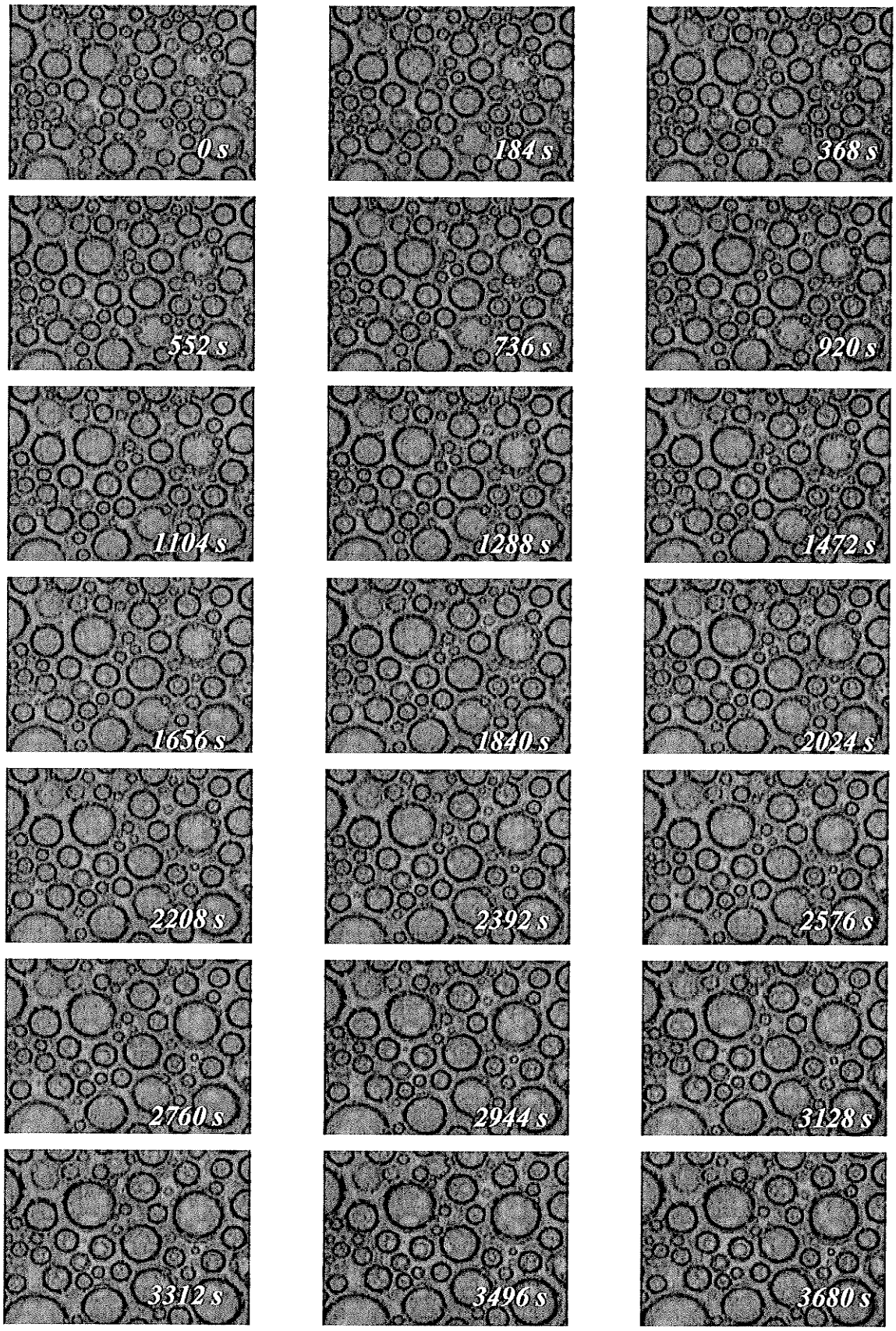

Figure 51: Time delayed photographs of an egg white foam mixed for 60 s. Image dimensions 0.7 mm x 0.52 mm.

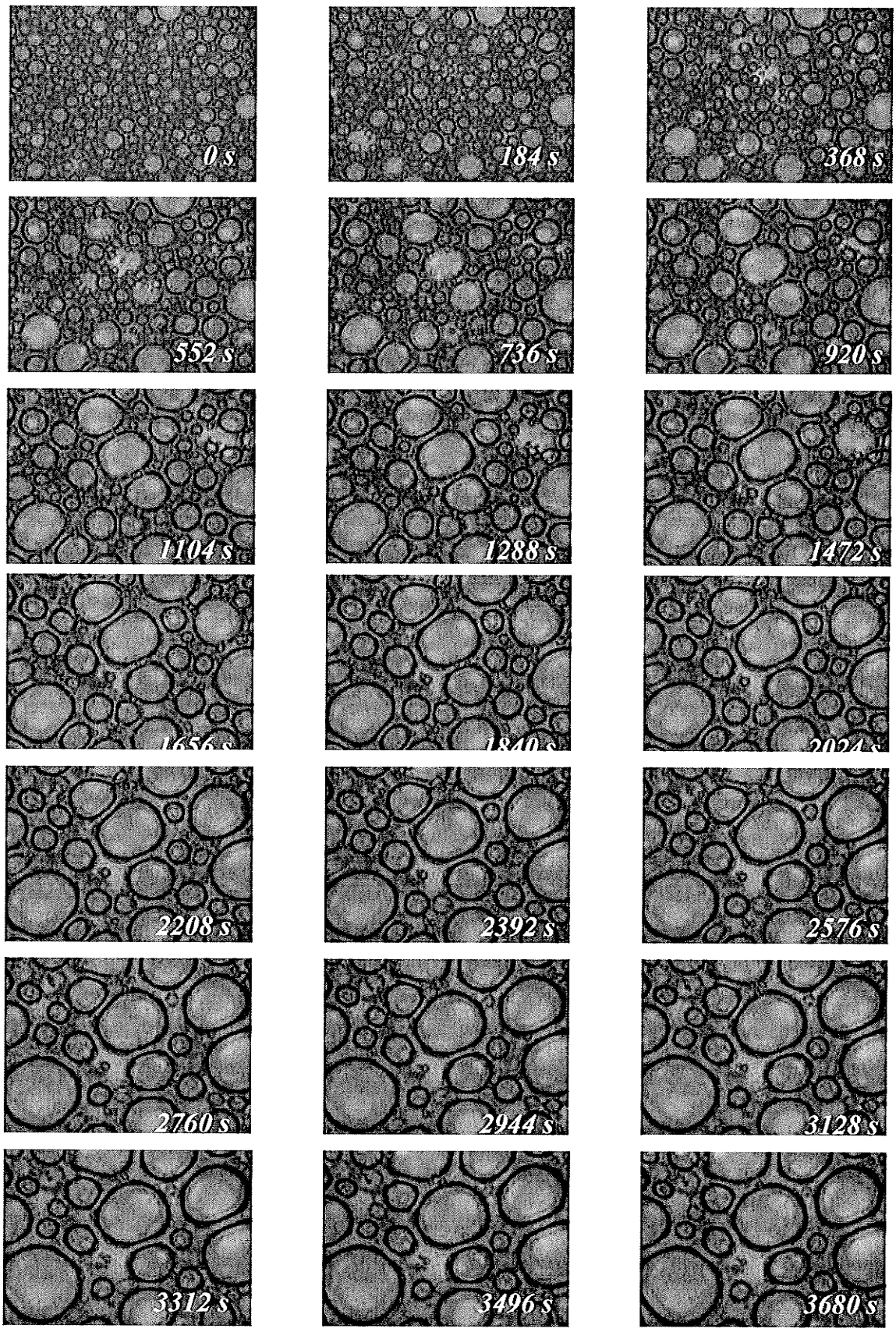

Figure 52: Time delayed photographs of an egg white foam mixed for 1065 s. Image dimensions 0.7 mm x 0.52 mm.

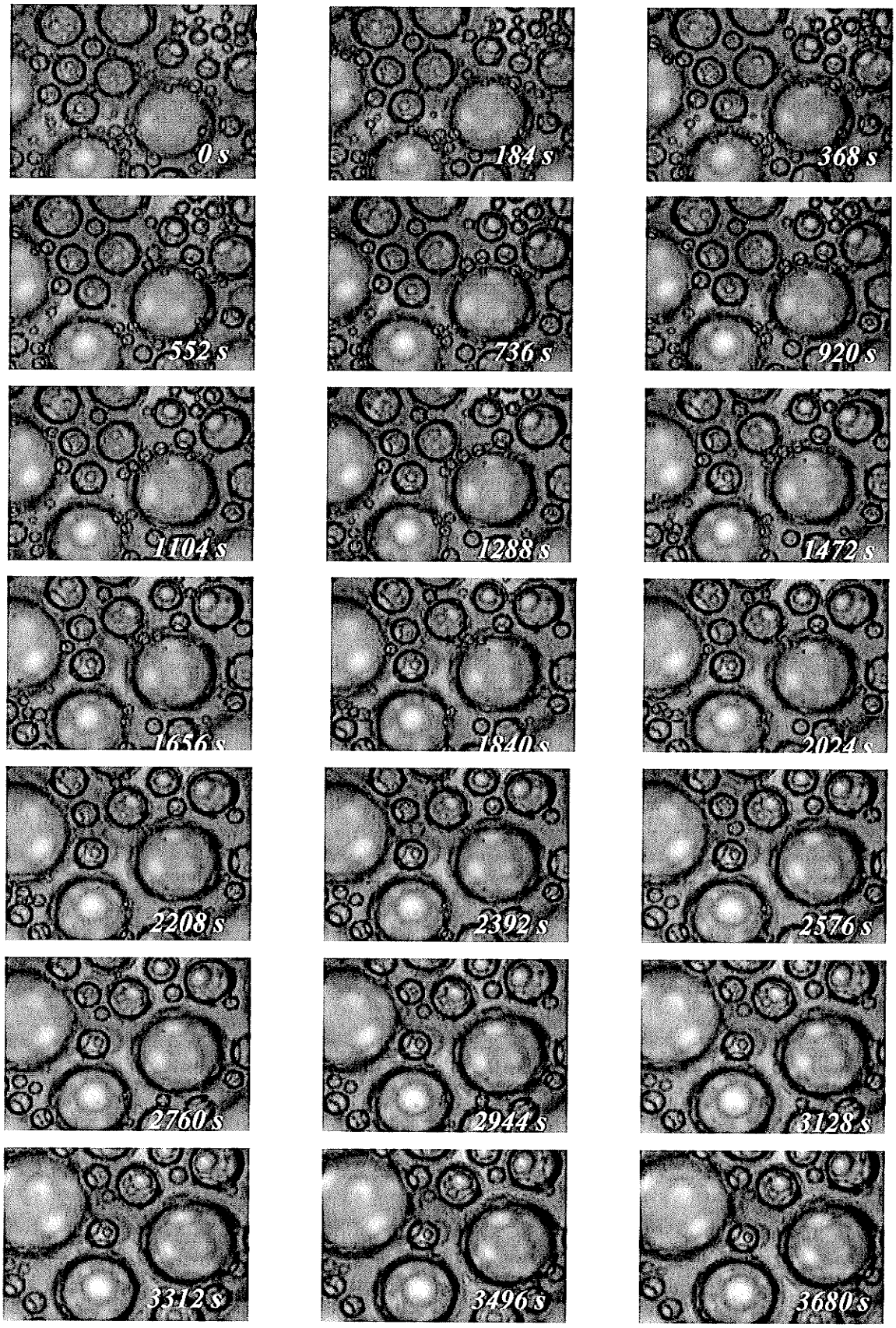

Figure 53: Time delayed photographs of a whole egg foam mixed for 60 s. Image dimensions 0.7 mm x 0.52 mm.

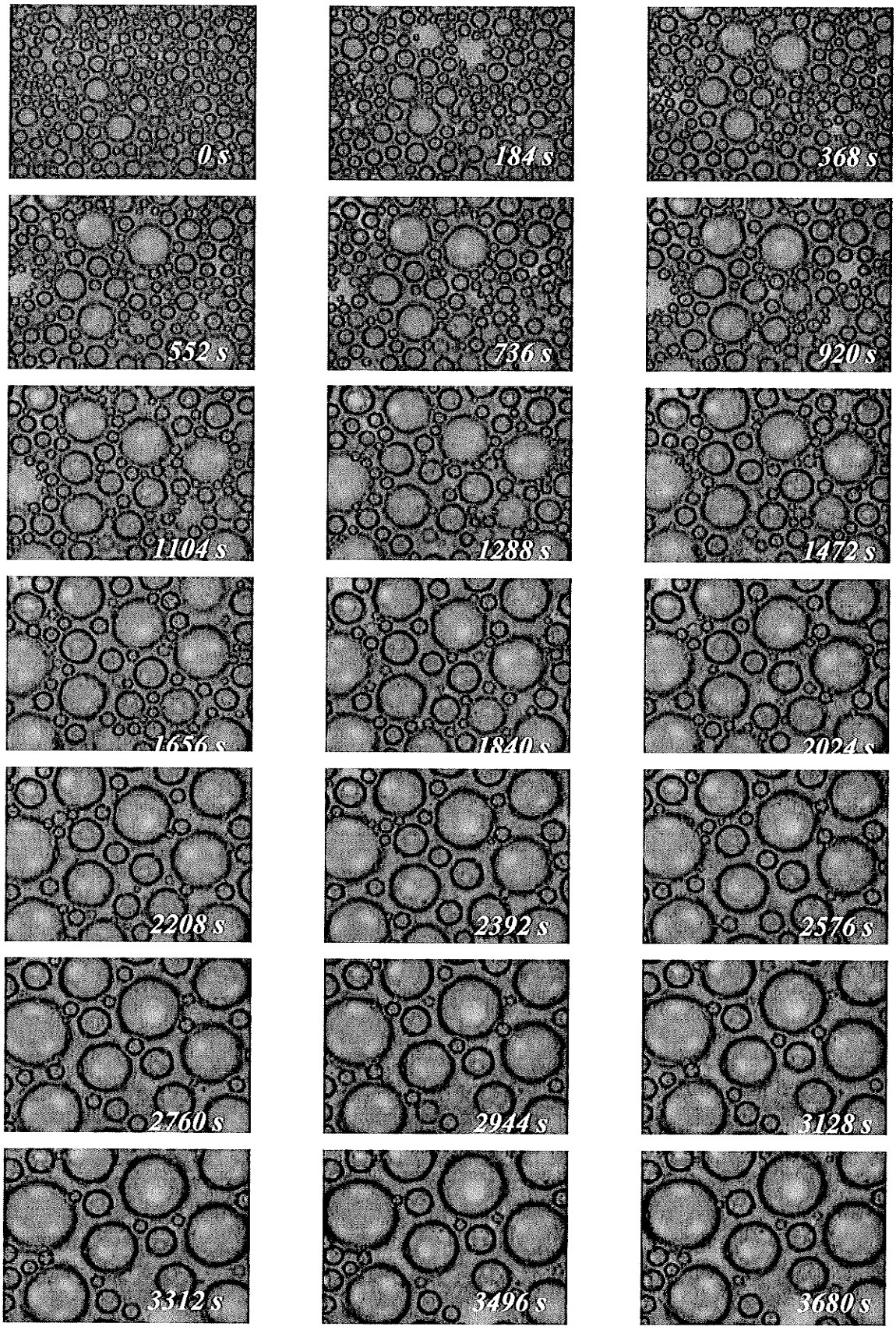

Figure 54: Time delayed photographs of a whole egg system mixed for 1065 s. Image dimensions 0.7 mm x 0.52 mm.

The significant change in rheology is likely due to gravity driven liquid drainage out of the foam system and the development of a dry foam skeleton linearly with time (Weaire & Hutzler, 1999). Visual inspection of the images confirms the fact that bubble sizes are not changing (Figures 51 & 53). A growth in bubble sizes would be seen if disproportionation were occurring. This visual evidence supports the conclusion that in the lower bubble volume fraction systems, those which approach a +1 slope, drainage rather than disproportionation is the dominant aging mechanism of the foams, and is responsible for the stiffening effect that occurs which scales approximately linear with time (as seen by the +1 slopes). Therefore, the rheological changes are consistent with the dry foam skeleton developing linearly with time.

Figures 52 and 54 show images aging over the one hour period for egg white and whole egg systems, respectively; both of which approach a −0.5 slope on the small strain scaling factor graphs. It is evident from both these figures that a significant change in the bubble size occurs during the one hour period which the foams were allowed to evolve. This is an expected result since Weaire and Hutzler (1999) have shown that bubble radius increases due to disproportionation. In contrast to the systems which exhibit a stiffening effect over the aging period, these systems showed a loss in elasticity over the same aging time (Section 4.5). As mix time, and consequently bubble volume fraction increases, the scaling of this loss in elasticity approaches a −0.5 slope. This result is in good agreement with the fact that the static shear modulus has been shown to be proportional to the inverse of the bubble size (Princen & Kiss, 1986). If bubble radius evolves according to the square root of time (Weaire & Hutzler, 1999) then the static shear modulus should change inversely in proportion to the square root of time (Princen & Kiss, 1986; Weaire

& Hutzler, 1999), which is in good agreement with the rheological scaling of high bubble volume fraction foams.

6.2 Bubble Size Distributions & Geometric Mean Bubble Sizes

Although a visual inspection of Figures 51 – 54 seems to confirm the mechanisms of foam decay qualitatively, a quantitative analysis of changes in bubble sizes over the one hour period is necessary to further support the conclusions and to apply models used on industrial foams to food foams (Princen & Kiss, 1986). Image J (v.1.35q) shareware image analysis software was used to determine bubble perimeter which was then used to calculate bubble radius as outlined in the procedures of Section 3.6. In order to construct bubble frequency distributions, bubble radii were tabulated in ascending order and then grouped into classes over the relevant range of sizes. Class width varied depending upon the system analyzed. The number of bubbles in each class was expressed as a percentage of the total bubbles in the field of view and plotted against the midpoint of each class. Figure 55 shows the distribution for an egg white system when no aging has occurred at a mix time of 60 s (representing a +1 slope), while Figure 56 shows an egg white system at a mix time of 1065 s (representing a −0.5 slope). Error bars represent the standard deviation in frequency arising from the two duplicate trials. Regardless of the mix time (and slope of the scaling factor plot) bubble size distributions were asymmetrical and skewed to the left at initial time (when no aging had occurred), suggesting a log-normal distribution. Similar distribution shapes were observed for the whole egg systems. The solid lines on Figures 55 and 56 represent the probability density function of the bubble radii distributions plotted automatically by OriginPro software (v.7.5) using a two-parameter log-normal distribution to characterize the bubble size distribution (Equation 23).

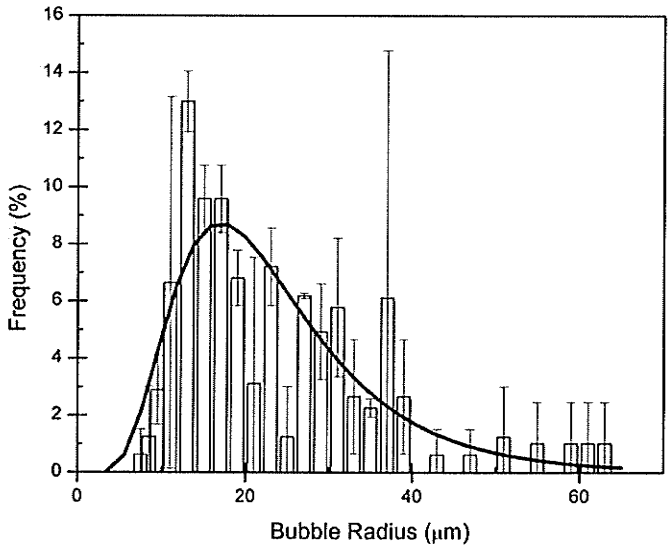

Figure 55: Bubble radius distribution of an egg white system mixed for 60 s at zero aging time. Solid line represents the probability density function based on a two parameter log-normal distribution.

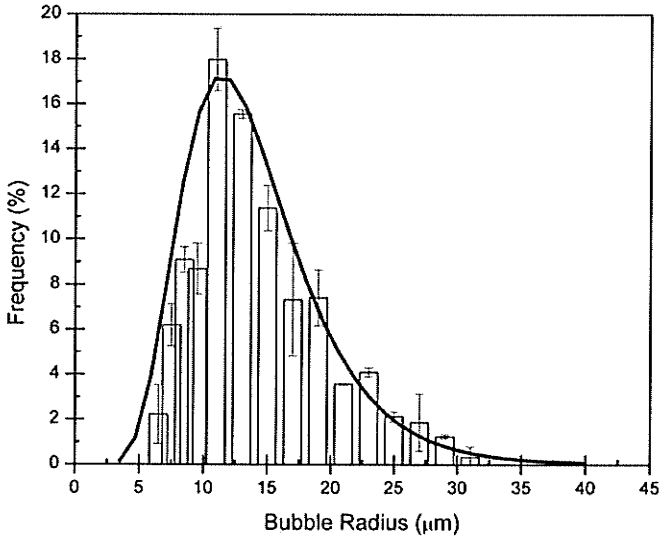

Figure 56: Bubble radius distribution of an egg white system mixed for 1065 s at zero aging time. Solid line represents the probability density function based on a two parameter log-normal distribution.

$$f(r_i) = \frac{1}{\sigma \cdot r_i \sqrt{2\pi}} \exp\left(\frac{-(\ln r_i - \mu)^2}{2\sigma^2}\right) \qquad [23]$$

where: $f(r_i)$ = probability density function of r_i, r_i = midpoint of the i^{th} class in the histogram of bubble sizes, μ = mean of the log-normal distribution, σ = standard deviation of the log-normal distribution. The mean (μ) and standard deviation (σ) of the log normal distribution can be obtained from the raw data by using Equations 24 and 25:

$$\mu = \frac{1}{n}\sum_{i=1}^{k}[\ln r_i * f_i] \qquad [24]$$

$$\sigma^2 = \frac{1}{n}\sum_{i=1}^{k}[(\ln r_i)^2 * f_i] - \left[\frac{1}{n}\sum_{i=1}^{k}\ln r_i * f_i\right]^2 \qquad [25]$$

where k = the number of classes, n the total number of bubbles, and f_i = the number of bubble in class i.

Using Equation 23 from above, the probability density functions at an aging time of one hour were then determined from the actual bubble radius distribution to visualize how the bubble size distributions changed as the systems age. Figure 57 shows the original (0 aging time) distribution and the one hour aged distribution for an egg white system which approaches the +1 slope. Minor differences in the distribution are seen, and although at the one hour aging time some larger bubbles did develop (as shown by the longer tail), the peak of the log-normal distribution occurs at the same bubble size. With only a 1% lowering of the peak over the one hour period, only minor growth in the bubble size is observed.

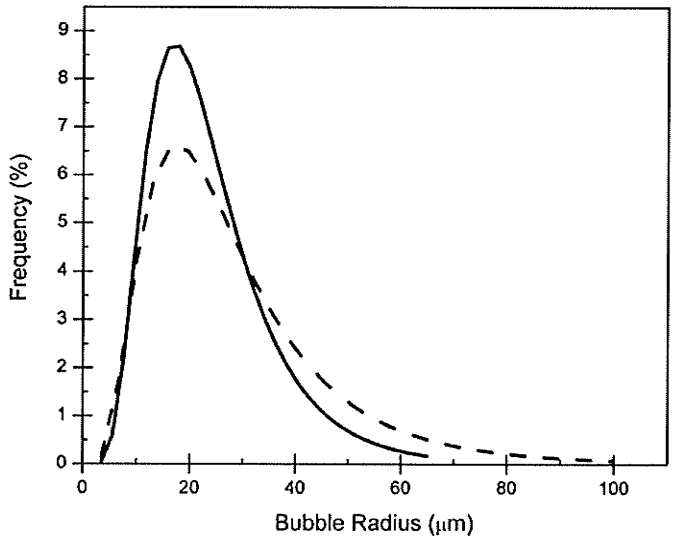

Figure 57 Probability density function of bubble radius distributions for an egg white system mixed for 60 s at zero aging time (solid line) and 1 hour aging time (dashed line).

Figure 58 shows the original and one hour aged distributions for an egg white system which approaches the −0.5 slope. In this case, both a shift in the peak of the log-normal distribution and a broadening of the distribution is apparent, both of which support the fact that there is a significant increase in the bubble size as the foam evolves.

In order to convert μ and σ from the log scale back to the original scale for easier interpretation, the geometric mean (x_g) and geometric standard deviation (σ_g) were determined by Equations 26 and 27:

$$x_g = \exp(\mu) \qquad [26]$$

$$\sigma_g = \exp(\sigma) \qquad [27]$$

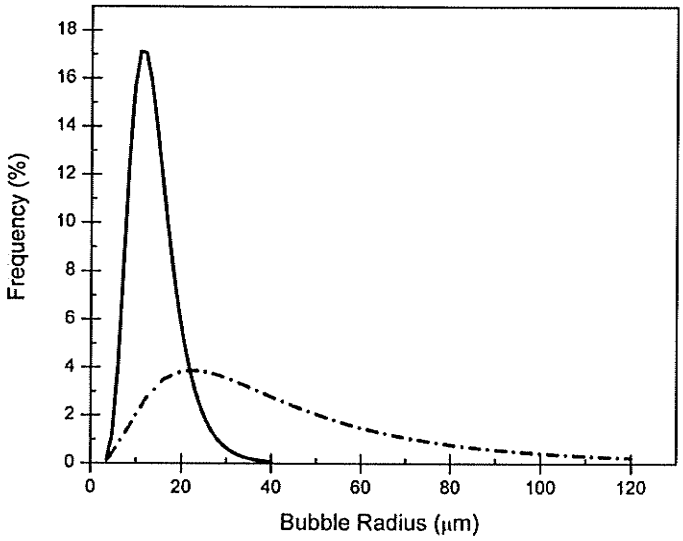

Figure 58 Probability density function of bubble radius distributions for an egg white system mixed for 1065 s at zero aging time (solid line) and 1 hour aging time (dashed line).

It was previously shown that there is a significant change in the bubble size distributions for those systems which approach a −0.5 slope on the small strain scaling factor versus aging time graphs (Figure 58). Conversely, there was very little change in the bubble size distribution for those systems which approach a +1 on the scaling factor graphs (Figure 57). Comparison of the geometric means plotted against aging time further confirms the theory that low bubble volume fraction (+1 systems) have very little disproportionation occurring and that high bubble volume fraction (−0.5 slopes) have significant disproportionation occurring. Figure 59 and 60 show the geometric means plotted versus aging time for egg whites and whole eggs, respectively, and these are systems which represent −0.5 and +1 slopes on the small strain rheology scaling factor graphs. Error bars represent the standard deviation as a result of duplicate trials and are shown on every fourth data point to limit congestion on the graph. A best fit linear line

was fit to the data of the +1 system to obtain a rate of change in the geometric mean radius with aging time. In both the egg white (Figure 59) and the whole egg (Figure 60) the systems exhibiting the +1 slope, have higher initial geometric mean radii than the systems which exhibit a −0.5 slope, an expected result considering that as mix time is increased more air is entrained and the bubbles are subdivided to become increasingly smaller (Jang *et al.*, 2005; Pyler, 1988). The geometric mean radius for these systems remains fairly constant over the one hour period which supports the conclusion that disproportionation is limited and drainage is the dominant aging mechanism. Conversely, the geometric mean radius of the −0.5 systems for both the egg white and whole egg increases over the one hour period; confirming that disproportionation is occurring in these high bubble volume fraction foams. Since the bubble radii of these systems are expected to evolve proportionally to the square root of time (Weaire & Hutzler, 1999), a fit proportional to $(t\text{-}t_0)^{0.5}$, where t_0 is an arbitrarily chosen reference time is plotted (dotted line). In the egg white systems (Figure 59) the geometric mean radii begin to evolve proportionally to $(t\text{-}t_0)^{0.5}$ at long aging times. It is unclear why the geometric mean radius evolves in a linear fashion at earlier aging times. The $(t\text{-}t_0)^{0.5}$ fit for whole egg foams (Figure 60) is not as good, perhaps reflecting the fact that the evolution in rheological properties in whole egg foams is not as close to $t^{0.5}$ for the egg white foams.

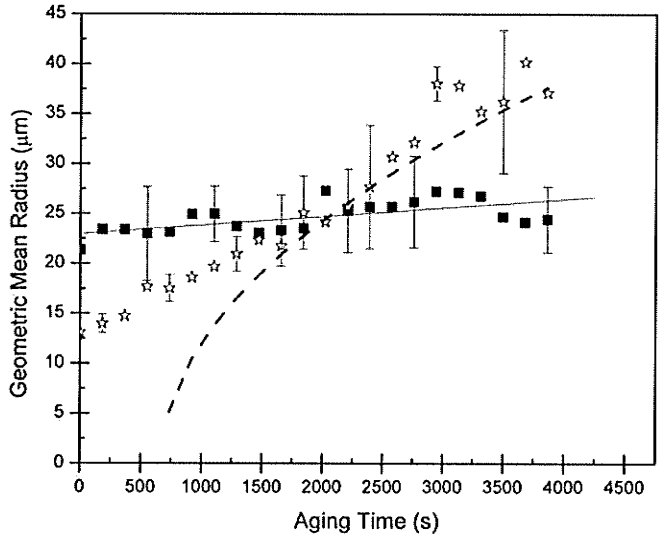

Figure 59: Evolution of the geometric mean radii for egg white systems mixed for 60 s (■) and 1065 s (☆), systems whose scaling factor slopes are +1.19 and −0.52 respectively. Solid line represents best linear fit. Dotted line represents a fit where $R \sim (t-t_0)^{0.5}$, with t_0 = 675 s.

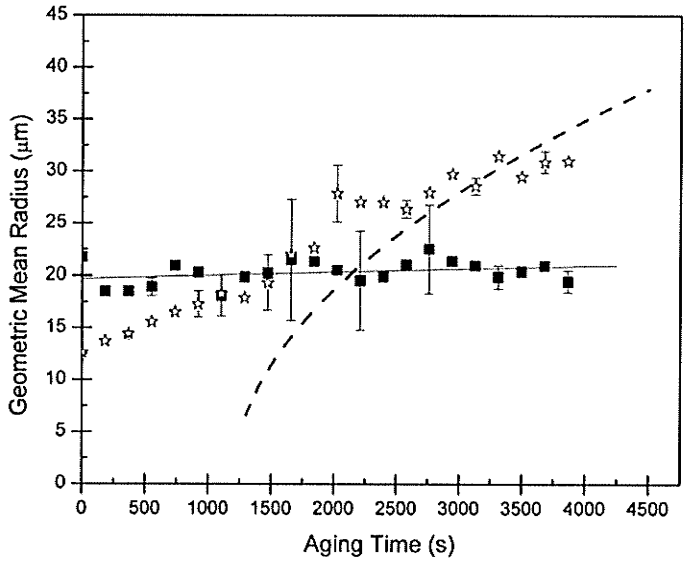

Figure 60 Evolution of the geometric mean radii for whole egg systems mixed for 60 s (■) and 1065 s (☆), systems whose scaling factor slopes are +0.358 and −0.385 respectively. Solid line represents best linear fit. Dotted line represents a fit where $R \sim (t-t_0)^{0.5}$, with t_0 = 1200 s.

Chapter 7: General Discussion

7.1 General Discussion

To this point, three separate techniques have been used to derive information about the structure and change in structure with aging time for foams and batters of two different egg systems and of varying bubble volume fractions. Small strain rheological analysis provided information about shear moduli as a function of frequency; the data followed a scaling law which allowed for considerations of changes in moduli with aging time. Large strain rheological analysis provided information on the shear rate response of the foams and batters, and allowed for visualization of the development of a yield stress in high bubble volume fraction egg white foams. Scaling laws were also obeyed by the large strain data which allowed changes in rheology with aging time to be easily characterized. Image analysis was used to analyze bubble size distributions and visually confirm mechanisms of foam evolution with time.

Although the three techniques have all been dealt with separately, an integration of the three results could strengthen conclusions made on foam decay, and may allow for the prediction of structure and mechanical response for a given set of conditions. The upcoming sections attempt to apply theories and models previously applied to industrial foams and/or systems which should exhibit similar mechanical properties.

To some extent the integration of small strain and large strain rheological results has already been dealt with in Section 5.2, which uses the Cox-Merz rule to support the application of the small strain scaling laws to the large strain data. Figures 35-39 showed us that although the apparent viscosity values and complex dynamic viscosity values do not fall directly on the same curve as predicted by the Cox-Merz rule, similar trends are seen in how the large strain apparent viscosities change as a function of rate of testing.

The downward shift of the large strain apparent viscosity is attributed to the damaging of the bubble network by the imposed shear stress during the large strain testing (Heller & Kuntamukkula, 1987).

7.1.1 Bubbly Egg Systems as Soft Glassy Materials

To further integrate small and large strain rheological results and further understand foam and batter mechanical behavior, we attempt to apply a theory developed to characterize materials that exhibit both structural disorder and metastability (Sollich, 1998). This theory of soft glassy materials rheology (SGMR) is particularly suited to descriptions of the small and large strain shear rheological properties of both power law fluids and Herschel-Buckley materials. On the basis of the coefficients of determination for fits of the large strain rheological data, most of the 32 systems studied are power law fluids (Tables 6-9) but as shown in Figure 46 from Section 5.3 a yield stress develops with higher concentrations of bubbles in the egg white systems. In the SGMR model, predictive capacity is governed by an effective noise temperature, x, that determines the probability of structural rearrangements in the material. To test the suitability of this parameter to characterize the properties of these bubble-filled systems, we examined how the small strain moduli scale with frequency and how the large strain data scale with shear rate, since the SGMR model provides predictions for such data according to the effective noise temperature of the system (Sollich, 1998). It is important to note that x is governed by the structure built into these bubbly systems by mixing, since changes in foam structure due to drainage and disproportionation have been accounted for in the $b(t,t_o)$ scaling procedures employed in Sections 4.4 for small strain and $b^*(t,t_0)$ scaling procedures in Section 5.4 for large strain results.

For the small strain data, both G'' and G' should scale according to ω^{x-1} at lower frequencies for power law fluids. Technically these lower frequencies are defined by $\omega x^{-1} << 1$ (Sollich *et al,* 1997; Sollich, 1998), but the validity of the model will be assessed for $\omega < 1$ rad s^{-1} since there is no evidence of a decrease in G'' as ω increases (Sollich *et al*, 1997) in this frequency region. Therefore, the first test of the model is whether a single power law exponent defines the low frequency response of both the real and imaginary parts of the complex shear modulus for systems with a given volume fraction of bubbles. For whole egg systems, this criterion is met, with the scaling exponent agreeing at an average of 3% difference for all eight mix times (Table 10). For

Table 10: Effective noise temperatures as determined by scaling of small and large strain rheological data for whole egg foams.

Mix Time (s)	(x) Determined from $G'(\omega)$	(x) Determined from $G''(\omega)$	(x) Determined from Large Strain Rheology
0	1.496	1.527	1.830
30	1.609	1.706	1.789
60	1.840	1.779	1.758
120	1.724	1.660	1.762
180	1.503	1.483	1.692
345	1.402	1.365	1.631
705	1.402	1.353	1.625
1065	1.405	1.369	1.623

egg white systems, agreement between the scaling response is within 4% for mix times of 30 s and 60s (ϕ is 0.31 and 0.46, respectively) (Table 11), and for these two mix times, r^2 values for power law fits (0.991 and greater) are better than fits to the Herschel Buckley equation (0.97 and greater) (Table 7). Therefore, small strain data support the view that whole egg systems and egg white systems of low mix times behave as soft glassy materials. Although r^2 values indicate that whole egg and egg white batters behave as

power law fluids (Tables 8 & 9), the batters did not exhibit a common value of x for $G' \sim \omega^{x-1}$ and $G'' \sim \omega^{x-1}$, so that the SMGR model does not appear to be appropriate for describing batter properties (data not shown).

Table 11: *Effective noise temperatures as determined by scaling of small and large strain rheological data for egg white foams which behave as either Power law fluids, or Herschel-Buckley materials.*

	Power Law Systems			Herschel-Buckley Systems	
Mix Time (s)	**(x) Determined from $G'(\omega)$**	**(x) Determined from $G''(\omega)$**	**(x) Determined From Large Strain Rheology**	**(x) Determined from Small Strain Rheology**	**(x) Determined From Large Strain Rheology**
0	1.645	1.836	1.914	N/A	N/A
30	1.219	1.154	1.680	N/A	N/A
60	1.264	1.235	1.766	N/A	N/A
120	1.150	1.034	1.740	1.034	0.087
180	1.124	0.964	1.616	0.964	0.184
345	N/A	N/A	N/A	0.937	0.281
705	N/A	N/A	N/A	0.933	-0.133
1065	N/A	N/A	N/A	0.384	0.096

For the longest three mix times for the egg white systems, a yield stress is definitely observed, and r^2 values for Herschel Buckley fits are similar or better to those for power law fluids (Table 7). For Herschel Buckley materials, the SGMR model predicts the onset of a glass transition, so that G' should be independent of frequency and G'' should scale according to ω^{x-1}. Although experimentally G' is not a constant, it rises only slowly with frequency ($G' \propto \omega^{0.13}$ for $\omega < 1$ rad s^{-1}). In addition, for these Herschel Buckley materials, x should be less than 1 for $G'' \sim \omega^{x-1}$, a criterion that is met for mix times of $\geq$ 180 s, so that small strain data support the SMGR model for egg white systems of long mix times.

For the large strain data, SGMR predictions for scaling are:

$\sigma \propto \dot{\gamma}^{x-1}$ (power law fluids)

$\sigma - \sigma_y \propto \dot{\gamma}^{x-1}$ (Herschel Buckley materials)

where σ is the shear stress, σ_y is the yield stress, and $\dot{\gamma}$ is the shear rate. The effective noise temperature was derived from the power law fits of the scaled large strain data for each mix time. These results have been included in Tables 10 and 11. A summary plot of x versus mix time shows how the effective noise temperature changes for the whole egg and egg white systems based on both the large and small strain data (Figure 61). Data for batters have not been included due to the poor agreement for the small strain data to the SGMR model.

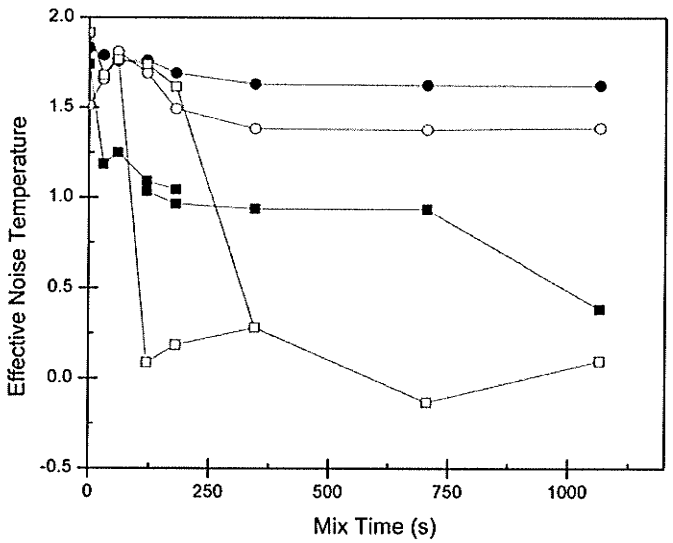

Figure 61: Change in effective noise temperature of whole egg (circles) *and egg white* (squares) *foams as a function of mixing time as assessed by large strain* (closed symbols) *and small strain* (open symbols) *techniques.*

It can be observed from Figure 61 that as more bubbles are entrained and subdivided the effective noise temperature decreases, i.e., the systems become less susceptible to change. This is true for both egg systems. There is reasonable agreement

between values of x derived from the large and small strain data for the whole egg systems, but values derived from large strain data are consistently greater. The greater "fluidity" observed during large strain testing implies that the shearing process itself allows easier propagation of rearrangements in foam structure. For the egg white systems, there is a transition to glass-like behaviour ($x \leq 1$) as mix time increases, and this transition is sharp based on assessments by large strain techniques. There is uncertainty in where this transition occurs based on these data. Certainly, a transition is expected when the volume fraction reaches 0.64 (Mason, 1999) at a mix time of ~180s, but since the development of a protein network structure may be essential for stable foam structures (Murray & Ettelaie, 2004), the transition line at the shorter mix time could be equally valid (since the volume fraction of proteins in egg albumen is approximately 0.08).

7.1.2 Static Shear Modulus Calculation

To this point small and large strain rheological results for foams and batters have been integrated to some extent; this integration has been more successful with the foam systems. However, image analysis, and consequently, bubble sizes, has yet to be incorporated with the small and large strain rheological results. It has previously been shown that the static shear modulus (G_0) of highly concentrated foams is inversely proportional to the surface-volume mean radius of the bubbles (R_{32}), and can be calculated using Equation 11 from Section 2.5.1 (Princen & Kiss, 1986). Since separate estimates of the static modulus can be taken from experimental parameters of both the small and large strain rheological data, the static modulus serves as a logical comparison parameter.

Since Equation 11 is only valid for foams with bubble volume fractions greater than 0.74 ($0.74 < \phi < 1$), an egg white foam mixed for 1065 s ($\phi = 0.81$) is used as a benchmark for the comparison of the static modulus determined by the three different experimental techniques. Using the bubble size distributions for the egg white foam ($\phi = 0.81$) R_{32} values are calculated using Equation 8 from Section 2.4.3; results are tabulated in Table 12. Using these R_{32} values, the experimentally determined bubble volume fraction, and a literature value for the surface tension of egg white, 0.53 Nm^{-1} (Vadehra & Nath, 1973; Ma *et al,* 1986), the static modulus at various age times is calculated using the Princen and Kiss equation (Equation 11). The calculated results are shown in Figure

Table 12: R_{32} values for an egg white foam that has been mixed for 1065 s ($\phi = 0.81$) determined from image analysis.

Aging Time (s)	Average R_{32} (μm)
0	20.2
184	27.1
368	41.6
552	58.4
736	53.9
920	50.3
1104	53.9
1288	61.4
1472	61.0
1656	60.1
1840	61.4
2024	62.3
2208	68.5
2392	66.1
2576	64.8
2760	67.5
2944	68.9
3128	69.1
3312	70.1
3496	66.3
3680	73.6
3864	73.8

62 as closed square symbols. As expected from the Princen and Kiss equation and from the fact that disproportionation is occurring, and thus an increase in bubble size is expected with aging time, the static modulus decreases as the foam ages.

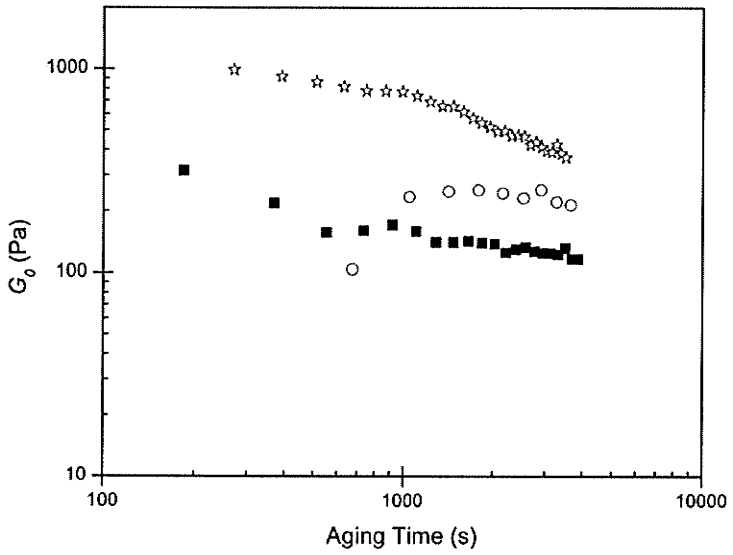

Figure 62: Estimates of the static shear modulus and its evolution with foam aging of an egg white foam mixed for 1065 s as obtained from: image analysis equation (■), small strain rheological analysis (○), and large strain rheological analysis (☆).

The next step is to assess how well Equation 11 predicts the modulus value by comparing calculated results with static modulus values estimated from both the small and large strain rheological analyses. Although an experimentally determined value cannot be extrapolated from the frequency sweep data, an estimate can be made. The estimate is made on the same assumption used for the SGMR model that at low frequencies a plateau is seen in the response of G'. By taking the lowest experimental frequency value and by assuming a plateau response at frequencies prior to this point the static modulus, G_0, is estimated as shown in Figure 63. Estimates from the small strain frequency response data for various aging times are shown as open circles in Figure 62.

For the majority of aging times the estimated static modulus values are greater than the static modulus values calculated by the Princen and Kiss Equation by a factor of approximately 2 for a given age time. This result is somewhat expected since the

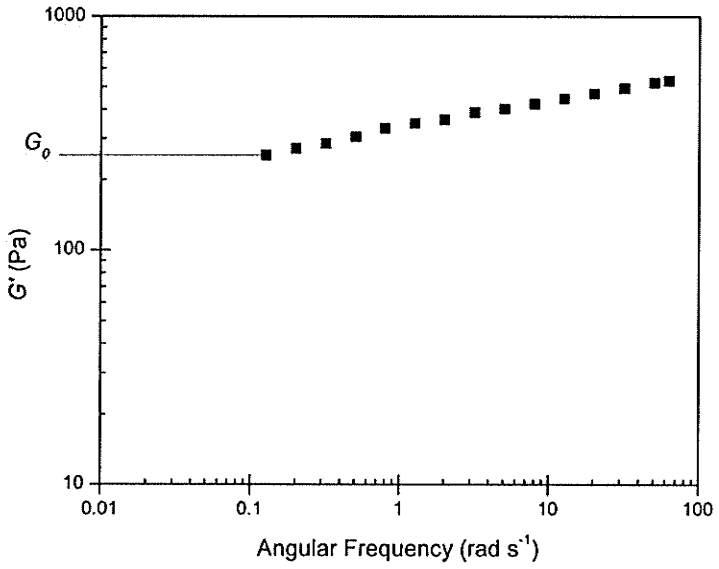

Figure 63: Visual representation of how the static shear modulus (G_0) was obtained from small strain rheological data.

frequency sweep data shows a slight increase in G' with frequency rather than the assumed plateau at low frequency ($G' \propto \omega^{0.13}$ for $\omega < 1$ rad s^{-1}), and therefore one would expect G' to continue to decrease as frequency is lowered and an overestimate of the static modulus at our lowest measured frequency would occur. At the shortest aging time there is one data point that falls below the Princen and Kiss estimated values for the static modulus. This deviation is presumably due to the larger amounts of error seen in the small strain frequency sweeps for high bubble volume fraction foams at early aging times caused by the potential for occurrence of voids in the sample cup as previously explained.

Using the large strain rheological results a second estimate of the static shear modulus can be made and compared to the static modulus calculated using the image

analysis data and Equation 11. This estimate also takes into account the small strain stress sweeps covered in Section 4.2. Figure 64 shows a stress sweep performed at a frequency of 6.284 rad s^{-1} with both the resulting G' and strain; the solid vertical line represents the stress at which breakdown of the structure

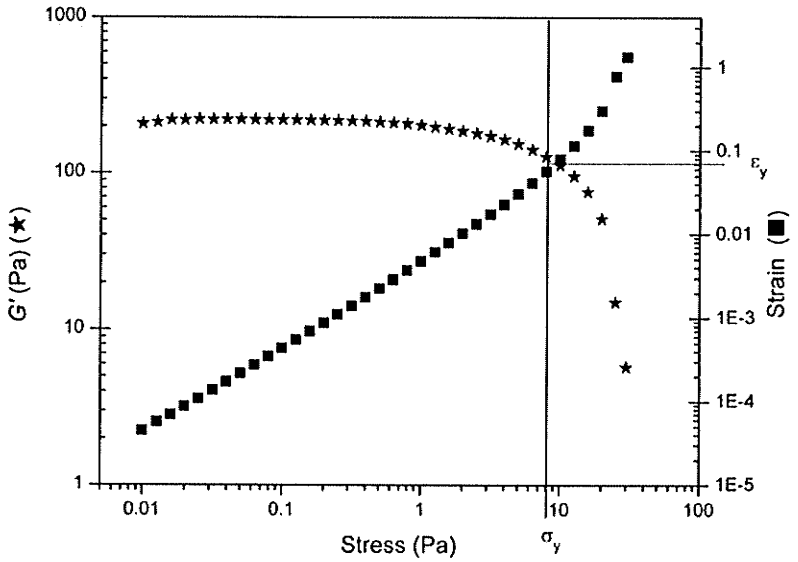

Figure 64: Visual representation of how yield stress and yield strain were obtained from small strain stress sweep data (6.284 rad s^{-1}) for an egg white foam mixed for 1065 s.

occurs and the foam begins to flow. This stress allows an estimation of the yield stress (σ_y), and the corresponding strain is the yield strain (ε_y) as shown by the dotted line on Figure 64. Assuming this yield strain holds constant for this foam as it ages, the yield stress values determined from the large strain rheological Herschel-Buckley fits at various aging times can be used to calculate the static modulus using Equation 28.

$$G_0 = \frac{\sigma_y}{\varepsilon_y} \qquad [28]$$

where G_0 is the static modulus, σ_y is the yield stress obtained from the y-intercept on the large strain Herschel-Buckley fits (Table 7), and ε_y is the constant yield strain obtained from the small strain stress sweeps.

The calculated G_0 values obtained from Equation 28 are also plotted on Figure 62 as open star symbols. As was seen with the small strain estimates for G_0, the large strain estimates are much greater (approximately 4 times) than the predicted values from the Princen and Kiss equation, as well as even greater than the estimates obtained from the small strain data. The disparity of estimates of G_0 derived from the large strain and small strain results most likely arises from the variation in determination of the yield stress from the stress sweeps and from the fitting of the Herschel-Buckley model to the large strain data. The constant yield strain obtained from the stress sweeps is used to calculate G_0 in Equation 28; however, the yield stress obtained from the stress sweeps is much less than the yield stress observed from the Herschel-Buckley fits. This would lead us to believe that either the constant yield strain used is an underestimate of the actual yield strain, or that the yield stress obtained from the Herschel-Buckley fits is inflated, both of which would lead to the calculation of higher than expected G_0 values.

Chapter 8: Conclusions & Future Work Consideration

8.1 Conclusions

By varying mixing time, foams and batters displaying a range of reproducible bubble volume fractions for both whole egg (sponge cake) and egg white (angel food cake) systems were successfully created. The resulting systems ranged from low bubble volume fraction systems behaving as bubbly liquids to high bubble volume fraction stiff foams.

Using small strain rheological analysis, the frequency dependence of both the shear storage and shear loss moduli were measured at ten different foam aging times over a one hour period. Scaling laws, which scale the aged moduli data to a reference time, previously employed on industrial foams (Cohen-Addad *et. al*, 1998) were adapted and successfully used to condense the aging time data to a single reference curve. Plots of the scaling factors, $b(t,t_0)$, versus aging time allowed for the identification of two distinct trends. Low bubble volume fraction bubbly liquids exhibited a stiffening effect with aging time, and thus the slope of their scaling factor versus aging time plot approached +1. High bubble volume fraction foams exhibited a decrease in G' as the foam aged and the slope of the scaling factor plot approached −0.5. Using theories previously applied to emulsions and industrial foams (Princen & Kiss, 1986; Weaire & Hutzler, 1999) the conclusion derived was that in systems which approached a +1 slope drainage was the dominant mechanism for foam aging, while in systems which approached a slope of −0.5 disproportionation was shown to be the dominant aging mechanism. The addition of flour to the foam systems to create a batter greatly slowed the evolution of modulus as the cake systems aged, regardless of whether drainage or disproportionation was dominant.

Large strain rheological analysis allowed for the monitoring of development in different shear flow properties as bubble volume fraction increased, specifically the development of a yield stress in high bubble volume fraction egg white foams. Shear rate ramps at 30 different aging times over a one hour period allowed for the monitoring of changes in the flow characteristics as the foams and batters aged. Making use of the Cox-Merz rule, the same scaling principles used for the small strain (Cohen-Addad *et al*, 1998), were successfully applied to condense the large strain rheological data to a single reference time. Plots of the scaling factors versus aging time seemed to mimic those of the small strain data although the extent of evolution was not as pronounced as in the small strain data regardless of whether disproportionation or drainage dominated. This limited evolution of the systems under large strain analysis was attributed to a disturbance of the bubble network that is in contact with the rotating surface (Heller & Kuntamukkula, 1987). As was observed for the small strain data, batter evolution was slowed significantly regardless of the aging mechanism.

In order to confirm the mechanisms of foam aging proposed, image analysis was used to monitor changes in bubble sizes over the one hour aging period. Image analysis supported the descriptions that systems which approach a +1 slope on the scaling factor graph have little change in the bubble size over the one hour period, suggesting that disproportionation is not taking place and that drainage is predominantly responsible for changes in the mechanical response. On the other end of the spectrum, image analysis showed a large increase in bubble sizes for systems which approached a −0.5 slope on the scaling factor graph, confirming the fact that disproportionation is occurring. Batters were not analyzed by image analysis due to their opacity and limited evolution over the one hour period.

In order to integrate the methods used for foam and batter analysis a theory on soft glassy materials was applied to the cake systems. This theory showed potential to model the rheology of both the whole egg and egg white foam systems, but did not appear to work well for their corresponding batter systems.

A second approach at integration of the three testing methods looked at how well a model developed for the prediction of the static shear modulus of emulsions and foams, based upon a measure of bubble size (R_{32}) obtained from image analysis, compared to experimentally derived estimates of the static modulus from both small strain and large strain rheological results. Although the equation was successful at predicting the trends as the foams age, the predictions proved to be approximately 2 times lower than the experimental estimates from the small strain rheology, and nearly 4 times lower than those estimated from the large strain rheology. The prediction equation was only examined for the high bubble volume fraction systems ($0.74 < \phi < 1$).

8.2 Future Work Considerations

Based on the outcome and conclusions made from this study, it would appear that there is still a need for developing a model which would allow for the accurate prediction of the mechanical response of food foams. Prior to this however, better agreement between results obtained from small and large strain rheological analysis would allow for better interpretation of the underestimate of the current Princen and Kiss (1986) model. Additionally, no prediction mechanism was found to exist for lower bubble volume fraction systems. Although these systems do not have a yield stress, they do possess interesting and dynamic flow properties. The ability to predict the mechanical response of foams could allow for the development of better stabilizing mechanisms and eventually greater consistency in the textural quality of the end food product.

Ideas of the disparity between small and large strain rheological analysis may be explored by employing a new frequency regime to explore the rheological properties of these foam systems. Recently, ultrasonic measurements have been used to obtain information on other cellular food materials (Elmehdi *et al*, 2003; Ross *et al,* 2004), and may prove useful in exploring the mechanical properties of these similar foam systems.

References

Bennion EB, Bamford GST (1973). The Technology of Cake Making. Leonard Hill Books, United Kingdom.

Bordel S, Mato R, Vilaverde S (2006). Modeling of the evolution with length of bubble size distributions in bubble columns. *Chemical Engineering Science*, 61: 3663-3673.

Brooker BE (1993). The stabilization of air in foods containing fat – a review. *Food Structure*, 12: 115-122.

Butt H-J, Graf K, Kappl, M (2006). Physics and Chemistry of Interfaces. WILEY-VCH Verlag GmbH & Co. KGaA, Germany.

Carlin GT (1944). Microscopic study of cake batter. *Cereal Chemistry*, 21: 189-199.

Cipelletti L, Ramos L (2002). Slow dynamics in glasses, gels and foams. *Current Opinion in Colloid and Interface Science*, 7: 228-234.

Cohen-Addad S, Höhler, R (2001). Bubble dynamics relaxation in aqueous foam probed by multispeckle diffusing-wave spectroscopy. *Physical Review Letters*, 86: 4700-4703.

Cohen-Addad S, Hoballah H, Höhler R (1998). Viscoelastic response of a coarsening foam. *Physical Review E*, 57: 6897-6901.

Coughlin MF, Ingenito EP, Stamenovic D (1996). Static shear modulus of gas-liquid foam determined by the punch indentation test. *Journal of Colloid and Interface Sceince*, 181: 661-666.

Cox S, Weaire D, Glazier JA (2004). The rheology of two-dimensional foams. *Rheologica Acta*, 43: 442-448.

Durian DJ (1995). Foam mechanics at the bubble scale. *Physical Review Letters*, 75: 4780-4783.

Damodaran S (2005). Protein stabilization of emulsions and foams. *Journal of Food Science,* 70: R56-R66.

Elmehdi HM, Page JH, Scanlon MG (2003). Using ultrasound to investigate the cellular structure of bread crumb. *Journal of Cereal Science*, 38: 33-42.

Gardiner BS, Dlugogorski BZ, Jameson GJ (1998). Yield stress measurements of aqueous foams in the dry limit. *Journal of Rheology,* 45: 1437-1450.

Gonatas CP, Leigh JS, Yodh AG, Glazier JA, Prause B (1995). Magnetic resonance imaging of coarsening inside a foam. *Physical Review Letters*, 75: 573-576.

Gopal AD, Durian DJ (2003). Relaxing in foam. *Physical Review Letters,* 91: 188303-1 - 188303-4.

Hammershøj M, Prins A, Qvist, KB (1999). Influence of pH on surface properties of aqueous egg albumen solutions in relation to foaming behavior. *Journal of the Science of Food and Agriculture,* 79: 859-868.

Heller JP, Kuntamukkula MS (1987). Critical review of the foam rheology literature. *Industrial Engineering Chemistry Research*, 26: 218-325.

Herzhaft B (1999). Rheology of aqueous foams: A literature review of some experimental works. *Oil and Gas Science and Technology*, 54: 587-596.

Jang W, Nikolov A, Wasan DT, Chen K, Campbell B (2005). Prediction of the bubble size distribution during aeration of food products. *Industrial and Engineering Chemistry Research*, 44: 1296-1308.

Khan SA, Schnepper CA, Armstrong RC (1988). Foam Rheology 3: Measurement of shear-flow properties. *Journal of Rheology*, 32: 69-92.

Lau K, Dickinson E (2004). Structural and rheological properties of aerated high sugar systems containing egg albumen. *Journal of Food Science*, 69: E232-E239.

Lauridsen J, Twardos M, Dennin M (2002). Shear-induced relaxation in a two-dimensional wet foam. *Physical Review Letters*, 89: 098303-1 - 098303-4.

Ma CY, Poste LM, Holme J (1986). Effects of chemical modification on the physiochemical and cake-baking properties of egg white. *Canadian Institute of Food Science and Technology Journal*, 19: 17-22.

Marze SPL, Saint-Jalmes A, Langevin D (2005). Protein and surfactant foams: linear rheology and dilatancy effect. *Colloids and Surfaces A*, 263: 121-128.

Mason TG (1999). New fundamental concepts in emulsion rheology. *Current Opinion in Colloid and Interface Science*, 4: 231-238.

Mason TG, Weitz DA (1995). Linear viscoelasticity of colloidal hard sphere suspensions near the glass transition. *Physical Review Letters,* 75: 2770-2773.

Mason TG, Lacasse MD, Grest GS, Levine D, Bibette J, Weitz DA (1997). Osmotic pressure and viscoelastic shear moduli of concentrated emulsions. *Physical Review E*, 56: 3150-3166.

Maurdev G, Saint-Jalmes A, Langevin D (2006). Bubble motion measurements during foam drainage and coarsening. *Journal of Colloid and Interface Science*, 300: 735-743.

Mayer P, Bissig H, Berthier L, Cipelletti L, Garrahan JP, Sollich P, TrappeV (2004). Heterogeneous dynamics of coarsening systems. *Physical Review Letters*, 93: 115707-1-115707-4.

McGinnis DF, Little JC (2002). Predicting diffused-bubble oxygen transfer rate using the discrete bubble model. *Water Research*, 36: 4627-4635.

Meinders MBJ, van Villet T (2004). The role of interfacial rheological properties on Ostwald ripening in emulsions. *Advances in Colloid and Interface Science*, 108-109: 119-126.

Murray BS, Ettelaie R (2004). Foam stability: proteins and nanoparticles. *Current Opinion in Colloid and Interface Science,* 9: 314-320.

Pal R (2006). Rheology of high internal phase ratio emulsions. *Food Hydrocolloids*, 20: 997-1005.

Phillips MC (1981). Protein conformation at liquid interfaces and its role in stabilizing emulsions and foams. *Food Technology,* 35(1): 51-57.

Princen HM (1985), Rheology of foams and highly concentrate emulsions, II. Experimental study of the yield stress and wall effects for concentrated oil in water emulsions. *Journal of Colloid and Interface Science*, 105: 150-171.

Princen HM, Kiss AD (1986). Rheology of foams and highly concentrated emulsions. III. Static shear modulus. *Journal of Colloid and Interface Science,* 112: 427-437.

Pugh RJ (2005). Experimental techniques for studying the structure of foams and froths. *Advances in Colloid and Interface Science*, 114-115: 239-251.

Pyler EJ (1988). Baking Science & Technology Third Edition Volume II. Sosland Publishing Company, USA.

Reiner M (1964). The Deborah number. *Physics Today*, 17: 62-62.

Ross KA, Pyrak-Nolte LJ, Campanella OH (2004). The use of ultrasound and oscillatory tests to characterize the effect of mixing time on the rheological properties of dough. *Food Research International*, 37: 567-577.

Rouyer F, Cohen-Addad S, Höhler, R (2005). Is the yield stress of aqueous foam a well-defined quantity? *Colloids and Surfaces A – Physiochemical and Engineering Aspects*, 263: 111-116.

Sahi SS, Alava JM (2003) Functionality of emulsifiers in sponge cake production. *Journal of the Science of Food and Agriculture*, 82: 1419-1429.

Saint-Jalmes A, Langevin D (2002). Time evolution of aqueous foams: drainage and coarsening. *Journal of Physics: Condensed Matter*, 14: 9397-9412.

Saint-Jalmes A, Peugeot M-L, Ferraz H, Langevin D (2005). Differences between protein and surfactant foams: microscopic properties, stability and coarsening. *Colloids and Surfaces A,* 263: 219-225.

Sakiyan O, Sumnu G, Sahin S, Bayram G (2004). Influence of fat content and emulsifier type on the rheological properties of cake batter. *European Food Research and Technology*, 219: 635-638.

Sollich P, Lequeux F, Hébraud P, Cates, ME (1997). Rheology of soft glassy materials. *Physical Review Letters*, 78: 2020-2023.

Sollich P (1998). Rheological constitutive equation for a model of soft glassy materials. *Physical Review E,* 58: 738-759.

Thakur RK, Vial C, Djelveh G (2003). Influence of operating conditions and impeller design on the continuous manufacturing of food foams. *Journal of Food Engineering*, 60: 9-20.

Thomas PD, Darton RC, Whalley PB (1998). Resolving the structure of cellular foams by the use of optical tomography. *Industrial and Engineering Chemistry Research*, 37: 710-717.

Vadehra DV, Nath KR (1973). Eggs as a source of protein. *CRC Critical Reviews in Food Technology*, 4: 193-309.

Wang ZB, Narsimhan G (2006). Model for Plateau border drainage for power-law fluid with mobile interface and its applications to foam drainage. *Journal of Colloid and Interface Science*, 300: 327-337.

Weaire D, Fortes MA (1994). Stress and strain in liquid and solid foams. *Advances in Physics*, 43: 685-738.

Weaire D, Hutzler S (1999). The Physics of Foams. Oxford University Press, New York.

Weaire D, Hutzler S (2003). Dilatancy in liquid foams. *Philosophical Magazine*, 83(23): 2747-2760.

Weaire D, Pittet N, Hutzler S, Pardal D (1993). Steady-state drainage of an aqueous foam. *Physical Review Letters,* 71: 2670-2673.

Wilde PJ (2000) Interfaces: their role in foam and emulsion behaviour. *Current Opinion in Colloid and Interface Science,* 5: 176-181.

Yu C, Gunasekaran S (2001). Correlation of dynamic and steady flow viscosities of food materials. *Applied Rheology,* 11: 134-140.

Yuan XF, Edwards, SF (1995). Flow behavior of 2-dimensional random foams. *Journal of Non-Newtonian Fluid Mechanics*, 60: 335-348.